Detailed Modeling and Simulation of Distribution Systems

Using Sub-Transmission-Distribution Co-Simulation

by

Sushrut Thakar

A Dissertation Presented in Partial Fulfillment
of the Requirements for the Degree
Doctor of Philosophy

Approved April 2023 by the
Graduate Supervisory Committee:

Vijay Vittal, Co-Chair
Raja Ayyanar, Co-Chair
Mojdeh Hedman
Amarsagar Reddy Ramapuram Matavalam

ARIZONA STATE UNIVERSITY

May 2023

ABSTRACT

There has been a significant growth in the distributed energy resources (DERs) connected to the distribution networks in recent years. For a distribution system with a high penetration of DERs, a detailed modeling and representation of the distribution network is needed to accurately assess its steady-state and dynamic behavior.

In this dissertation, a field-validated model for a real sub-transmission and distribution network is developed, including one of the feeders modeled with the secondary network and loads and solar PV units at their household/user location. A procedure is developed combining data from various sources such as the utility database, geoinformation data, and field measurements to create an accurate network model.

Applying a single line to ground fault to the detailed distribution feeder model, a high voltage swell, with potentially detrimental impacts on connected equipment, is shown in one of the non-faulted phases of the feeder. The reason for this voltage swell is analyzed in detail. It is found that with appropriate control the solar PV units on the feeder can reduce the severity of the voltage swell, but not entirely eliminate it.

For integrated studies of the transmission-distribution (T&D) network, a T&D co-simulation framework is developed, which is capable of power flow as well as dynamic simulations, and supports unbalanced modeling and disturbances in the distribution as well as the sub-transmission system. The power flow co-simulation framework is developed as a module that can be run on a cloud-based platform.

Using the developed framework, the T&D system response is studied for balanced and unbalanced faults on the distribution and sub-transmission system. For some faults the resultant loss of generation can potentially lead to the entire feeder tripping due to high unbalance at the substation. However, it is found that advanced inverter controls may improve the response of the distribution feeders to the faults. The dissertation also highlights the importance of modeling the secondary network for both steady-state and dynamic studies. Lastly, a preliminary investigation is conducted to include different dynamic elements such as grid-forming inverters in a T&D network simulation.

ACKNOWLEDGMENTS

I would like to express my sincere gratitude to my advisors, Professor Vijay Vittal and Professor Raja Ayyanar. Their valuable insights and inputs have been critical throughout my PhD at Arizona State University. They have been very supportive and encouraging and provided critical feedback at the same time – they have been instrumental in my growth both academically and as a person during my PhD.

I would also like to thank my committee members, Professor Mojdeh Hedman and Professor Amarsagar Reddy Ramapuram Matavalam for being a part of my graduate committee and for their feedback and time throughout the PhD.

I would like to thank other students I have had the chance to work with, specifically Dr. Karen Montaño-Martinez, Madhura Sondharangalla, Dr. Nikhil Korada, Dr. Shanshan Ma, Zahra Soltani, Jingyi Yuan, Jiaqi Wu, Mengxi Chen, Arnab Acharya, Giritharan Vijay Iswaran, Dan Moldovan, Mengzhi Wang. I learned a lot while working with you and it was a great pleasure to work with you all.

I have also had a chance to work with different teams from outside ASU during my research. I would like to thank and more specifically Jeff Loehr, Ken Brown and Ernest Palomino from Salt River Project, Dr. Daniel Haughton and Cynthia Rojas from Arizona Public Service, Dr. Michael Emmanuel from National Renewable Energy Laboratory, Dr. Joseph (Panitarn) Chongfuangprinya and Nicky (Natsuhiko) Futamura from Hitachi America, Professor Ravikumar Gelli from Iowa State University, and Dr. Deepak Ramasubramanian from Electric Power Research Institute and others from these

institutions who worked on the same projects. Their insights and feedback were valuable in giving me different perspectives and ways of looking at a topic.

I would like to thank the IEEE PES ASU Student Chapter teams I was a part of during 2021-23 – working with them to arrange various events related to power systems was a really great process where I learned a lot. I would like to express my gratitude towards all my friends at Arizona State University – my time at Arizona State University was a really beautiful and enjoyable journey because of all of you. Finally, I wish to thank my parents and relatives for all their support and love.

TABLE OF CONTENTS

CHAPTER Page

LIST OF TABLES

Table Page

LIST OF FIGURES

Figure Page

Figure Page

Figure Page

Figure Page

Figure Page

Figure Page

Figure Page

1 INTRODUCTION

Distribution systems are one of the key elements of the overall power system network. They are at the same time the part of the electrical network that interfaces with the end users and have been relatively neglected compared to the transmission and generation systems in terms of detailed modeling or analysis. Historically, the distribution systems would be oversized and operated for a large part in a 'connect-and-forget' manner [1]. While analyzing the transmission systems, until the 1990s, entire distribution systems including the distribution substation and feeders and loads were merely represented by static loads [2].

However, the recent decades have brought a lot of changes in the electric grids – there is an increasing proliferation of distributed energy resources (DERs) connected to the distribution systems. There is also a movement of the electrical industry (and society at large) towards giving a preference to using sustainable and renewable energy resources. This shift has resulted in significant distribution connected renewable resources such as solar photovoltaic (PV) units in today's feeders and the penetration of these DERs in the distribution systems is only expected to increase in the future. Some smaller grids such as that of Hawaii now have more than 71% of their daytime load and 11% of annual energy supplied by these DERs. Furthermore, even larger grids across the United States of America and the world expect the share of DERs to grow significantly in the near future[3].

These DERs, especially solar PV units, incorporate advanced control techniques and show nonlinear dynamic behavior. Hence, the distribution feeders of today need to be

carefully modeled and studied. These resources play an increasingly important role in determining the response of the distribution systems both in steady state operation as well as in their response to various grid disturbances and dynamic events. Recognizing the increased penetration of DERs in the distribution resources, the IEEE 1547 Standards (with the latest version being released in 2018 with an addendum in 2020) [4] specify the minimum requirements for the DERs which include the capabilities of the DERs to provide active and reactive power support in regular operation as well as during abnormal conditions. Hence, modeling the DER controls is important while studying distribution systems with high DER penetration.

Another set of advanced inverter-based devices are "grid-forming" inverters, that are capable of providing frequency as well as voltage support [5]. These inverters are designed to be able to maintain a local grid through a main grid disconnection or islanding event. Although these inverters are more relevant for microgrids or for bulk-system connected large-scale resources, they may become more prevalent for distribution grids of the future.

In addition to the advanced DER devices, load modeling is another important aspect ensuring accurate response from distribution grids to dynamic events. Devices such as single-phase induction motors are important in capturing the delayed voltage recovery events that are visible at the distribution as well as transmission levels.

Due to the presence of these DERs as well as other technologies such as electric vehicles and demand side management interacting with the distribution grid, there is a need to model the distribution systems in detail. Since late 1990s, there have been efforts to

switch from a static model for the distribution systems to a composite load model with DERs [2]. However, the distribution systems are still represented as aggregated models in this framework. As will be shown in this dissertation, on systems with high penetration of renewables, certain dynamic events may not affect the entire distribution system equally. Hence, it is important to model the distribution system in detail to study its response to various disturbances.

On the other hand, traditionally the sub-transmission/transmission systems are represented using voltage sources behind impedances in distribution system studies. With this modeling, a lot of work is required to study how the sub-transmission level events impact the distribution system in detail. This provides another impetus for modeling the sub-transmission and distribution systems together.

One method to combine a detailed distribution system model with the sub-transmission/transmission system is to create an integrated model involving both the sub-transmission and distribution systems. There are some commercial software packages like DIgSILENT PowerFactory [6] which support this. However, a large number of available transmission/distribution software packages are either just intended for the study of the transmission or for the distribution systems. In addition, usually the transmission-level software packages model the system in sequence domain, while the distribution system is usually analyzed in the unbalanced three-phase domain. Hence, creating an integrated model requires significant effort and may not take advantage of the domain-specific (transmission or distribution specific) advances in simulation which rely on a particular problem structure. Co-simulation is one possible method to connect and

simulate the distribution and transmission models together while being able to model the distribution and sub-transmission models in their own software packages and domains. A co-simulation power flow and dynamic simulation thus provide the benefit of being able to model the sub-transmission and distribution models in software packages designed for modeling those, while still performing a common simulation involving both systems. This dissertation provides a power flow as well as dynamic co-simulation with the sub-transmission modeled in three-sequence detail and the distribution network modeled in three-phase unbalanced detail.

Considering these important challenges, this dissertation aims to achieve the following objectives:

- A detailed distribution system model for a real feeder in Arizona for power flow and dynamic simulations (with a detailed representation of the solar PV units) is created. In addition, four other feeders at the same substation and the sub-transmission circuit in the vicinity of this substation are modeled to create a sub-transmission-distribution circuit model.
- A three-sequence – three-phase sub-transmission-distribution co-simulation framework is developed for both power flow and dynamic co-simulations. The solar PV units are represented in this framework using a custom user model to enable a detailed representation of the solar PV units including the controls.
- For an unbalanced fault, the modeled feeder experiences voltage swell in one of the non-faulted phases. This phenomenon is investigated, and the impact of the solar PV units on this voltage rise is studied with different controls.

- Utilizing the developed co-simulation framework, the response of the distribution-sub-transmission system is assessed for various faults on the distribution and sub-transmission network.

The dissertation is organized in the following manner:

- Chapter 1 (this chapter) provides the background and introduction for the dissertation /research
- Chapter 2 provides the procedure and results for the detailed feeder model created
- Chapter 3 describes the developed sub-transmission distribution co-simulation framework and describes the models for solar PV model, grid-forming inverters and single-phase induction motors that can be used in conjunction with the co-simulation framework
- Chapter 4 describes the dynamic simulations showing the voltage swell for unbalanced fault. This chapter also discusses the impact of the solar PV units on this voltage swell.
- Chapter 5 describes the developed T&D network model and the validation of this model against field measurements, and the impact of modeling the secondary network in steady state.
- Chapter 6 discusses some case studies involving various faults on the distribution/sub-transmission networks using dynamic transmission-distribution co-simulation formulation developed in Chapter 4. It also discusses the importance of modeling the secondary network via dynamic simulations.

- Chapter 7 concludes the dissertation and presents some future research questions building on material presented in this dissertation.

2 DETAILED FEEDER MODEL CREATION

Modeling distribution systems in detail is important in order to study the phenomena which impact them, especially for feeders with a high number of DERs or other smart devices connected to the distribution. In this dissertation, an actual feeder from Arizona is modeled in detail to study the impact of a high penetration of solar PV generation on some aspects of the steady state operation as well as the response of this feeder to dynamic events. Various data are acquired from an electric utility in order to create the feeder model. The feeder model is created in OpenDSS [7], which is an open-source distribution system simulation and analysis software with advanced modeling and simulation capabilities. When creating the feeder model, the primary as well as secondary network are represented in detail including individual residences, and the loads and the solar PV units are modeled at their actual residential locations.

The selected feeder serves 1715 residential customers via 371 distribution transformers. The feeder includes 5700 primary sections and 1790 secondary sections and is approximately 9 kilometers in length, consisting of underground cables. Including the single and three-phase buses in the primary and secondary circuits, the circuit model for this feeder consists of 7800 buses. The peak active power demand for the feeder was 7.35 MW in 2019, and the corresponding reactive power demand was 1.15 MVAr. There are 4 three-phase capacitor banks installed on the feeder with 1200 kVAr rating each. This feeder has one of the highest penetration levels of solar PV among the feeders operated by this utility – with peak solar PV production around 3.8 MW resulting in reverse active power flow of around 2.1 MW during March 2019. The circuit diagram of this feeder including the locations of various key elements is shown in Figure 2.1.

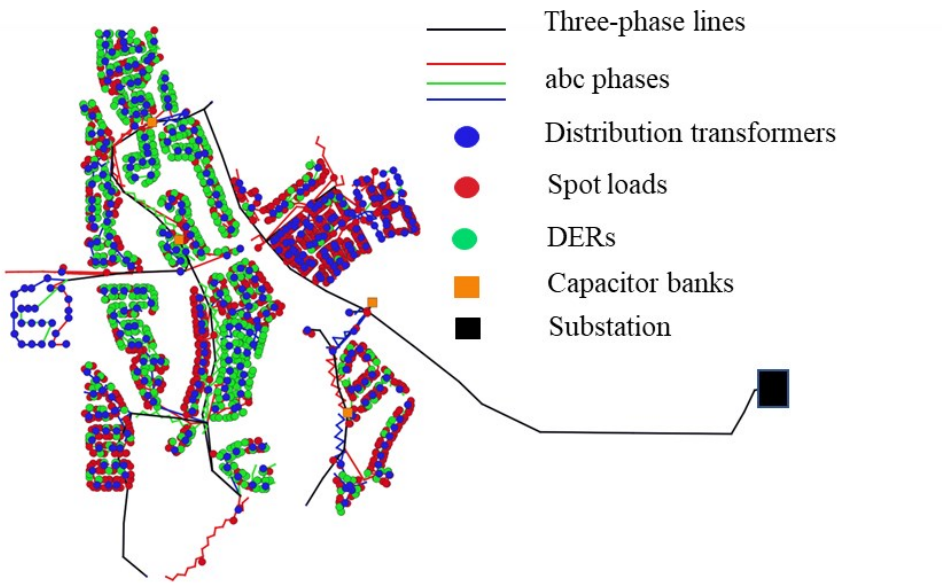

Figure 2.1 Circuit Diagram of the Selected Feeder with Different Elements

This chapter begins by presenting the available literature covering the detailed modeling of utility distribution feeders, in Section 2.1. Section 2.2 describes the data acquired and used for creating the feeder model (which includes a network model plus the time series profiles for the loads, solar PV units and the source voltage). The process of creating the network model is described in Section 2.3, while the process of creating the time series model/profiles is described in Section 2.4. The time series model is then compared with some field measurements as a validation in Section 2.5. The importance of modeling the feeder in detail is highlighted in Section 2.6. For some studies presented in this dissertation, the penetration level of the DERs is increased beyond the present level, these scenarios are described in Section 2.7. A large part of this chapter is reported as a part of a publication [8].

2.1 Detailed Modeling of Distribution Feeders

Historically, distribution systems have been modeled using numerous approximations and simplifications. Such simplifications can be found in the textbooks on distribution system modeling and analysis [9], [10]. However, with the increased penetration of the DERs and the smart grid technologies, it is important to model the distribution system in detail [11]. Hence, there have been efforts to create detailed models of real distribution networks for research. There are two aspects to creating a detailed network model:

- A detailed network model corresponding to the actual feeder, with the primary and secondary networks as well as elements such as distribution transformers and capacitors, loads and solar PV units accurately represented at their locations
- An accurate assignment of the load and solar PV active and reactive powers and the source voltage at the substation, obtained based on measurements. If the purpose is to create a time series data, using the measurements to create accurate power profiles for the loads and solar PV units leads to an accurate time series model.

A distribution feeder model of a real distribution system from Iowa is provided in [12]. It is a 240 bus model for a circuit from Midwest US comprising of three feeders. The provided data contains the network data as well as time series profiles corresponding to all four seasons. To preserve privacy, the time series data at each primary node is aggregated from the customer measurements. However, the network model provided does not contain any information about the secondary network or the loads. As a part of another project from Arizona, a feeder from Flagstaff, AZ is modeled in [13] by

combining the available GIS data from the utility with the AMI measurements. These data are combined to create an accurate feeder time series model. Further, the AMI data is combined with the higher resolution data acquisition system (DAS) measurements from several locations of the feeder to create higher resolution data. However, the feeder model again does not include the secondary network. Another project from Washington [14] uses measurements from a large number of meters installed for the project to create load models at each node in the system by allocating the closest available meter to that location.

Due to the smart devices, there is an increasing need for modeling the secondary network in addition to the primary network including detailed models of the network elements [15]. Thus, there has been an effort to approximate the secondary network where the data is not available. The authors of [16] model a low voltage network, where they aggregate the meters at individual poles to create a model including the low voltage buses. However, this study does not utilize any field measurements and creates a single snapshot model. The authors of [17] model an actual distribution network from Hawaii with a high solar PV penetration, and show that for different estimates of the secondary network, the voltage profile of the secondary nodes can vary significantly, thus establishing the importance of modeling the secondary network. Here, the primary network is modeled in detail, and the time series model is created using AMI meter measurements. Approximate secondary network models are created by selecting secondary cable/line types based on factors such as the transformer size and the number of customers. In [18], it is shown that using an inaccurate model of the secondary network or not accounting for a diversity of customer load profiles can misrepresent the impact of the secondary network and result in

incorrect voltages and powers losses across the secondary network. Hence, modeling the secondary network accurately to reflect the actual network is important. There are some approaches to estimating the secondary network parameters using the AMI data as well [19], [20]. In this dissertation, the secondary network impedances are obtained from the network model provided by the utility.

The rest of the chapter provides the methodology used in this project to create a detailed and accurate distribution system model for a real feeder from Arizona by combining data from various sources, including the network model and time series profiles.

2.2 The Data Used for Creating the Feeder Model

A variety of data was acquired from the utility and used to create an accurate model for the selected feeder. Using this data, a network model as well as time series profiles for two selected days were created. The selected days included one day in summer (15 July 2019) corresponding to the peak load of the system and one day in spring (15 March 2019) corresponding to the peak reverse active power flow from the feeder. The data acquired included the following:

1. Base network model of the feeder: The base network model of the feeder including the primary and secondary network was prepared by the utility and provided as a database file for the commercial distribution system software CYME/CYMDIST [21]. This database contains the information for the network model elements including the sections, distribution transformers, loads, capacitors and switching elements in the circuit as well as the locations of the loads and solar PV units in the system (as shown in Figure 2.2 which shows a small portion of the

circuit model from CYME) and the snapshot values of the loads corresponding to a snapshot (5 PM on 15 July 2019).

2. Geographic Information System (GIS) data: The utility also provided the GIS data including the latitude and longitude for all the sections in the system as well as for the meters installed in the system.
3. Feeder-head measurements: The measurements of active power, reactive power (both for combined three phases), the magnitudes of phase A voltages and the individual phase currents were included in the available feeder-head measurements. The resolution available for these measurements was 10 seconds.
4. Advanced metering infrastructure (AMI) meter measurements: The measurements of active power and voltage was available from 1652 load (billing) meters and 784 solar PV meters, and voltage magnitude measurements were available from 1194 of those meters for the selected days. A large number of meters out of these report the values hourly, but there are some meters reporting the values each 15 minutes for the selected days.

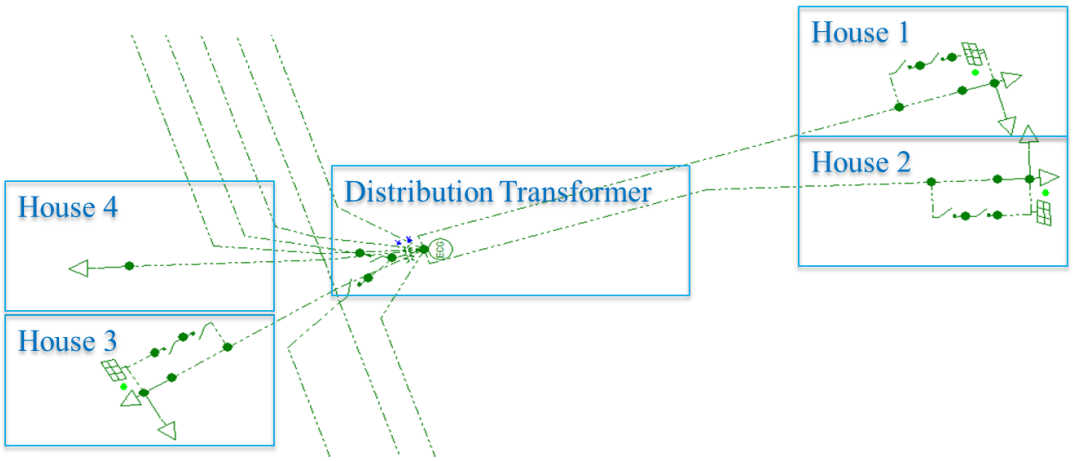

Figure 2.2 Single Line Diagram of a Small Portion of the CYME Model

2.3 Creating the Feeder Network Model

The initial network model in OpenDSS is obtained based on the CYME model database by the utility. The ready-made data converters available did not support the particular version of CYME data (8.1) out of the box, hence, a new tool was developed for this process. The developed converter was written in Python language and a version of this tool is released as an open-source software [22].

The overall process of the conversion tool can be explained via Figure 2.3. The CYME database provided was in '.sxst' format, which is an extensible markup language (XML) based database read by the CYME software. From CYME, the database can also be exported as a set of three text files describing the equipment, network and the loads in the system. These text files are read by the developed tool to form lists of tuples for each kind of element in the converter. The main task of the converter is to map the parameters for each element from the format in CYME and convert them to the format required by OpenDSS. In some cases, this involves computing the equivalent values between two different representations of elements like transformers and cables. Another challenge is to relate different tables/elements from the database: for instance, the equipment database and the network database often contain different information about a network element which must be combined and converted to a form required by OpenDSS. For this feeder, additionally, the section impedances were directly exported from CYME and read separately for more accurate network modeling, rather than relying on converting the

underground cable parameters. Finally, the conversion script writes the OpenDSS model including all the elements in a format readable by OpenDSS.

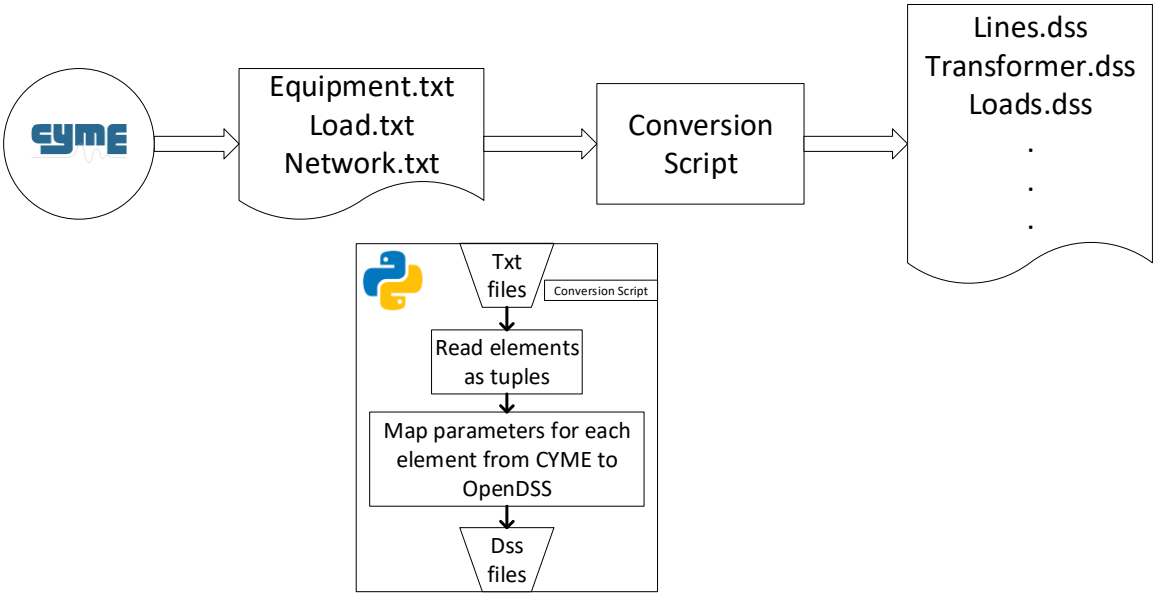

Figure 2.3 Flowchart for the CYME to OpenDSS Conversion Tool

The values of active and reactive powers of the loads corresponding to a snapshot were available in the CYME database, however, the values of solar PV unit generation were not available in the database. They were obtained based on the AMI meter measurements. The AMI meter measurements of active powers were provided for billing meters and production meters. Out of these, the production meters record the active power output of the solar PV units. Each meter is associated with a customer number and a premise number. Using the customer numbers, the meters were mapped against the loads available from the CYME database which also contains the information about the customer number each load is associated with. Hence, the active power values for the

solar PV units for the network model for were used from the available meter measurements corresponding to the same timestamp as the CYME database. Note that all solar PV units installed operate in a 'unity power factor' mode, hence, the reactive power exchanged by the solar PV units with the network is always zero.

For loads with available meter measurements (not all loads had a corresponding meter measurement of active power available), the load active power was updated based on the meter measurement. At a house/premise, there are two types of meters installed: billing meters and production meters. Production meters measure the output from the solar PV units (in terms of kWh per each 15 minutes or hour) installed at that house, while the billing meters are bidirectional, measuring the net energy provided to the house ("delivered") and the net reverse energy flow from the house to the grid ("received") in each 15 minutes or hour. This structure can be explained via Figure 2.4. From the figure, it is clear that the gross load at the house must be estimated by combining the different meter readings. The net and gross load for each house can be calculated as follows:

$$Net\ load\ = Billing_{Delivered} - Billing_{Received} \tag{2.1}$$

$$Gross\ load\ = Net\ load + \ Production \tag{2.2}$$

The reactive parts of the loads were retained from the CYME database, since the meter measurements did not contain any reactive power measurements.

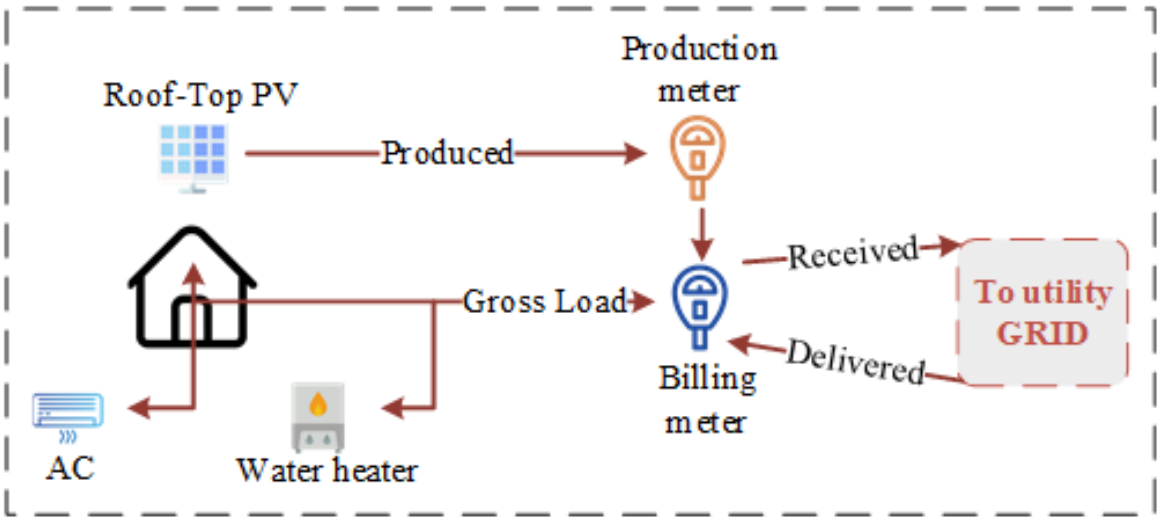

Figure 2.4 Metering Infrastructure at a Typical House for the Modeled Feeder

A GIS model was created for the circuit based on the GIS data acquired from the utility using QGIS [23] software. Further, to validate the circuit, aerial imagery obtained from Google Maps was added to the QGIS project. It can be seen from Figure 2.5 that the secondary locations of loads and PV units correspond to the individual houses.

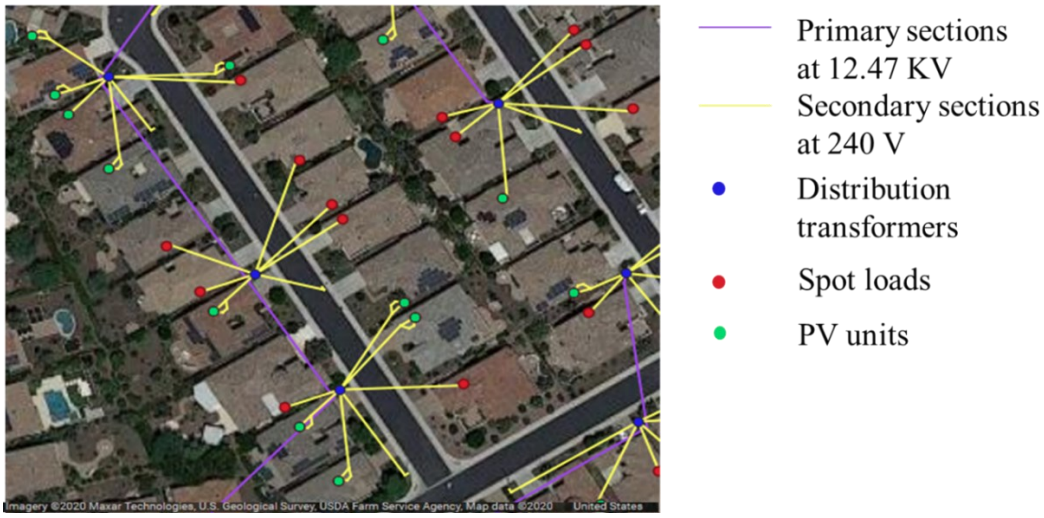

Figure 2.5 GIS Model of the Feeder

The load values from CYME were retained for the houses without any measurements, identified using the GIS representation of the network. Further, it was found that two of the distribution transformers in the CYME database fed a large number of loads. Using the customer numbers to find the associated meters for those loads and then using the GIS data/addresses associated with the meters, these loads were moved to appropriate locations within the feeder. Remaining excess loads at these transformers were moved to houses with no apparent load in the electrical model, as identified using the GIS representation.

2.4 Creating the Time Series Model

In addition to creating a detailed network model, time series profiles are also created using the feeder-head and AMI measurement data available for the feeder. Since a large number of the meters provide hourly measurements, hourly time series profiles are created for the active and reactive loads, solar PV units and the source voltage for the two selected days.

The active power profiles for the loads with meters are formed by calculating the gross load using (2.1) and (2.2) for all hours. Multipliers for active power are then obtained by comparing these gross load values to the active power set in the load definition. For solar PV units, the active power profiles are created similarly, using the production meter values for all hours and comparing them with the active power value used in the element definition. For loads without meter measurements, profiles based on the active power calculation for the distribution transformer they are connected to are used: these are created by adding the active powers from all the loads connected to that transformer which do have meter measurements.

For reactive power profile, since no measurements were available along the feeder except at the feeder-head, the following formula was used to estimate the combined reactive power from all the loads:

$$Q_{feederhead} = Q_{load} + Q_{loss} + Q_{capacitor} \quad (2.3)$$

To calculate the reactive load using this equation, a time series power flow is run with an initial estimate of the reactive load assuming a power factor of 0.9. By measuring the reactive losses and since the reactive power from the capacitors are known, a better estimate of the reactive loads is obtained and used to create the reactive power profile for the loads. This process is repeated iteratively, using the reactive power profile obtained in the previous iteration to obtain a new estimate till it converges.

For the voltage profile for the voltage source at the head of the feeder, a profile based on the phase A voltage measurements at the feeder-head is created. Note that a balanced source behind the source impedance obtained from the CYME database is used for the OpenDSS source model. This impedance corresponds to the Thevénin equivalent impedance obtained at the feeder-head to represent the rest of the utility network. Note that because of the presence of this impedance, due to the different phases having different magnitudes of currents/powers, the voltage in the OpenDSS model at the feeder-head is not necessarily balanced between the three phases.

2.5 Validation Against Field Measurements

The feeder time series model created using the procedure described in the previous two sections is validated against two sets of field measurements:

- The values of total active and reactive power at the feeder-head are compared against the feeder-head measurements available
- For the AMI meters installed on the feeder from which there are voltage magnitude measurements available, the voltages at corresponding buses from the OpenDSS model are compared with the meter measurements.

A good match between the measured values and the values obtained from the OpenDSS feeder highlight the accuracy of the model. For the selected summer day (15 July 2019) the feeder-head active and reactive powers have root mean square (RMS) errors over a day (24 measurements) of approx. 1.56% and 0.02%, respectively. Note that since the reactive power profile is created using the reactive power feeder-head, the error for it is expected to be quite low. Figure 2.6 shows the feeder-head active and reactive power from the OpenDSS model for July 15 compared with the field measurements. The voltage measurements from the AMI meters also match the voltages obtained from the OpenDSS model well – for all the meters the RMS error is below 5%, as shown in Figure 2.7 for the summer day. Three of these meters are selected (their locations shown in Figure 2.8), and the measured and OpenDSS voltages for these meters for the summer day are plotted in Figure 2.9. For the spring day, similar values of RMS errors are obtained, indicating that the created circuit model accurately represents both summer and spring conditions. In another publication, efforts have been made to improve this feeder model further using optimization to match the voltages from the meter measurements better by allowing different reactive load profiles and unbalanced voltage source model [24].

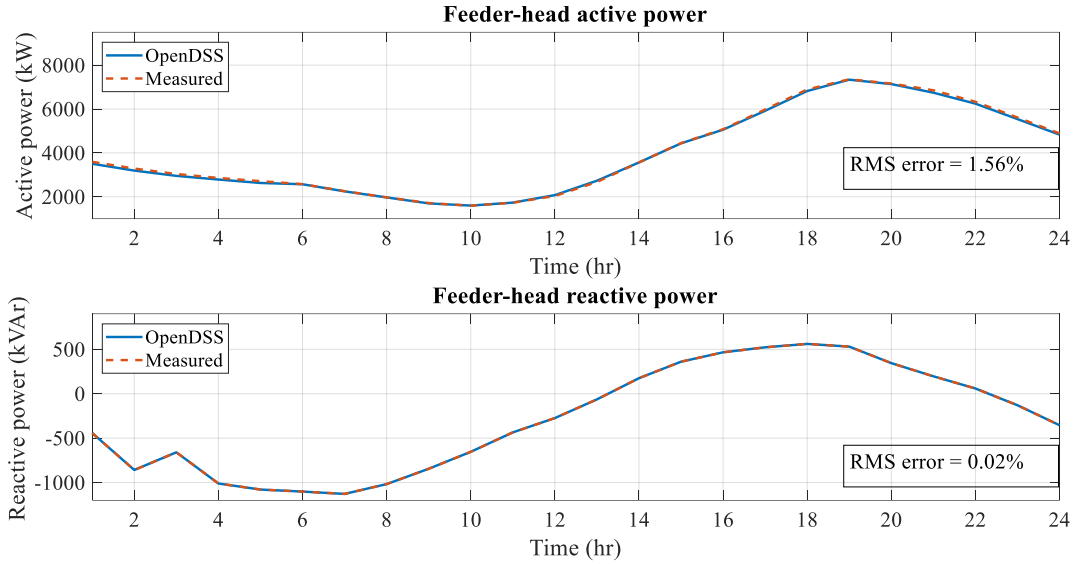

Figure 2.6 The Comparison Between the Feeder-head Active and Reactive Power from the OpenDSS Model and Measurements

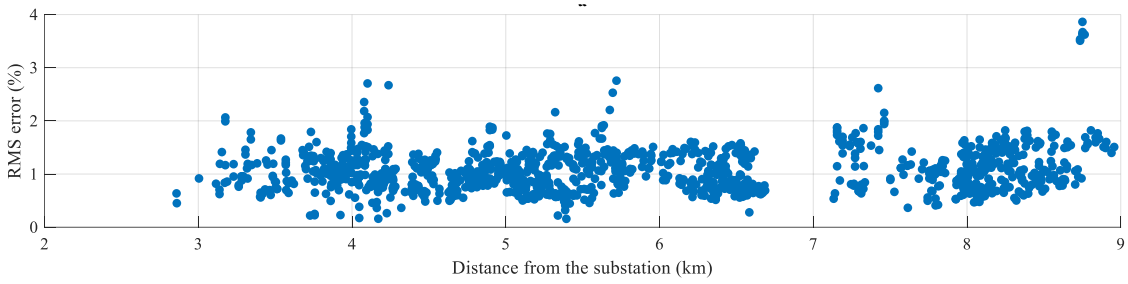

Figure 2.7 RMS Errors for All Voltage Meter Locations Between the OpenDSS Model and the Measured Values

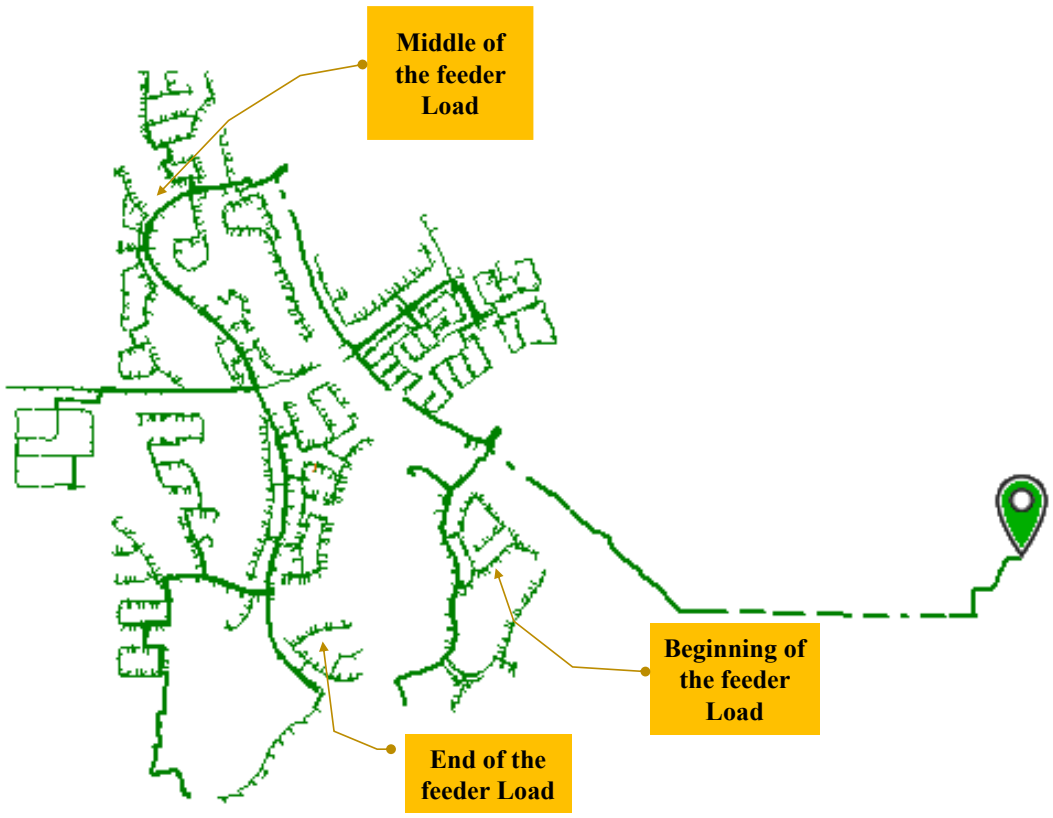

Figure 2.8 Locations of the Meters Selected for Comparing the Voltage Profiles

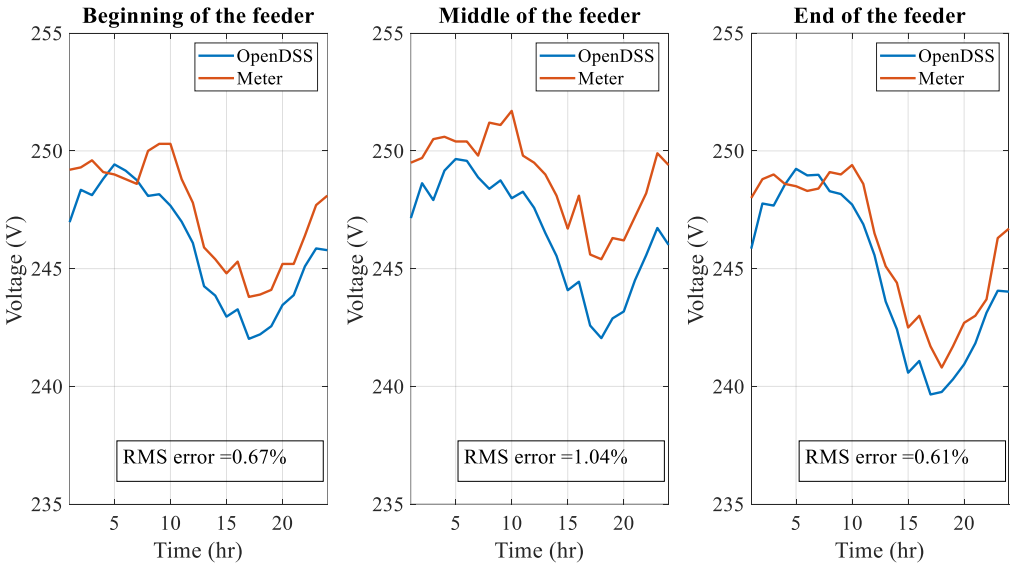

Figure 2.9 Voltage Comparison for the Three Selected Locations Between the OpenDSS Model and Measured Values for the Summer Day

2.6 The Importance of Modeling the Feeder in Detail

The previous sections in this chapter so far have described the procedure used to create a detailed and accurate model for the selected feeder and the validation of the model against field measurements. This section highlights the importance of creating such a detailed model.

Two days, one in summer and one in spring, were selected for creating the feeder model. These two days represent very different conditions. The summer day is characterized by a very high load and a moderately high solar PV generation, whereas the spring day sees a very high solar PV generation and low load leading to high reverse active power flow for certain hours. The gross load, solar PV production and net load for the feeder for these two days is shown in Figure 2.10. The voltage profiles for two snapshots are shown in Figure 2.11 – these snapshots correspond to summer evening (6 PM on 15 July 2019) and spring early afternoon (12 PM on 15 March 2019). For the summer snapshot, since the load is very high, the voltages decrease as we travel along the feeder. However, for the spring snapshot, the trend is opposite: because of the reverse active power flow due to high solar PV generation, the voltages along the feeder increase with the distance, and in fact, there are a lot of voltage violations seen for this snapshot because of the high solar PV penetration level where the voltages go above 1.05 p.u.

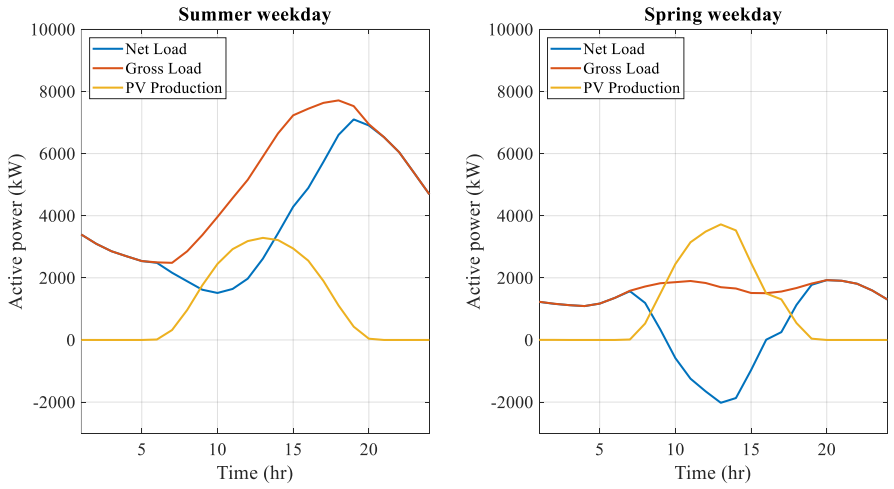

Figure 2.10 The Gross Load, Net Load and the PV Generation for Summer and Spring Weekday Modeled

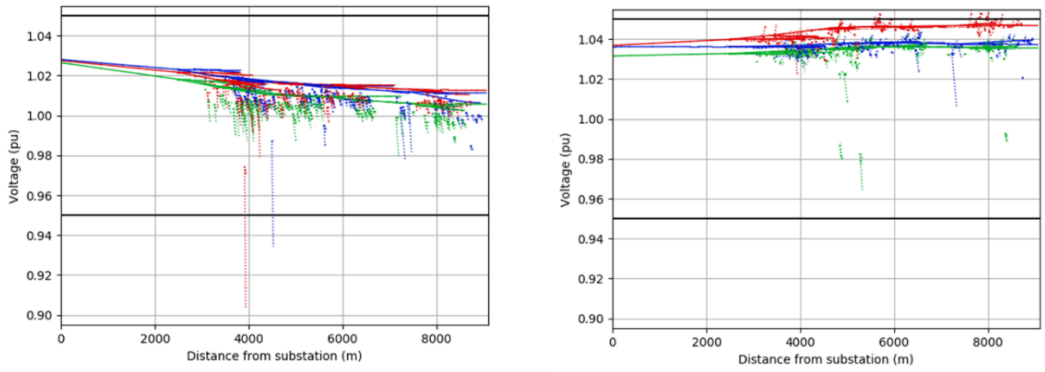

Figure 2.11 The Voltage Profile for the Selected Feeder for Summer Evening (15 July 2019 at 6 PM, Left) and Spring Early Afternoon (15 May 2019 at 12 PM, Right)

Another important feature of the created model is that the secondary network is modeled in detail. Modeling the secondary network becomes especially important for a feeder with a high penetration level of solar PV resources. For the spring day, Figure 2.12 shows the voltages from the OpenDSS time series power flow solution recorded at a distribution transformer as well as at the houses served by this transformer. It is seen that there is a significant voltage difference between the voltage recorded without modeling the

secondary network (which would be approximately the voltage at the transformer) and the voltage recorded with the detailed model and that different houses connected to the same distribution transformer can have different voltages. Another feature highlighting the importance of modeling the network in detail is that without modeling the secondary, the voltage violation seen in Figure 2.12 would be missed. Hence, it can be concluded that a detailed model is able to capture the network conditions more accurately. The next chapter explores the feeder model described in this chapter further using dynamic simulations.

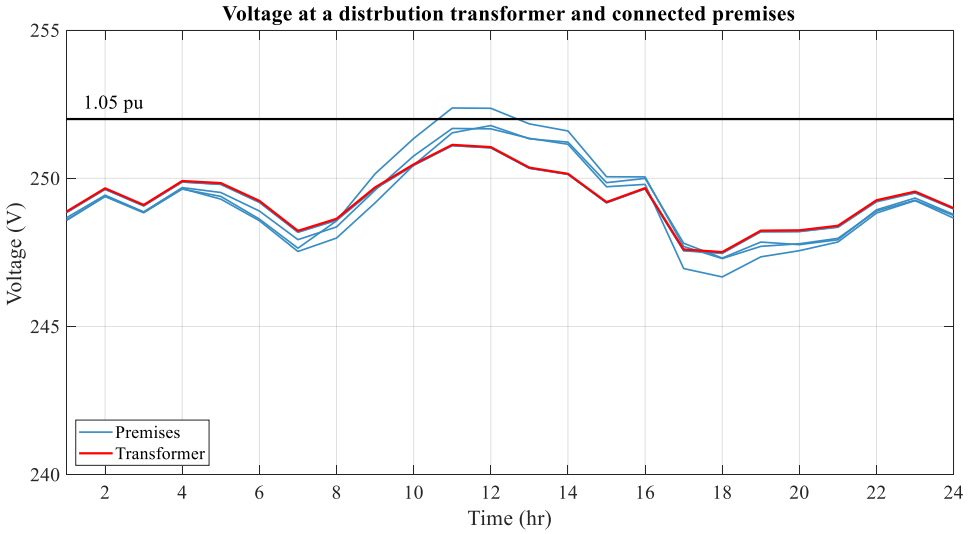

Figure 2.12 Distribution Transformer Voltage (Red) and the Premise Voltages (Blue) for the Premises Connected to the Transformer for the Spring Day

2.7 Creating High Penetration Scenarios

For some of the case studies presented in this dissertation, an analysis is performed for the distribution feeder with a higher penetration of solar PV resources. For the modeled feeder the penetration level of solar PV is approximately 237%, calculated by comparing

the hourly active load and solar PV generation for the maximum reverse active power flow (15 March 2019 at 1 PM) scenario. While this has a high solar PV penetration, several cases of higher solar PV penetration up to 800% are constructed for this feeder by adding additional solar PV units at various randomly selected customer locations. The procedure developed by the National Renewable Energy Laboratory during their LA100 study is used to create these high penetration cases [25]. At the highest penetration level case (801%), there would be almost 13 MW of solar PV generation assumed to be installed in the feeder, as opposed to the present value of approximately 3.8 MW at the present 237% penetration.

3 DYNAMIC CO-SIMULATION ANALYTICAL FORMULATION

The previous chapter has described the procedure followed for modeling a real feeder in detail. The modeled feeder has a high penetration of solar PV resources, and the response of the feeder for such faults can affect the sub-transmission system as well. Further, accurately representing the behavior of such a feeder for faults on the sub-transmission system is also important. Hence, to explore the impacts of various faults (applied both on the distribution as well as sub-transmission network) on this feeder further, a co-simulation approach is adopted in this project.

This chapter begins by presenting the literature review of various approaches for conducting T&D co-simulation as well as the applications of T&D co-simulation in Section 3.1. The formulation used for the co-simulation in this project both for power flow (Section 3.2) as well as dynamic co-simulation (Section 3.4) is described. The T&D co-simulation power flow code is further developed as a module that can be run on cloud platforms – the process of creating this module is described in Section 3.3. When performing dynamic T&D co-simulations, one of the key dynamic models considered is the dynamic model of the solar PV DER, especially for a distribution system with a high penetration of such solar PV units. A custom user model is created to represent the solar PV unit in the distribution system software, both for power flow as well as dynamic simulation, allowing the modeling of advanced inverter control. This user model is described and validated against a detailed model in Section 3.5. The model for the grid-forming inverter implemented is presented in Section 3.6 and a model of the single phase induction machine suitable for implementation with the rest of the network is presented in Section 3.7. Some portion of this chapter is published as a part of [26].

3.1 Transmission-distribution (T&D) Co-simulation

Historically, distribution and transmission systems have been analyzed independently, with different requirements, paradigms and software packages. In this framework, distribution systems are represented as loads in the transmission system model, and transmission/sub-transmission systems are represented as voltage source(s) in the distribution system models. However, representing both the systems adequately becomes important especially for studying phenomena impacting both the systems. Due to the increased penetration of distribution-connected DERs and smart devices, there has been an increased need for studies involving both distribution and sub-transmission/transmission systems.

There have been several studies in recent years highlighting the need of studying distribution and transmission/sub-transmission systems together. The authors of [27] describe a large scale synthetic T&D co-simulation power flow. They compare the time series power flow voltages for the distribution feeders against modeling the same distribution feeders with a constant voltage source instead of interacting with the transmission-level network. The comparison shows that representing the transmission system rather than using a constant voltage source is a more accurate representation of the circuit. The authors of [28] also show that a coordinated power flow between the transmission and distribution systems is more accurate than solving the transmission and distribution systems independently. This added discrepancy for the power flow performed independently for the distribution and transmission systems rather than via a co-simulation further impacts factors such as voltage profiles and voltage regulator operations [29] and prices for price responsive loads [30]. The load dependent losses and

reactive power from DERs are shown to be different with a detailed feeder model compared to representing distribution feeders as loads [31].Some of the reasons and motivation behind studying integrated T&D analysis or T&D co-simulation are delineated in [32]. Not just for power flow, but the impacts of the transmission/sub-transmission and distribution systems on each other are also important in dynamic simulations. The authors of [33] note that the feeder response to transmission voltage sags is dependent on factors such as feeder loading, solar PV generation and sag severity. The authors of [34] conduct a fault-induced delayed voltage recovery (FIDVR) study where they couple the transmission and distribution simulations, and find out that the response from distribution systems and especially the behavior of DERs during the fault impacts the bulk system. Another study [35] uses combined T&D simulations to form dynamic equivalents of distribution networks. The authors report that the combined T&D models are critical to accurately capture low voltage trips of distribution connected inverter-based generation to form an appropriate aggregate model. The authors of [36] show that with explicit models of high, medium and low voltage circuits, coordinating proper response from DERs to support high voltage grid is possible. Hence, there is clearly a need for studying integrated T&D systems.

One approach suggested is to model the entire network including T&D circuits in a single framework or platform. There are different approaches suggested for this: one approach uses equivalent circuit based methods and network tearing to represent the network coupling in a single framework [37]. A three-phase unified model of the T&D network for voltage stability is proposed in [38]. Another three-phase model for dynamic studies is proposed in [39]. Domain-decomposition and Schur complement approach coupled

with parallel processing is applied to combined T+D simulation and is shown accurate and fast for a large network [40]–[42]. Combined modeling of a very large grid (100,000 vertices and edges, 10,000 IBRs) using graph computing is presented in [43]. Another study [44] comparing a unified approach to decoupled power flow solution, and finds that the power flow solutions obtained from both the methods are similar, while [45] suggests that integrated modeling may be faster and more accurate, taking advantage of parallelizing the solution process for a the network described in a single suitable framework, especially when topology changes are considered. On the other hand, a comparison of unified Newton-Raphson power flow approach compared with a sequential solution approach from [46] finds the sequential approach to be robust while the unified approach to require a good initial guess for convergence. There are several studies modeling integrated T&D systems in commercial tools: a study [47] compares a co-simulation to a combined model of T&D circuit in DigSILENT, some other studies show that T&D circuits can be modeled in ePHASORsim/OPAL-RT for both power flow and dynamic simulation [48], [49]. However, a large number of available tools for transmission and distribution systems do not support integrated modeling of both systems, hence, co-simulation is seen as a viable option which allows to use existing established software while connecting the different systems.

There are some tools developed specifically for co-simulation of power systems which control and coordinate between the distribution and transmission systems such as IC-GAMA framework interfacing Matpower and GAMS software package [50]; or a Matpower-OpenDSS co-simulation[51]; or a framework to coordinate three-phase/three-sequence power flow via Matlab [52], and another framework CoTDS which has been

shown useful for power flow, dynamic simulations as well as eigenvalue analysis [53]. A client-server type co-simulation between Matpower and Gridlab-D is proposed in [54]. A cyber-physical events emulation based platform connecting ANDES and OpenDSS with additional features added is described in [55]. The challenges of creating a T&D co-simulation tool are presented in [56] using the T&D co-simulation tool developed by them, TDcoSim, as an illustrative example. Some of the challenges mentioned include (1) passing messages between different software packages, (2) time synchronization, (3) ease of usage and onboarding, (4) capability to scale to a large system. The importance of model coordination in a T&D co-simulation of a large network is illustrated in [57]. Commercial options such as PSSE-PSCAD co-simulation module can also be used in particular cases [58].There are several general frameworks which have been developed over the recent years (and are in active development) for enabling co-simulation, such as bus.py (which is one of the earlier frameworks) [59], Integrated Grid Modeling System (IGMS) [60], functional mockup interface (FMI) based tools such as Cyder [61], and Framework for Network Co-Simulation (FNCS) [62], [63]. These are general purpose tools developed for co-simulation. Some of these tools are compared in [64]. Overcoming the drawbacks of some of these tools, a new tool for co-simulation, HELICS is described in the same study. A study reports using HELICS tool to implement a co-simulation using a commercial distribution system solver (CYME) running on a high performance computing (HPC) node [65]. Another paper uses HELICS to achieve a multi-timescale T&D co-simulation including power flow and dynamic simulation [66]. A review report from EPRI compares several available tools for co-simulation [67].

Another important aspect of co-simulation frameworks is the actual models for various systems which are used and the models for the interfaces between them, as well as how the co-simulation process coordinates the data and solution process between the different software. For example, a transmission system modeled in positive sequence-only fashion cannot model any unbalance at the boundary bus, and hence the unbalanced data from distribution system must be balanced before supplying to a positive sequence software. Transmission systems can be modeled in positive sequence-only fashion or can use a three-sequence model, whereas distribution systems are usually modeled in three-phase unbalanced domain.

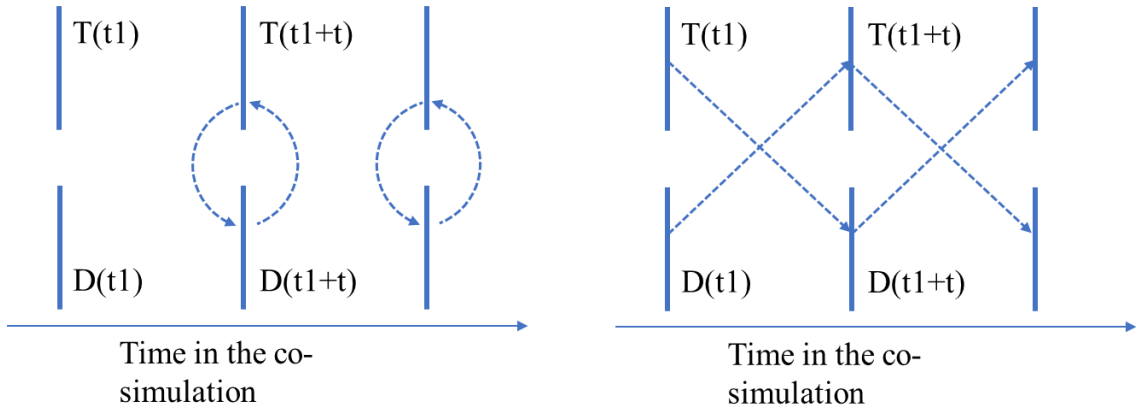

Figure 3.1 Iterative (Left) and Loosely-coupled Co-simulation Power Flow Schemes

Further, the power flow simulations can be performed iteratively or in a loosely-coupled manner and dynamic simulations can be performed in different systems using a parallel or series solution scheme in each time step. Here, for power flow (especially time series analysis), a system following a loosely-coupled scheme would use the inputs from other systems initially but is allowed to converge separately, only exchanging information with

other systems at the beginning of the next power flow solution, whereas in an iterative scheme all the systems must converge and the boundary values also must converge before moving to the next solution, as shown in Figure 3.1. A study comparing the tightly-coupled (iterative) and loosely-coupled power flow co-simulations concluded that tightly-couple solutions are more accurate but more time consuming, and that the loosely-coupled scheme has higher errors compared to the iterative scheme especially for stressed grid conditions such as high unbalance or high penetration of solar PV resources leading to higher variability of the load and generation [68]. Another study comparing the two schemes also finds that the iterative solution scheme better approximates the system conditions, and that a three-sequence transmission model has better accuracy than positive sequence-only transmission model [69]. However, [70] shows that if the three sequences are not coupled in the transmission software, that can lead to an error for transmission systems coupled through distribution systems, because the distribution system software packages do not neglect the coupling between the different sequences. This study also shows that such error due to the sequence coupling not being modeled are more prominent where wye-wye transformers are used compared to the systems using wye-delta transformers.

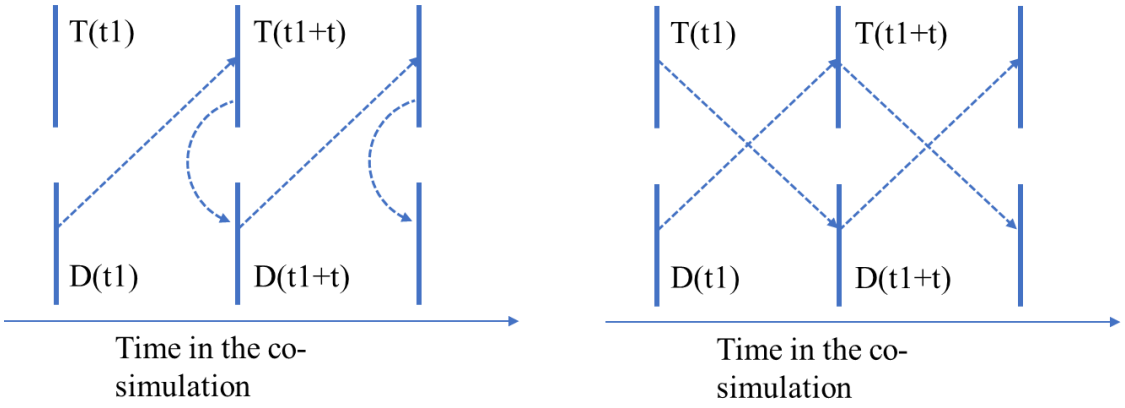

Figure 3.2 Series (Left) and Parallel (Right) Solution Schemes for Dynamic Co-simulation

For dynamic co-simulation, a parallel scheme uses inputs from other systems from previous time-step, whereas for a series solution scheme some of the inputs may be from the current time-step: this is illustrated in Figure 3.2. Another study [71] compares different interface techniques for dynamic co-simulation and shows that a three-sequence model of transmission systems is more accurate even for dynamic simulations, and that iterative/series schemes are more accurate. They also note that representing transmission system as a Thevénin equivalent is more accurate in capturing its impact on distribution systems, and that selecting adequate simulators for both the systems is important considering the accuracy of the co-simulation. For series solution scheme, the authors of [72] show that the sequence of simulation (transmission/sub-transmission followed by distribution versus the opposite) matters and can result in extra overshoot and delay in the response when there are large disturbances such as faults, but only for a few time steps – this might be an issue if a larger time step is used in the co-simulation. A comparison of the iterative versus non-iterative solutions in dynamic co-simulation is made in [73], and

it is found that while the iterative schemes have better stability and convergence, non-iterative schemes also exhibit good convergence and stability characteristics as long as the step size is small enough. A further comparison between different co-simulation frameworks and coupling/solution processes can be found in some recent review papers [74], [75].

Several studies highlight different impacts which can be observed through power flow/dynamic co-simulations. The authors of [76] find that the solar PV resources on the distribution system above a 50% penetration level cause the transmission voltages to drop because of the slack bus absorbing active power rather than injecting active power into the network using iterative three-phase/three-sequence co-simulation power flow. Another study examines the impact of the DER volt-VAr control mode on the bulk power system [54]. The voltage stability using a T&D co-simulation is found to be different than considering just the transmission model in [38], [77]. An optimal control to mitigate the delayed voltage recovery for distribution feeders is tested using a T&D co-simulation in [78]. The authors of [79] model a real network from Arkansas and conduct T&D powerflow and dynamic simulations using MATLAB and OpenDSS. It is shown that intermittency in the DER output can result in an increase in the number of LTC operations and result in increased flicker. It is also shown that DER fault ride-through can help with voltage recovery after short circuit faults at the expense of voltage overshoots. Comparing lumped and distributed motor models, distributed models show a higher current from DERs and higher voltage rise after fault is cleared in the presence of DER_A control units. Dynamic co-simulation is also used as a tool to characterize load parameters for representing the distribution system in transmission-level large studies

either as a static load [80] or composite load [81]. Via a T&D co-simulation, it is noted in [82] that at higher penetration the load and DER interactions on the distribution system may be important to represent in transmission planning studies and partial trip and rate-of-change-of-frequency based protection might be needed for aggregate distribution/DER models. Using DER primary and secondary frequency response to stabilize bulk system frequency under load change and generator outage contingencies using T&D co-simulation is considered in [83]. The frequency response provided by grid-following and grid-forming distribution connected inverter-based devices is studied with a co-simulation environment in [57], [84]. The impact of electric vehicles on the transmission systems is examined in [85] using T&D co-simulation. Another study [86] considers the frequency response/support using electric vehicle grid-to-vehicle mode using T&D co-simulation.

Hence, T&D co-simulation has been employed in a variety of studies examining the impact of different phenomena on the T&D system. However, several research efforts use small systems or large synthetic systems and do not model real-world data. To accurately capture the dynamic response of the T&D system, the DERs are represented using detailed custom user model including the phase locked loop, current control and the advanced active and reactive power controls in addition to the accurate network model. The rest of this chapter describes the T&D co-simulation framework and the dynamic models used in this dissertation.

3.2 T&D Co-simulation Power Flow

The developed co-simulation framework consists of the distribution system model, the sub-transmission system model, and the coordination between the two system models. In a T&D co-simulation, the distribution and sub-transmission systems are solved using separate tools and can use different modeling assumptions and domains, allowing the use of existing software for this purpose. However, these solutions are coordinated so that the values at the boundary (where the distribution and sub-transmission systems interface with each other) are consistent in both systems. For this project, the distribution system is modeled using OpenDSS and the sub-transmission system interfacing this distribution system is modeled in InterPSS [87]. The exchange of the information and timing coordination between these two systems/software packages is achieved using the HELICS framework. All three selected software packages (OpenDSS, InterPSS and HELICS) are open source.

The distribution system is modeled in three-phase unbalanced detail using OpenDSS. This approach allows modeling the distribution feeders in detail. The rooftop solar PV units installed on the feeder are represented by the created user model for OpenDSS. Using a custom model for the solar PV units enables a detailed representation of the solar PV units in the co-simulation.

For modeling the sub-transmission system, InterPSS is selected as the software of choice. Many popular software packages for transmission system analysis use only the positive sequence model. InterPSS supports a three-sequence model of the transmission system for performing power flow solution as well as dynamic simulation. The positive sequence

power flow in InterPSS is solved using the Newton-Raphson method, whereas a linear model is solved for the negative and zero sequence power flows.

In a T&D co-simulation, whether it be power flow or dynamic simulation, correct coordination of timing/data between the different sub-systems is vital. This is performed using HELICS, which is an open-source software specifically aimed at easing co-simulations. HELICS has an application programming interface (API) support for various programming languages, so the exact timing and data coordination can be controlled. In the present work, OpenDSS is controlled using its Python API, and InterPSS is controlled using its Java API.

During the power flow, the distribution system is represented as a constant power load in the positive sequence and as constant current injections in zero and negative sequences. In the distribution system model, the transmission system is represented by an unbalanced three-phase voltage source. This choice of the representation for the distribution/transmission system is made so as to accurately represent the unbalance at the distribution-sub-transmission boundary. Another reason for this representation is that it supports modeling symmetrical/unsymmetrical disturbances on both the transmission and distribution systems. The latter factor is not relevant when just the power flow is considered, but this project deals with co-simulation power flow as well as dynamic simulation, hence it is an important concern. Since the distribution system is modeled in three-phase fashion and the transmission system is modeled in three-sequence fashion, the conversion between the two representations is made before exchanging the data between the two systems.

Figure 3.3 shows a schematic of the models used in this co-simulation framework. As shown in this figure, the co-simulation is run using three scripts. Script 1 in Java calls the InterPSS routines and interacts with HELICS to send the boundary voltages in three-sequence details to two distribution systems (called by Script 2 and Script 3) and receive the three-sequence currents from these systems. Note, even though the figure shows one sub-transmission system and two distribution systems, the process described here will be the same for any number of systems/scripts. Script 2 and Script 3 in Python call OpenDSS routines to model the two distribution systems in addition to interacting with HELICS. Script 2 and Script 3 receive the three-sequence boundary voltages from script 1 via HELICS and send back the three-sequence boundary currents. These two scripts also perform the three-phase/three-sequence conversion since the distribution systems are modeled in three-phase domain in OpenDSS.

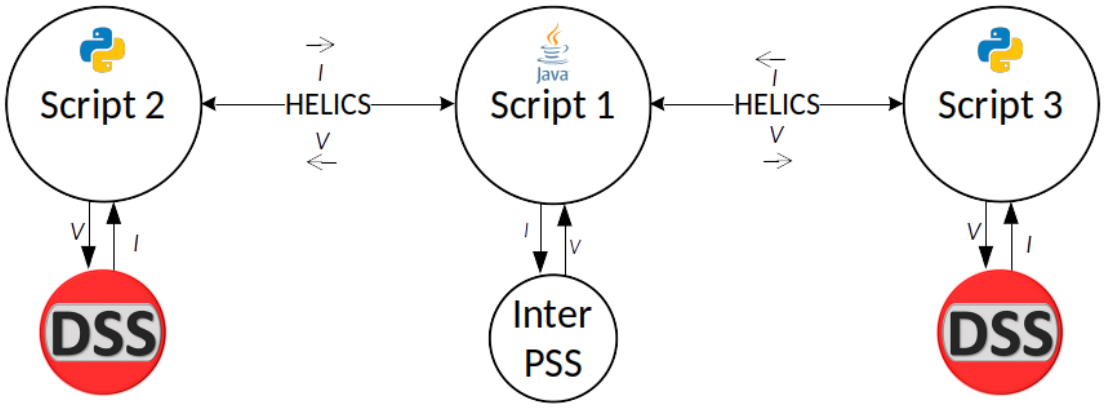

Figure 3.3 Schematic of the Co-simulation Showing the Software Packages and Data Flow

The process of co-simulation can be divided into three stages: initialization, execution, and finalization. The initialization involves setting up the distribution and sub-transmission circuits as well as the required HELICS components. The actual co-simulation takes part in the execution stage and the finalization stage involves finalizing the data and closing the HELICS components. Apart from taking care of the data transfer between the two systems, HELICS also takes care of the synchronization and makes sure that both systems enter the next stage at the same time.

For coordinating between different software packages, as a part of initializing HELICS, a "broker" must be created. This broker connects to different subsystems/software called "federates" in HELICS. Only one broker needs to be created, however, a different federate must be created for each different system in the co-simulation. Then, for defining the interface between different software or systems, HELICS uses "publications" (which "publish" or send the value) and "subscriptions" (which "subscribe to" or receive the value). In the codes calling different subsystems, appropriate publications and subscriptions must be defined according to the data being exchanged by that subsystem with other subsystems via HELICS.

HELICS uses special functions/commands to go into a particular mode. At the start, each federate or subsystem is in the "initialization" mode. A special command must be run in each federate for that federate to go into "execution" mode. Any actions performed before the execution mode are independent i.e. the different federates do not exchange data. The co-simulation does not begin for any subsystem until all the registered subsystems or federates go into execution mode. Once all federates or subsystems go into

execution mode, they can exchange values with each other according to how they are set up and begin the co-simulation. Similarly, to end the co-simulation, all federates must "finalize" to exit the execution mode.

The process followed by each federate or subsystem during co-simulation power flow is displayed in Figure 3.4. Here, an important aspect is choosing the convergence criteria for the co-simulation power flow. In addition to the requirement that power flow from each individual system should converge, the boundary values must be consistent across the different systems. Since in each iteration the boundary values from one system ("system 1") are sent to the other systems ("system 2", …, "system n") and used in those systems to represent system 1, as long as the values in each subsystem converge with respect to the iterations, they will also be consistent across the different systems. Hence, the chosen convergence criteria checks for the convergence of the shared boundary currents and voltages.

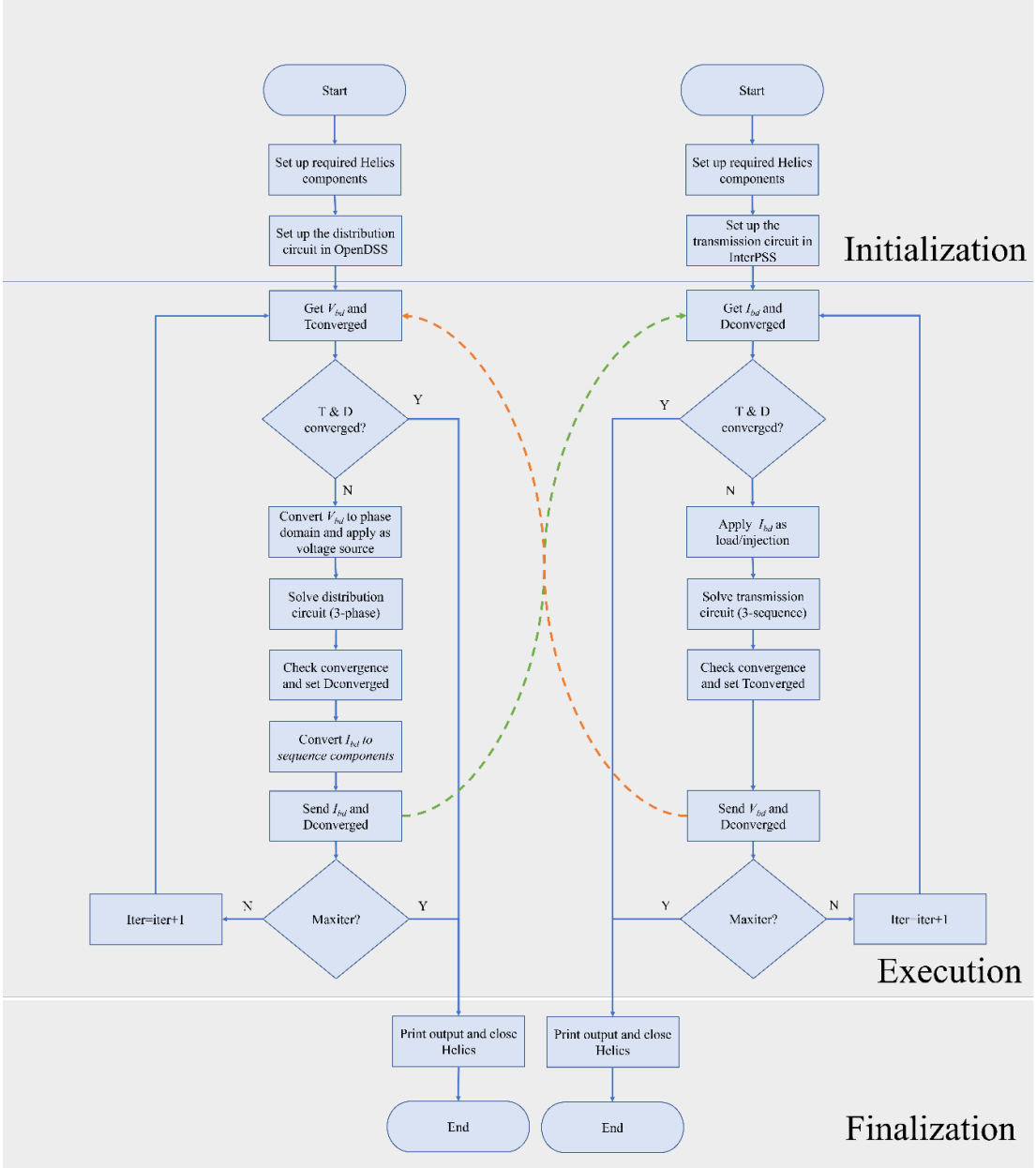

Figure 3.4 Flow Chart Representing the Operations in T&D Co-simulation Power Flow

The procedure of running a T&D co-simulation power flow is extended to create a T&D co-simulation time series power flow solution framework. In this framework, the sub-transmission sources as well as the distribution loads and solar PV units have time series

profiles associated with them. For each time step, the corresponding values for the sub-transmission sources as well as loads and solar PV generation are used to create a snapshot that represents the particular time step, and a power flow is performed. Once the T&D co-simulation power flow converges successfully for that time step, the results are stored and the next time step is considered. This process is repeated for all time steps. During each time step, the T&D co-simulation power flow iterates till the solutions from the different subsystems converge and the values across the boundary between the subsystems match for that time step. This process of T&D co-simulation time series power flow is described as a flowchart in Figure 3.5. Using this T&D co-simulation time series framework, a large number of power flow scenarios corresponding to different time instances over a day or over a year can be simulated together, instead of having to separately set the software packages and corresponding network snapshot cases manually for each time step.

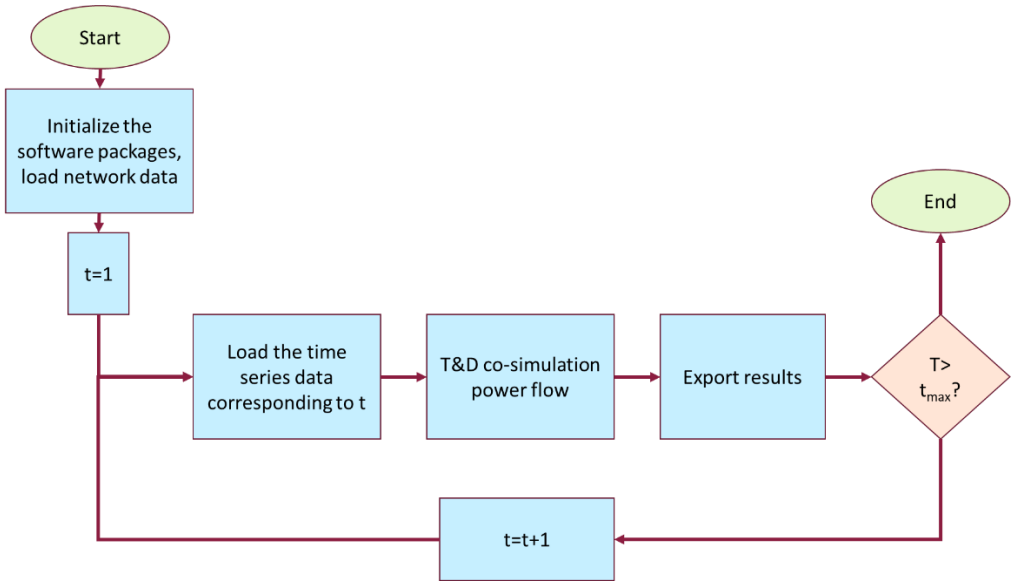

Figure 3.5 The Flow Chart Describing the T&D Time Series Power Flow Co-simulation Process

3.3 T&D Co-simulation Power Flow Module

It is shown in this chapter that a T&D co-simulation power flow can represent the state of a T&D network accurately. This accurate state of the network can in turn inform various other power system operational functions such as advanced coordinated DER control, substation transformer on load tap changer or voltage regulator control, feeder capacitor control, and other related features. These functions may be used to achieve different objectives such as eliminating or reducing the overloads or over/under voltages or reducing the losses in the network. To use the T&D co-simulation power flow for this purpose, the process to set up and run the T&D co-simulation power flow and exporting the results is automated to create a T&D co-simulation power flow module.

The functions served by the T&D module are shown in Figure 3.6. The inputs to the module include the load and solar PV generation for the modeled distribution feeders and the sub-transmission source powers and voltages for the particular time instance the user wants to run the module for. Using these data as input, the module has scripts to edit the circuit data for both OpenDSS and InterPSS automatically, resulting in a snapshot T&D model corresponding to the snapshot; running the T&D co-simulation power flow; and exporting various reports such as the voltages for all the buses, or the powers flowing through different elements in the network. These initial reports are then further analyzed to export lists of buses with voltage violations, sections and transformers operating close to the overload rating, and sections and transformers with reverse active power flow.

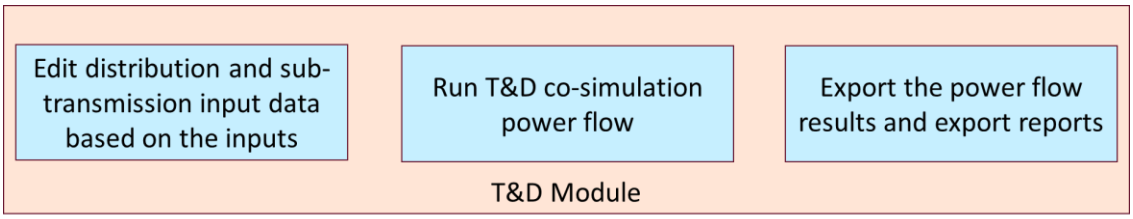

Figure 3.6 The Various Functions Implemented in the T&D Co-simulation Power Flow Module

The T&D module is designed to run on a Linux-based server environment. The software packages used for the T&D co-simulation, OpenDSS (via the Python package DSS-Python), InterPSS, and HELICS are all open-source, and can be set up to run on a Linux-based system. Note that HELICS package must be compiled on the system with the relevant language bindings enabled to be able to connect with the Python (for OpenDSS) and Java (for InterPSS) interfaces. Also note that since InterPSS is called through a Java interface, the corresponding Java code must be compiled before this module can be run. The processes of editing the circuit data and analyzing the outputs from the T&D co-simulation power flow to create different reports are formalized as Python scripts. Finally, the entire workflow of setting up and running the T&D co-simulation power flow and analyzing the results to create reports is written as a bash script file that successively calls relevant scripts or bash commands.

Since this module is created to automatically set up and run the T&D co-simulation based on the input data, it may be used in conjunction with other data management systems of a utility to provide real-time data to the module and estimate the network states using the T&D module. The outputs generated by the script can then be used for displaying

information such as voltage violations or reverse active power flow, such as the interface shown in Figure 3.7, or for analysis modules such as DER coordinated control. This application is shown in Figure 3.8.

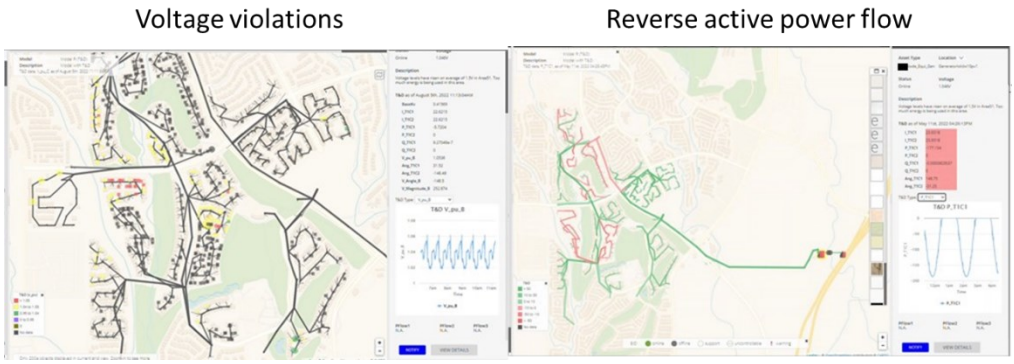

Figure 3.7 Example Outputs Obtained from the T&D Co-simulation Power Flow Module Displayed on the Circuit Plot

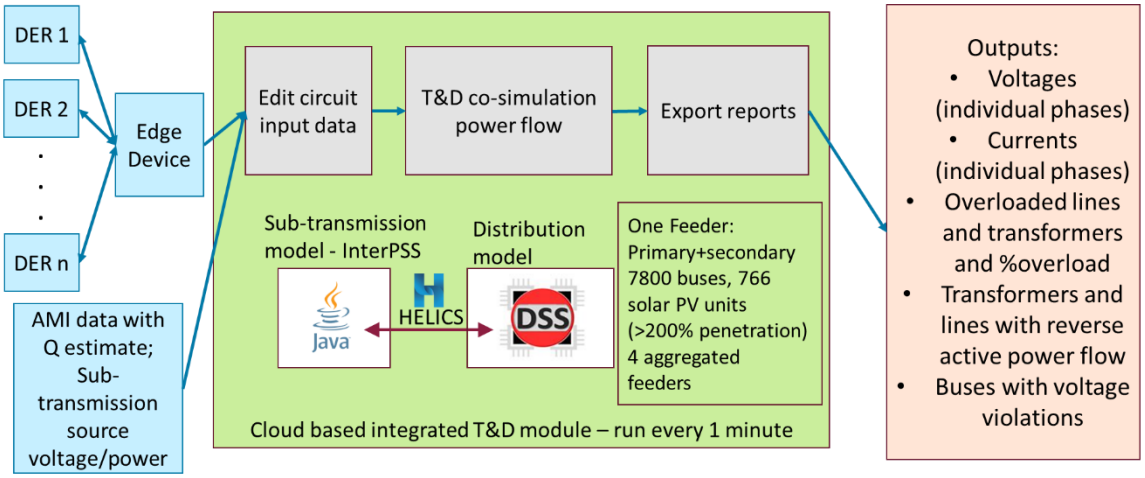

Figure 3.8 A Schematic Showing the T&D Co-simulation Power Flow Module Inputs, Functions and Outputs

3.4 Dynamic T&D Co-simulation

During the dynamic co-simulation, the distribution systems are represented in the sub-transmission model as current injections for all three sequence components. In the distribution system model, the transmission system is represented by an unbalanced three-phase voltage source, same as its representation for the power flow co-simulation. The overall data flow between the software packages remains the same as in the case of the power flow, represented by Figure 3.3, where the boundary bus voltages from the sub-transmission system are sent to the distribution systems and the distribution systems in turn send the boundary currents to the sub-transmission system. The distribution systems also continue to perform the three-phase/three-sequence conversion.

At the start of the dynamic co-simulation, both the sub-transmission and distribution system data are loaded in respective software packages. Then, the power flow solution is performed iteratively by updating the values in one subsystem based on the solution of the other subsystem(s). The iterative solution procedure is performed till the power flows and the boundary currents and voltages converge. After solving the co-simulation power flow successfully, the dynamic models in both the systems are initialized. For each time step, the sub-transmission system is integrated, and the boundary voltage(s) are sent to the distribution system(s), which are then integrated, and the updated boundary currents are sent back to the sub-transmission system. This process is depicted in Figure 3.9. At certain time steps, pre-determined disturbances are applied to the relevant subsystem as a part of the dynamic co-simulation. The overall dynamic co-simulation process can be represented as a block diagram as given in Figure 3.10.

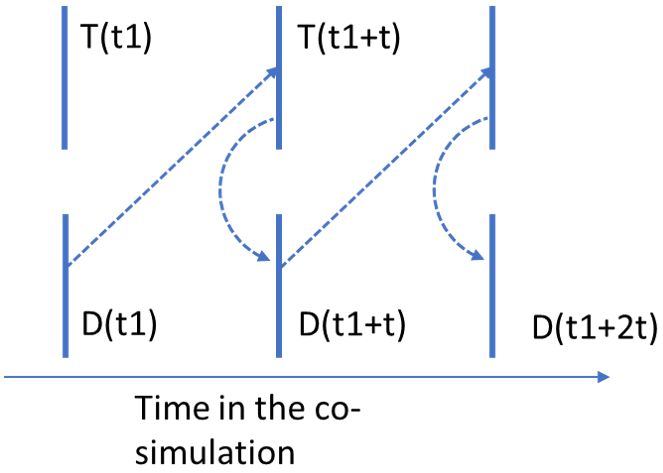

Figure 3.9 Timing Coordination in Dynamic Co-simulation

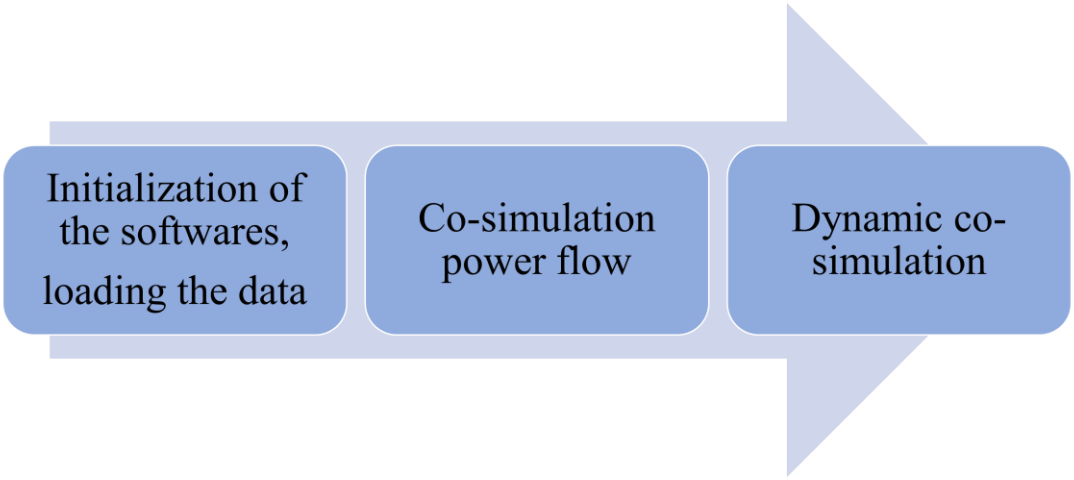

Figure 3.10 The Dynamic Co-simulation Process Block Diagram

In the next chapter, the framework for dynamic T&D co-simulation described here is utilized for various case studies involving dynamic T&D co-simulations involving various faults on the distribution as well as sub-transmission system. Both OpenDSS and InterPSS support applying different faults such as three-phase to ground (3ϕG) fault, single line to ground fault (SLG), double line to ground fault (LLG) and line to line fault

(LL). However, by default InterPSS only calculates the fault current in the positive sequence. Hence, the fault is represented in negative and zero sequence networks as current injections. For balanced 3ϕG fault, the fault current in negative and zero sequence networks is zero. However, for other unbalanced faults, the negative and zero sequence fault current is not zero and is calculated based on the sequence component analysis of unbalanced faults [88]. This involves the following formulae (reproduced from [88]):

For SLG faults:

$$I_{fa}^{0} = I_{fa}^{1} = I_{fa}^{2} \tag{3.1}$$

For LLG faults:

$$I_{fa}^{0} = -I_{fa}^{1} \frac{Z_{kk}^{0} + 3Z_f}{Z_{kk}^{0} + Z_{kk}^{2} + 3Z_f} \tag{3.2}$$

$$I_{fa}^{2} = -I_{fa}^{1} \frac{Z_{kk}^{2}}{Z_{kk}^{0} + Z_{kk}^{2} + 3Z_f} \tag{3.3}$$

For LL faults:

$$I_{fa}^{0} = 0 \tag{3.4}$$

$$I_{fa}^{2} = -I_{fa}^{1} \tag{3.5}$$

In these formulae, $I_{fa}^{0}, I_{fa}^{1}, I_{fa}^{2}$ respectively represent the zero, negative and positive sequence fault currents, Z_{kk}^{0}, Z_{kk}^{2} represent the pre-fault equivalent Thevénin impedance representing the network in zero and negative sequence at the fault location, and Z_f

represents the fault impedance. When using these formulae in InterPSS, the impedances are calculated using InterPSS functions, and using the positive sequence fault current from InterPSS for the given fault, the zero and negative sequence fault currents can also be calculated and applied to the corresponding networks.

3.5 Solar PV Inverter Dynamic Model

One of the key dynamic models involved in the T&D co-simulations involving distribution systems with a high penetration of DERs is the model for these DERs. OpenDSS supports a wide array of components including generators and solar PV systems. However, many of these components are designed/intended for just power flow modes. Additionally, the default components available may not model the inverter control in detail. Hence, the solar PV units with their dynamic elements modeled are described as a custom user model for OpenDSS. The overall process followed for creating the user model and the validation of the user model is described in this section.

OpenDSS supports power flow (snapshot and time series) as well as dynamic simulation modes. During the dynamic simulations in OpenDSS, the network model uses algebraic equations (similar to the power flow mode) and the loads switch to constant impedance model instead of constant power model (which is used in this project for the power flow). The time step can be controlled via the OpenDSS graphical interface as well as via any programming language interface which OpenDSS supports. There are some dynamic models which are provided; however, a user defined model is created to represent the power flow as well as dynamic response from the solar PV units including advanced controls.

Custom user models for OpenDSS can be written either as a dynamic link library (DLL) or as the Python user model supported by the Python package DSS-Python [89]. User defined models allow users to model new components which interact with OpenDSS with any custom dynamic model. DLLs can be created using several programming languages, in the work presented, Embarcadero Delphi was chosen as the platform for developing a DLL since OpenDSS is written using it. A user model to represent solar PV units has been created both in the form of a DLL and a Python user model.

The advantages for the Python user model over DLL include:

- Python user model can be run on most operating systems (rather than being limited to Microsoft Windows)
- Once the Python user model is created, it is easier to edit it compared to the DLL since it does not require a separate program to compile and then use (for the DLL, a separate program, Delphi, is used to compile it before using it in OpenDSS)
- There is a vast array of libraries for Python programming language, and these can be incorporated into the model if needed.

The disadvantages of the Python user model over the DLL include:

- The user model cannot be used outside DSS-Python
- Since the Python user model is not compiled, the control equations are not hidden – this might be important from the perspective that companies may not want to make the exact control equations available for viewing and editing
- The computational speed for conducting the dynamic simulations was found to be lower compared to DLL. For example, for the controls implemented for this

project (described later in this section), simulating a solar PV unit connected to a source behind an impedance for 0.5s simulation time took approximately 0.11s with the DLL and 5.50s with the Python user model on the same machine.

From these advantages and disadvantages, it can be concluded that Python user model or DLL both have their advantages and might be more suitable depending on the application.

Writing a user defined model file consists of writing several functions which OpenDSS requires with their proper format/interface. These functions are invoked in the OpenDSS routines such as setting up the component in the circuit, power flow and dynamic solution. Functions such as Calc (which calculates the injected current by the selected component given the terminal voltage), Init (which initializes the component for dynamic simulation) and Integrate (which performs the integration step for the selected component) are the most important functions among these. By default, OpenDSS uses a predictor-corrector type explicit trapezoidal method for integration, but a new integration routine can be implemented if desired. Hence, both the steady state and dynamic model can be created/modified as per the need.

A detailed model for the single-phase solar PV units is created as a custom model including the advanced controls. The controls implemented are shown in Figure 3.11, and involve a phase locked loop (PLL) to track the voltage, a proportional-resonant (PR) current control, and active and reactive power controls. The active and reactive power controls implemented include different active and reactive power control modes from the IEEE Standard 1547-2018 including constant active and reactive power setpoints,

constant power factor, volt-VAr, volt-watt and watt-VAr modes. The default response curves for volt-VAr, volt-watt and watt-VAr curves from IEEE1547-2018 for category B inverters are used. The inverter switching is represented by an average model. The user model is developed as a differential algebraic model. The control equations are modeled using dynamic phasors, similar to the control model described in [90].

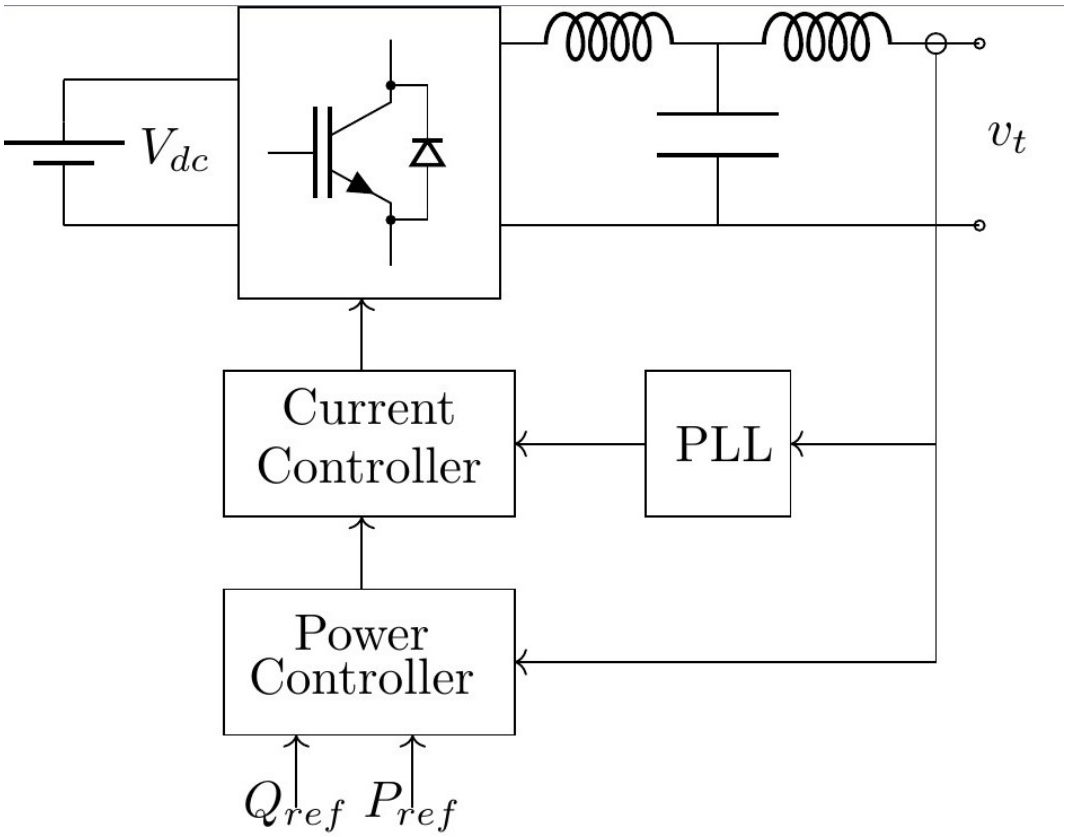

Figure 3.11 Block Diagram of the Control Modeled for the Solar PV Units as a User Model for OpenDSS

During low voltages, the inverter current is limited to twice the rated current (assumed to correspond to delivering the rated apparent power at 0.88 p.u. voltage, which is the lowest continuous mode operation voltage mandated by the IEEE 1547-2018 standard).

In addition, different abnormal voltage controls from IEEE 1547-2018 standard, specifically the trip/no-trip controls are also implemented. Some of the implemented abnormal voltage controls are described in Table 3.1. The values given in this table represent the limits of the clearing time, and when the maximum clearing time in the table is given as 0.16s, a clearing time of 1 cycle is implemented in the model. In the table, only the values corresponding to UV2 and OV2 undervoltage and overvoltage limits are shown because these limits are more relevant to the simulations performed using the user model, however, UV1 and OV1 limits can also be easily incorporated in the model.

Table 3.1 Some of the Trip/No-trip Abnormal Voltage Controls Implemented for Solar PV Units Based on The IEEE 1547-2018 Standard [91]

Inverter category	UV2 voltage (p.u.)	UV2 clearing time (s)	OV2 voltage (p.u.)	OV2 clearing time (s)
Category I	0.45	0.16	1.2	0.16
Category II	0.45	0.16	1.2	0.16
Category III	0.5	2	1.2	0.16

A detailed inverter model with the same control blocks is created in PLECS [92] and compared against the OpenDSS model as a validation. A small circuit is constructed in both OpenDSS and PLECS, shown in Figure 3.12 for this purpose. The circuit parameters are selected based on some of the network parameters of the modeled feeder and kept the same between OpenDSS and PLECS models. and the inverter models are operated under various disturbances including changes in active and reactive power setpoints (active power setpoint is changed at 0.15s and reactive power setpoint is changed at 0.3s), a

change in the terminal voltage of the inverter achieved by changing the source voltage (at 0.4s), and response to a single line to ground (SLG) fault applied on a neighboring bus (fault is applied at 0.6s and cleared after 0.08s). Note, the abnormal voltage tripping controls are not enabled for this comparison. Figure 3.13 and Figure 3.14 show the terminal voltage and current for the inverter modeled, and Figure 3.15 and Figure 3.16 show the active and reactive powers from the inverters for these disturbances. Note, OpenDSS provides the currents as phasors and Figure 3.14 compares the current obtained from PLECS with the current reconstructed based on the phasor values (RMS magnitude and phase angle) from OpenDSS. The good match between the two models validates the custom OpenDSS model.

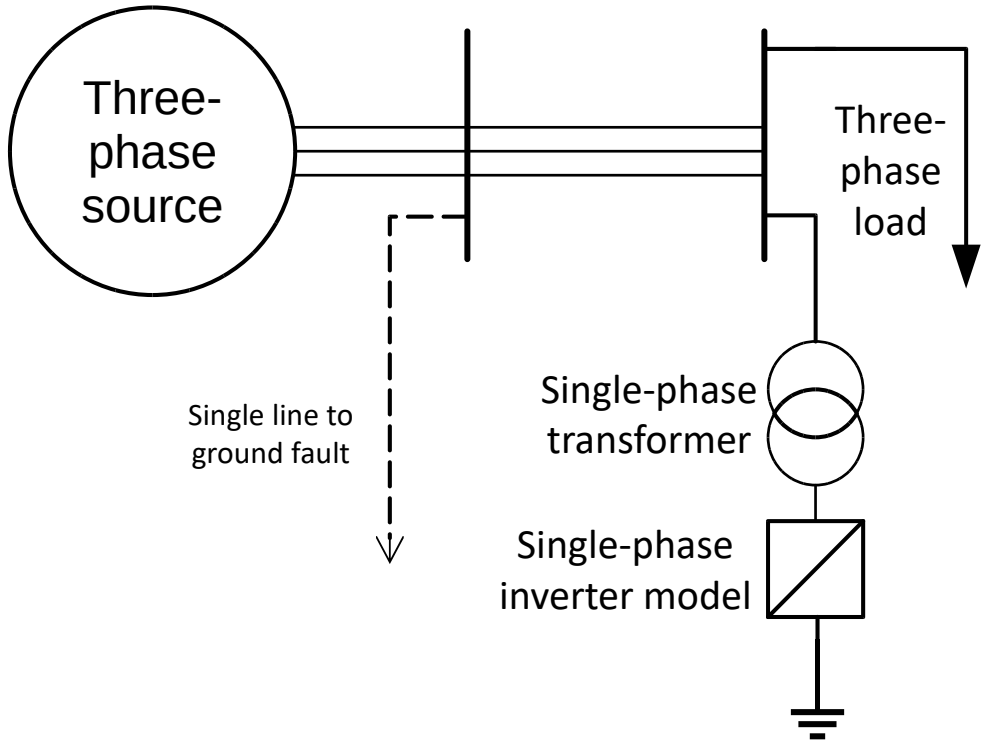

Figure 3.12 Small Test Circuit Used to Validate the Single-phase Inverter Model

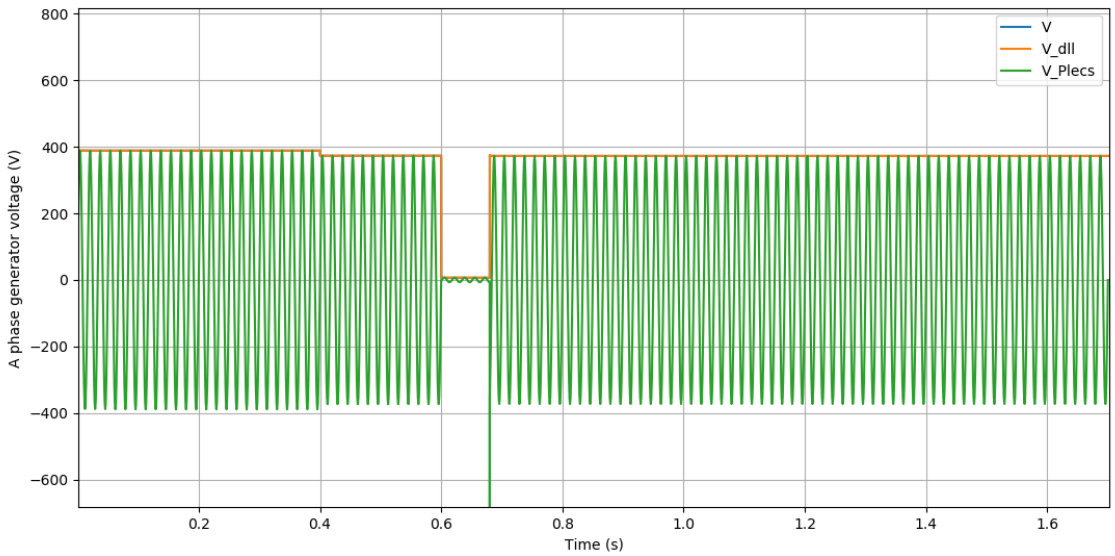

Figure 3.13 Comparison of the Voltage at the Terminal of the Inverter from the OpenDSS User Model (Both DLL and Python User Models) and the PLECS Model under Various Disturbances.

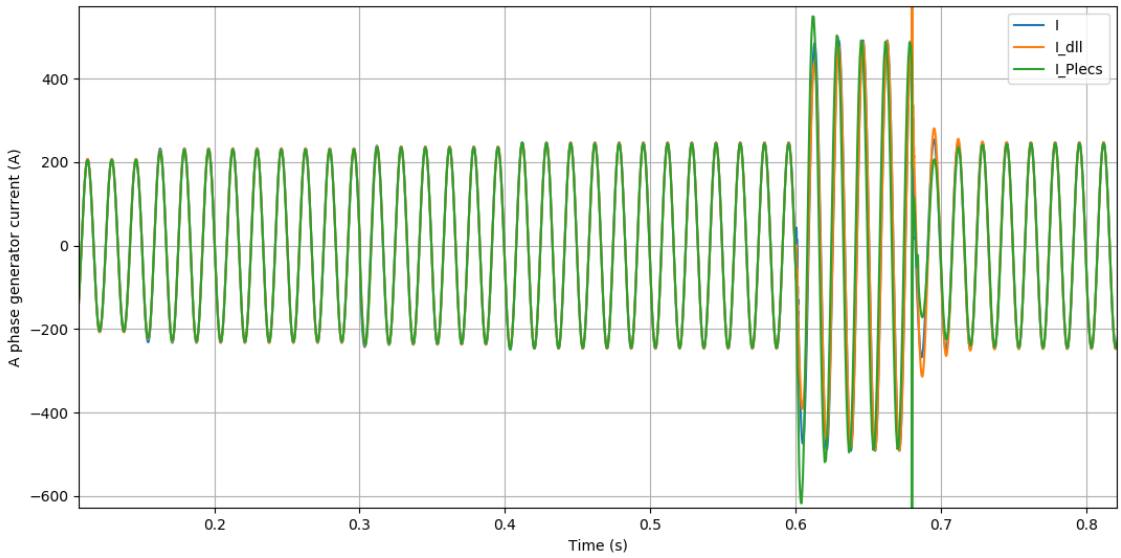

Figure 3.14 Comparison of the Current at the Terminal of the Inverter from the OpenDSS User Model (Both DLL and Python User Models) and the PLECS Model under Various Disturbances.

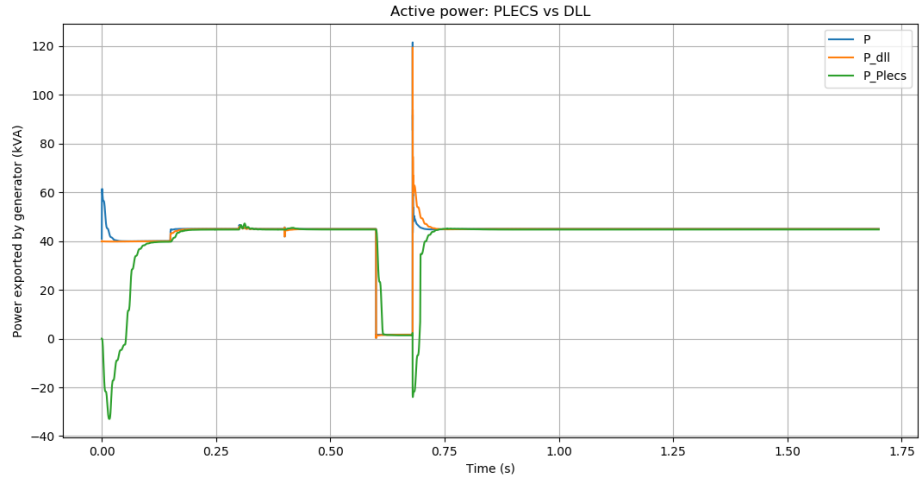

Figure 3.15 Comparison of the Active Power at the Terminal of the Inverter from the OpenDSS User Model (Both DLL and Python User Models) and the PLECS Model under Various Disturbances

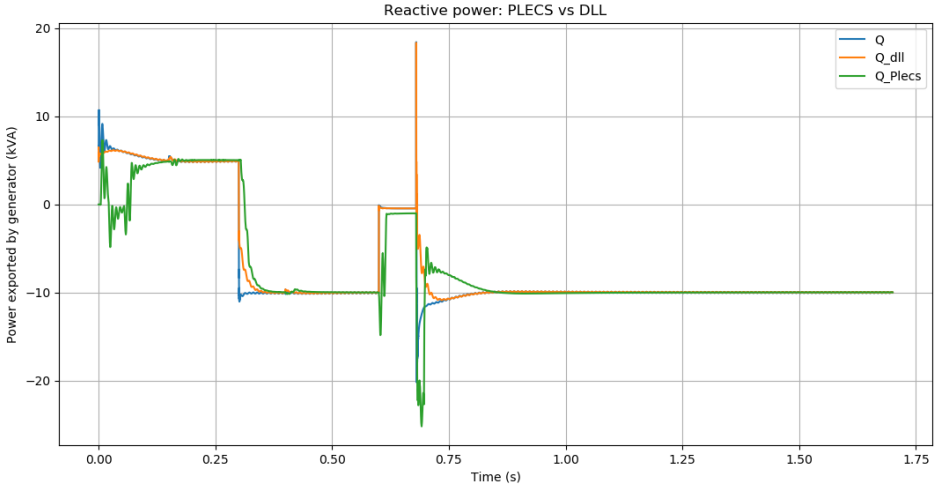

Figure 3.16 Comparison of the Reactive Power at the Terminal of the Inverter Form the OpenDSS User Model (Both DLL and Python User Models) and the PLECS Model under Various Disturbances

However, one of the downsides of the developed model is the requirement of a small time step. It is seen that the user model requires a time step less than 4e-5 s; a time step larger than this leads to numerical instability, as shown in Figure 3.17. The figure plots an internal variable from the solar PV user model for two different time steps, where the model is seen to be numerically stable for a time step of 1e-5s and unstable for a time step of 4.4e-5s. It is to be noted, however, that the usage of small time steps is not specific to the model constructed for this project, a previous study involving similar solar PV inverter OpenDSS model using dynamic phasors reported a similar usage of 5μs time step [90].

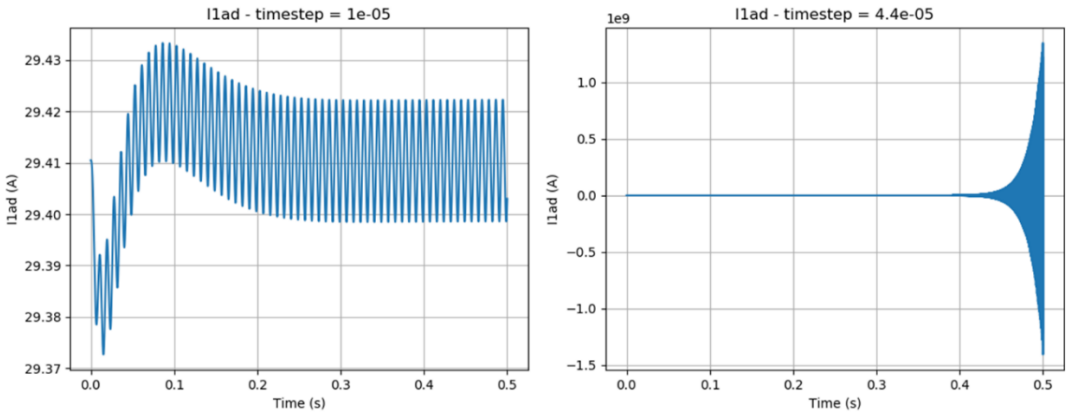

Figure 3.17 The Impact of Time Step on the Stability of the Solar PV Model

3.6 Grid Forming Inverter Model

Traditionally, the DERs connected to the distribution system operate in a “grid following” control paradigm. In the “grid following” control for DERs or other inverter-based resources, the inverter is not responsible for maintaining and “forming” the grid

voltage and frequency. The model presented in the previous section is a grid following inverter model, and majority of the inverters installed on distribution feeders would operate in a grid-following control mode in the field. In such case the inverter may be considered to be a current source that injects a particular current at its point of common coupling with the grid. On the other hand, with the newer "grid forming" control, an inverter-based resource is configured to maintain a certain voltage and frequency at the point of common coupling and can be represented by a voltage source. This difference is depicted pictorially in Figure 3.18. Note, the DER/inverter in either control paradigm can support different complex controls and functionality, such as the functionality described in Section 3.5. In this section, a simple model created to represent a grid-forming inverter is explained. One of the benefits of using a simple model with few dynamic components is that the model can be simulated at higher time steps. The simulations involving GFM models given in the dissertation are performed using 10 μs time step (higher than the 2 μs time step required by the model described in Section 3.5). model is intended to be used for preliminary studies of the combined T&D network. Some results implementing the model presented in this section with the utility network model are presented in Section 6.6.

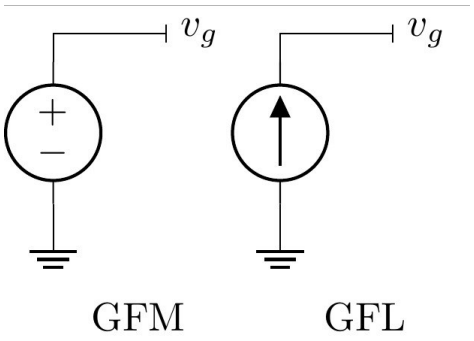

Figure 3.18 The Grid Forming and Grid Following Inverter Paradigms

Different grid-forming inverter control strategies have been proposed in the literature such as droop-based GFM [93], virtual synchronous generator [94], and virtual oscillator control [95]. While the initial development of the grid forming concept is considering a microgrid operation [93] or an application for a bulk system connected large inverter based generation [96], applications for distribution system connected GFMs are also considered in literature [97]–[99].

Here, a simple model is considered for representing the grid forming inverters connected to the distribution system. Since a large number of distribution-connected devices are single-phase, a single-phase model is considered. For this dissertation, the model is developed as a Python user defined model. Please note that this GFM model and the simulations using the model are conducted to illustrate the capabilities of the considered framework – using other GFM architectures or controls and a wider range of network models and timescales is possible depending on the study. The overall schematic of the grid forming inverter model is shown in Figure 3.19. The inverter is modeled in dq domain. This is a PLL/droop-based grid forming inverter model. The combined operation

of current control and switching is represented by delay blocks in the d and q domains, and a controlled voltage source behind an impedance is used as the model interfacing the network. The control block diagram of the PLL is shown in Figure 3.20.

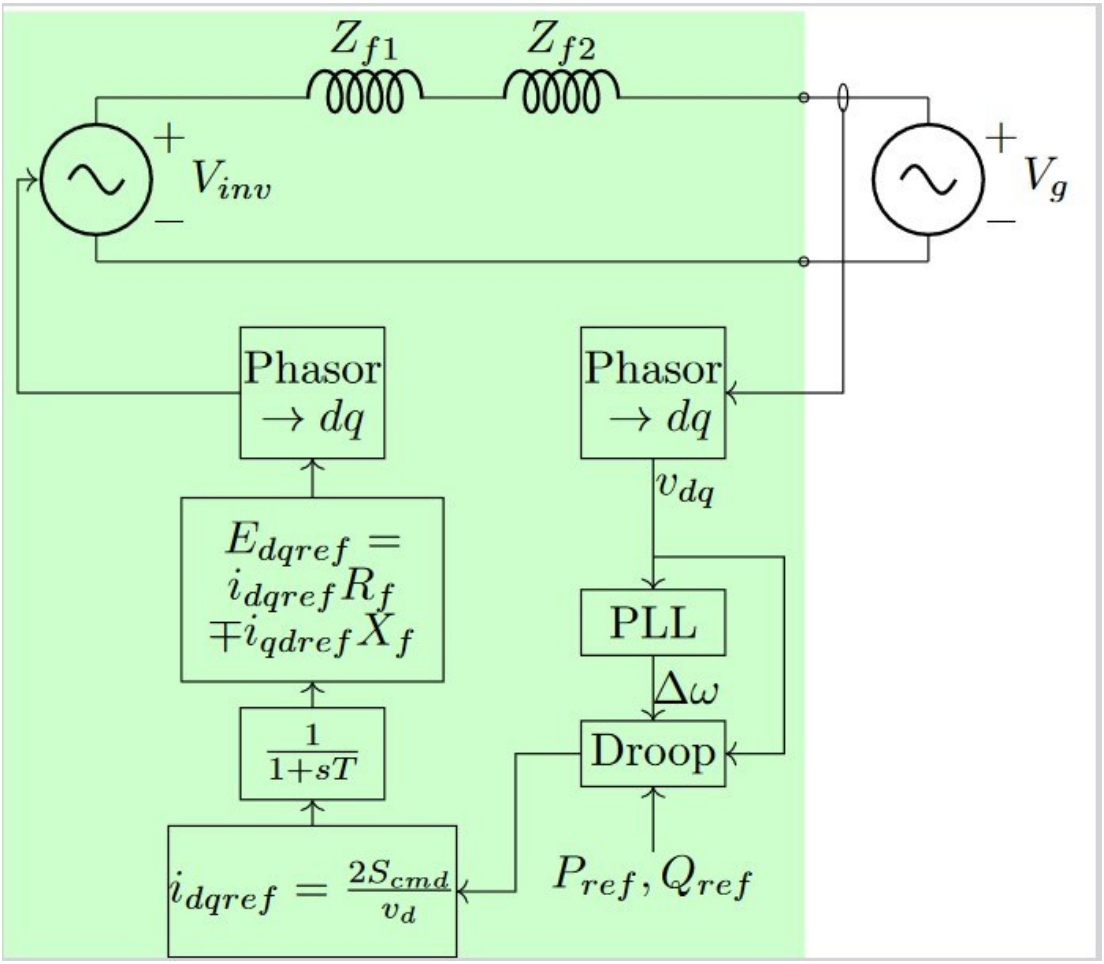

Figure 3.19 The Block Diagram Representing the Implemented GFM Controls

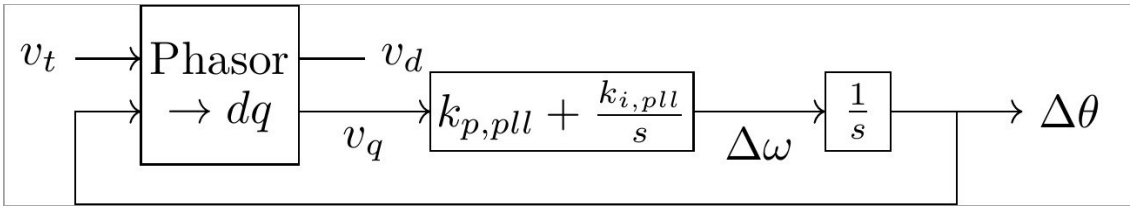

Figure 3.20 The Block Diagram of the Phase Locked Loop Implemented for the GFM Model

The active and reactive power commands are generated based on the active and reactive power references as well as the reactive power-voltage magnitude and active power-frequency droops:

$$P_{cmd} = P_{ref} - \frac{\Delta\omega}{m_p} \tag{3.6}$$

$$Q_{cmd} = Q_{ref} + \frac{V_{\text{ref}} - V_t}{m_q} \tag{3.7}$$

Here m_p and m_q are droop parameters, $P_{ref}, Q_{ref}, V_{ref}$ are the active and reactive power and voltage magnitude reference values, $\Delta\omega$ is the deviation in the angular frequency measured by the PLL, V_t is the magnitude of the voltage at the inverter terminal, and P_{cmd}, Q_{cmd} are the generated active and reactive power commands. The active and reactive power commands inform the current references. The current reference is limited to twice the rated current (calculated based on the rated apparent power and voltage supplied to the model). An algebraic equation representing the filter and coupling impedance (in the voltage source model) is used to estimate the required voltage source magnitude and phase angle:

$$E_{dq} = V_{t,dq} + i_{dq,cmd}R_f \mp i_{qd,cmd}X_f \tag{3.8}$$

Here E_{dq} represents the voltage commands for the controlled voltage source in the GFM model in dq domain, $i_{dq,cmd}$ are the commands for the dq domain inverter current, $V_{t,dq}$ is the inverter terminal voltage in dq domain, and $R_f + X_f$ is the filter impedance. This described GFM model is created as a Python user model for OpenDSS. A first order

delay is implemented to approximate the current control loop and switching delays – the outputs of the delay blocks form the current command that is passed to the algebraic equation.

This GFM model is tested using a small circuit, shown in Figure 3.21. In the first test, the load is modified at 0.5 s, the active and reactive power references are changed from 3.5 kW and 1 kVAr to 5 kW and 0.3 kVAr respectively, at 1.0s, and the voltage source magnitude is changed from 1.0 p.u. to 0.99 p.u. at 1.5s. The active and reactive power injected by the GFM model are shown in Figure 3.22. It is seen that the GFM model follows the active and reactive power reference at 1.0 p.u. voltage. When the source voltage is lowered, a corresponding change in the reactive power injected by the GFM is seen – this change reflects the reactive power-voltage magnitude droop law implemented.

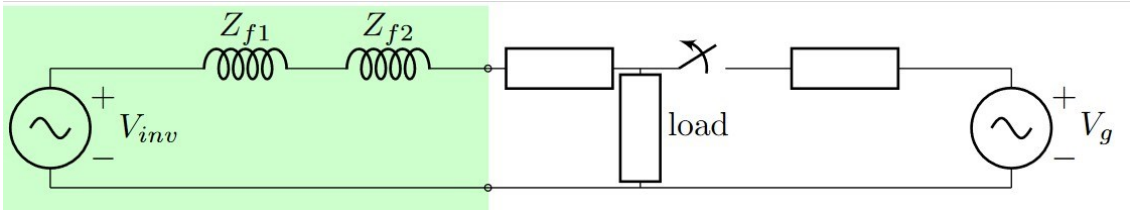

Figure 3.21 The Circuit Diagram for the Small Test Circuit

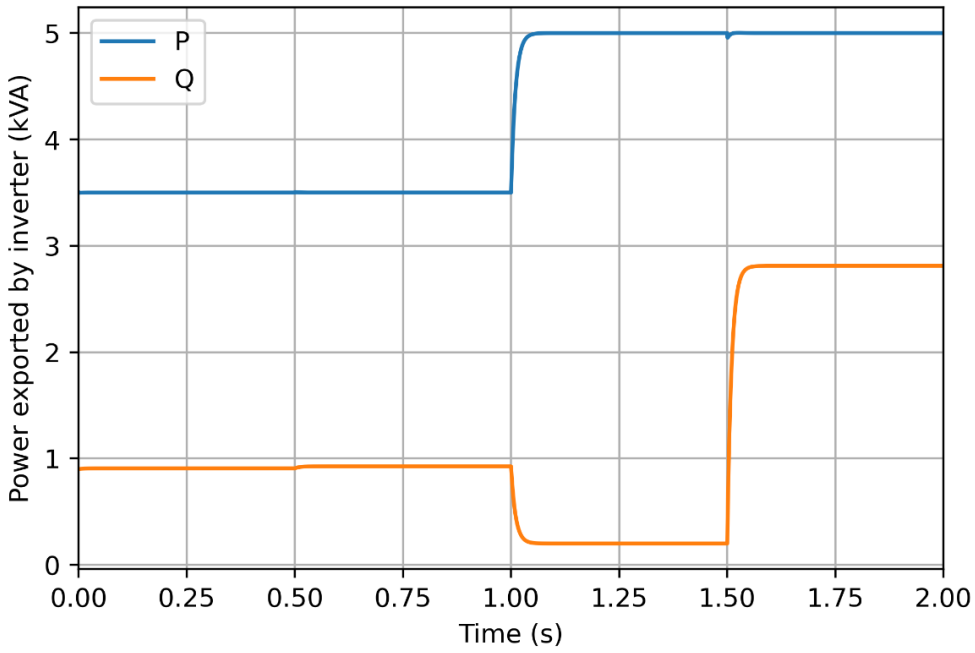

Figure 3.22 The Active and Reactive Power During the First Test from the GFM Python User Defined Model

As a second test, another simulation is conducted where the main grid is disconnected. For this case, it is seen that even after the main grid is disconnected at 0.5s. The initial inverter active and reactive power references are set to be equal to the load fed entirely by the GFM when the main grid is disconnected (1.152 kW and 0.5 kVAr). In this case, the inverter active and reactive power does not change significantly after the disconnection of the main grid, shown in Figure 3.23. The voltage magnitude as well as frequency are maintained very close to their values before disconnection, as shown in Figure 3.24 and Figure 3.25, respectively. On the other hand, if the initial power references are not set equal to the load fed by the GFM when the main grid is disconnected, a larger change in

the inverter active/reactive power as well as the maintained voltage magnitude and the frequency is expected. This is tested by setting the initial active and reactive power references to 3 kW and 0.5 kVAr – the corresponding plots of active and reactive power, shown in Figure 3.26; the voltage magnitude, shown in Figure 3.27, and angular frequency, shown in Figure 3.28 highlight this behavior. Note, the deviations in the frequency and voltage magnitude are dependent on the droop coefficients as well as the network connected with the GFM. However, it is seen that the GFM model successfully changes the active power setpoint to match the load to be fed and is able to maintain the voltage magnitude and frequency close to the nominal values. A preliminary study implementing this model with the developed T&D co-simulation framework is presented in Section 6.6.

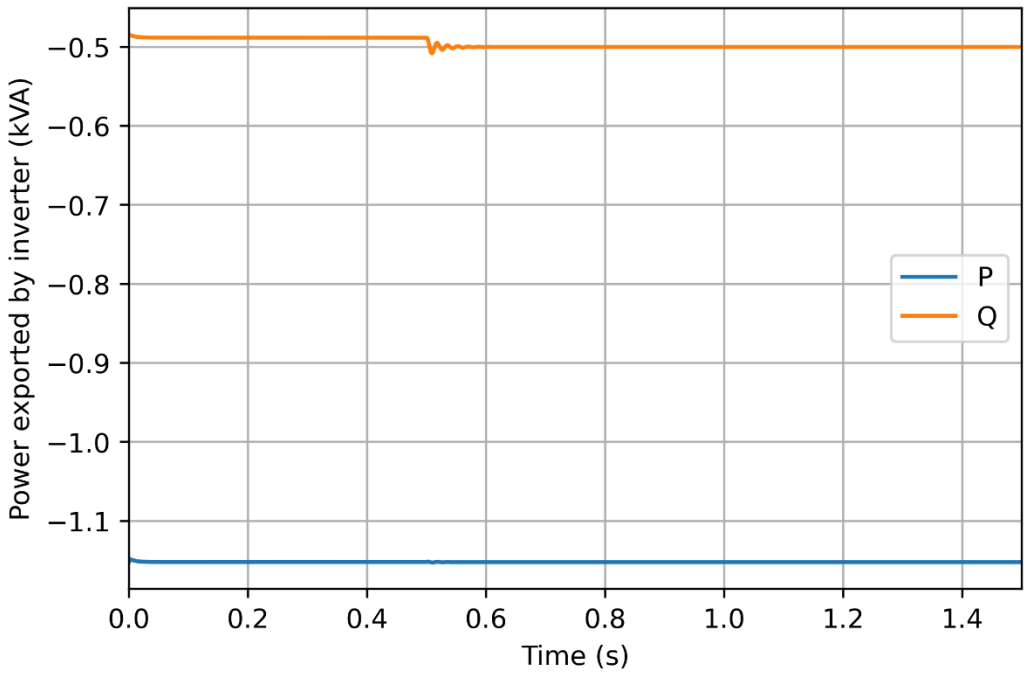

Figure 3.23 The Active and Reactive Power During the Second Test (Main Grid Disconnection) from the GFM Python User Defined Model, with Initial Powers Matching the Load

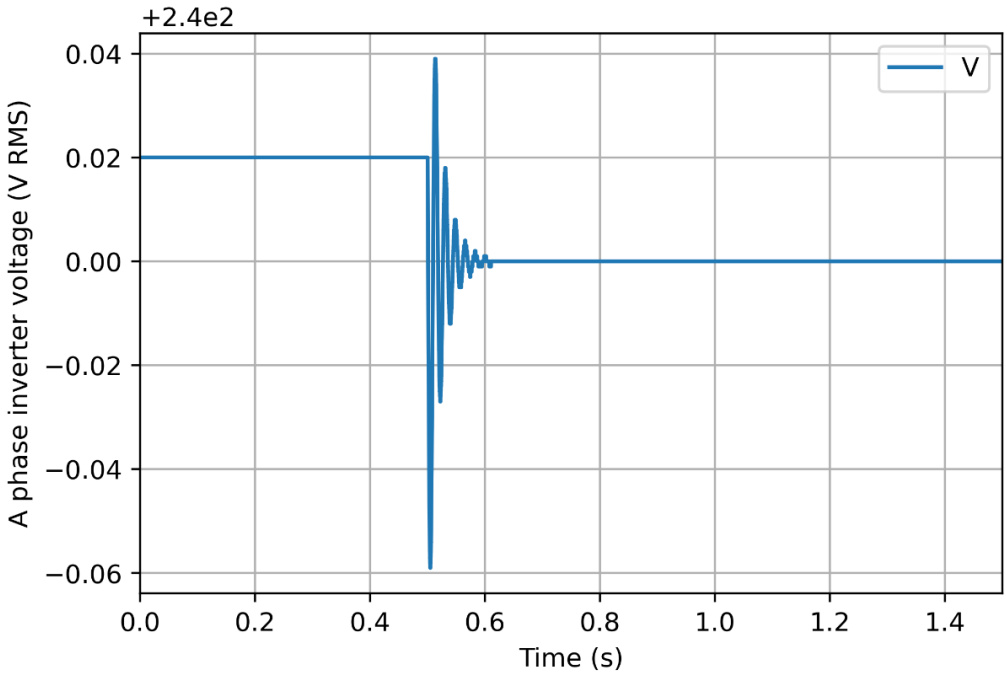

Figure 3.24 The Inverter Voltage Magnitude During the Second Test (Main Grid Disconnection), with Initial Powers Matching the Load

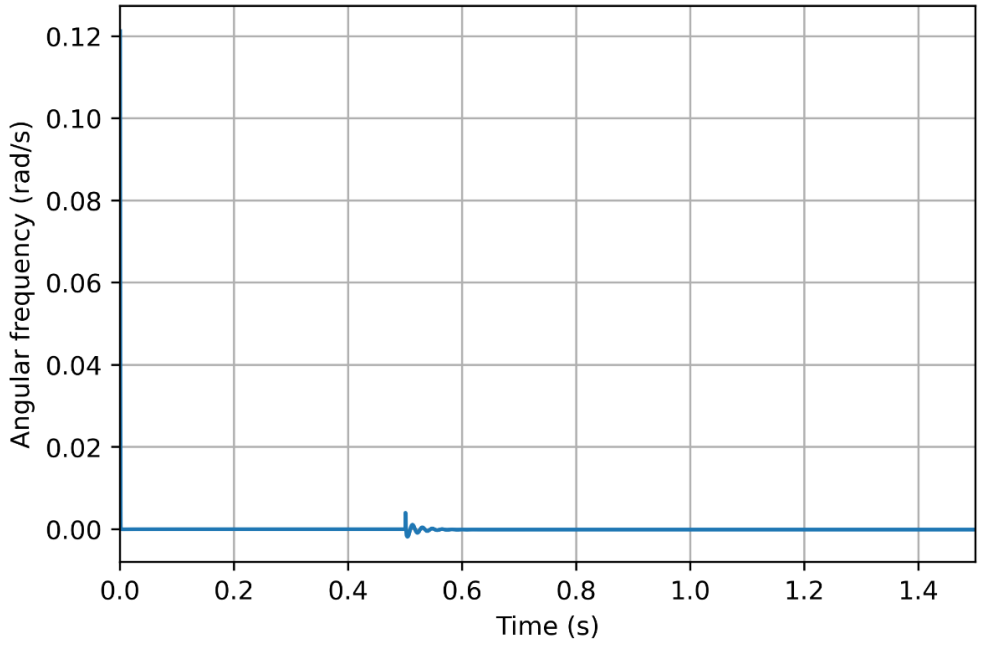

Figure 3.25 The Inverter Relative Angular Frequency Deviation During Second Test (Main Grid Disconnection), with Initial Inverter Powers Equal to the Load

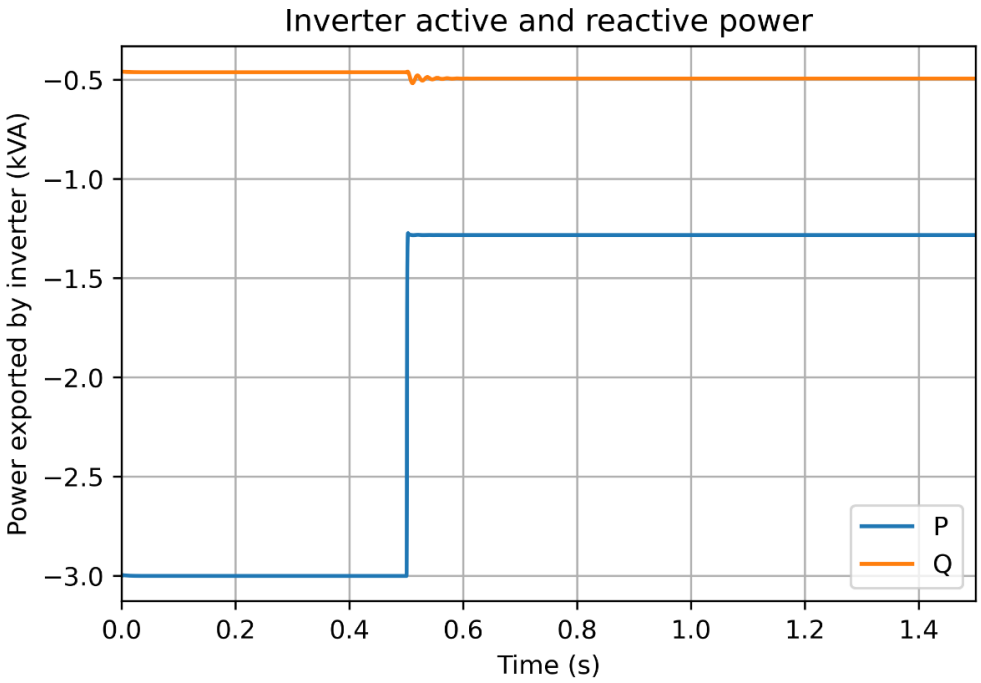

Figure 3.26 The Inverter Active and Reactive Power for Main Grid Disconnection, with Initial Inverter Powers Not Matching the Load

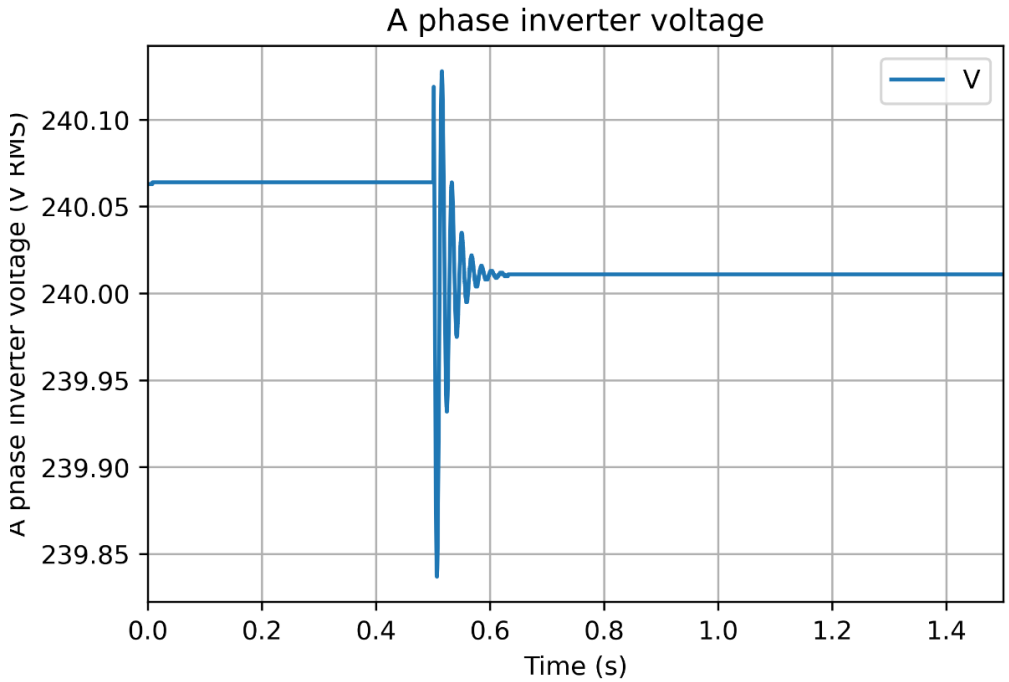

Figure 3.27 The Inverter Terminal Voltage Magnitude for Main Grid Disconnection, with Initial Inverter Powers Not Matching the Load

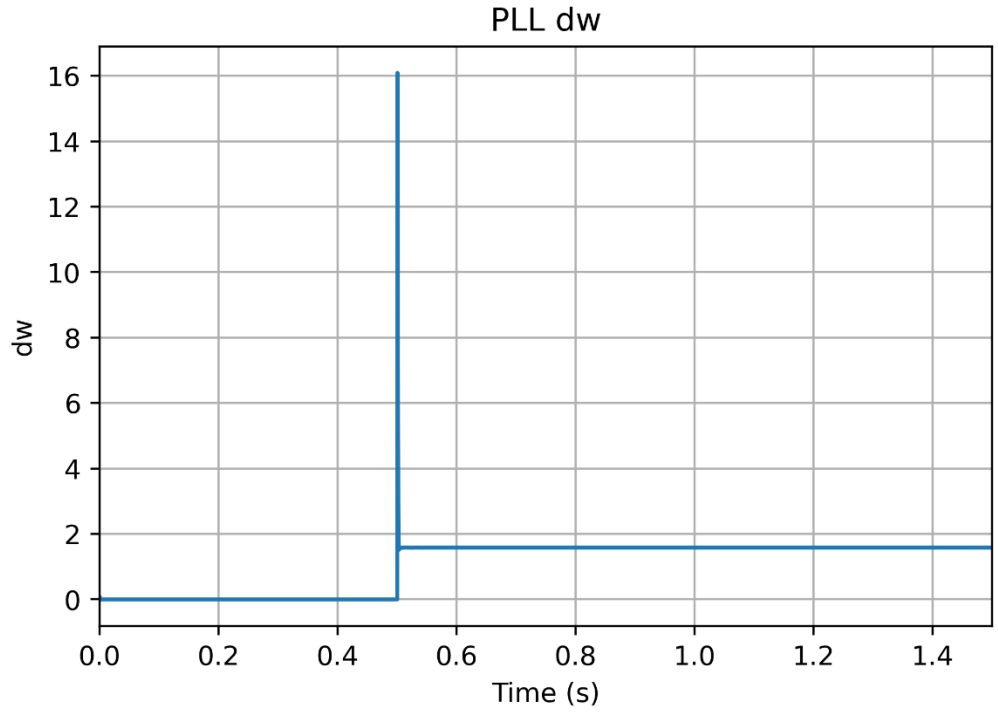

Figure 3.28 The Inverter Relative Angular Frequency Deviation for Main Grid Disconnection, with Initial Inverter Powers Not Matching the Load

3.7 Single Phase Induction Motor

Single phase induction motors connected to the distribution system are one of the key components in capturing the dynamic response of distribution feeders. Single phase induction motors can be found as a part of air conditioning units and refrigerators and fans, among other household devices. Single phase induction machine stalling is one of the key reasons for fault-induced delayed voltage recovery (FIDVR) seen in the electrical power systems. This section describes a possible approach to include a representation of the induction machine model in a T&D network study.

Classically, the single-phase induction motor can be analyzed by writing stator and rotor voltage and flux equations. The stator field produces a pulsating magnetic field and the induced current on the rotor produces another magnetic field – the torque driving the rotor is generated as a result of the interaction between these magnetic fields. There are three types of models available in the literature: performance based models [2], point on wave/EMT detailed models [100] and dynamic phasor models [101]. Performance based models are used in the commercial positive sequence-software as a part of composite load model. These were developed based on laboratory testing of a large number of single-phase induction motors and implemented as a part of composite load model [2]. Different sets of algebraic equations are used to represent normal operation and motor stall characteristics for these models. Hence, performance-based models are relatively straightforward to implement and use with a software (comparing with the point on wave or dynamic phasor models). However, these are intended to represent an aggregate impact of a large number of motors for bulk stability studies and are static models. Point on wave detailed models accurately represent the motor dynamics, however, they have high computational requirement, and need conversion between the point on wave and phasor representation if interfacing with phasor domain software. Dynamic phasor models are also physics-based, but have lower computational requirement for representing the motor dynamics and are implemented for commercial/open-source software such as PowerWorld [102] and Gridlab-D [103]. A downside of the dynamic phasor models compared to detailed point on wave models is that they do not capture the point on wave/phase impacts on the stalling of motors. For any motor model, additionally, it may be important to model the thermal tripping/protection of motors

especially for longer duration studies [103]. For application to a large-scale network model, dynamic phasor models may be appropriate to represent the dynamics including stalling without a prohibitive computational cost.

The dynamic phasor models [101], [104] are based on forward-backward component-based modeling of the induction motor equations. Another dynamic phasor model [105] uses multiple harmonic dynamic phasors to create an aggregated model. The model described in [103] builds on [101] by adding multistate model representing end use features such as 'off' state and thermal tripping. The model given in [106] is similar to [101] but uses phasor voltage instead of voltage magnitude. Since [101] has been tested experimentally and implemented in commercial/non-commercial software packages [102], [103] , it is considered suitable for studying the dynamic response of a large T&D network. The equations representing this model from [101] are reproduced below:

$$|V_s| = \left(r_{ds} + j\frac{\omega_s}{\omega_b}X'_{ds}\right)(I^R_{ds} + jI^I_{ds}) + j\left(\frac{\omega_s}{\omega_b}\right)\frac{X_m}{X_r}(\Psi^R_{dr} + j\Psi^I_{dr}) \tag{3.9}$$

$$|V_s| = \left(r_{qs} + j\frac{\omega_s}{\omega_b}X'_{qs} + j\frac{\omega_s}{\omega_b}X_c\right)\left(I^R_{qs} + jI^I_{qs}\right) + j\left(\frac{\omega_s}{\omega_b}\right)\frac{nX_m}{X_r}\left(\Psi^R_{qr} + j\Psi^I_{qr}\right) \tag{3.10}$$

$$\begin{bmatrix}\left(\Psi^R_f + j\Psi^I_f\right)\\ \left(\Psi^R_b + j\Psi^I_b\right)\end{bmatrix} = \left(\frac{1}{2}\right)\begin{bmatrix}1 & -j\\ 1 & j\end{bmatrix}\begin{bmatrix}\left(\Psi^R_{dr} + j\Psi^I_{dr}\right)\\ \left(\Psi^R_{qr} + j\Psi^I_{qr}\right)\end{bmatrix} \tag{3.11}$$

$$\begin{bmatrix}\left(\Psi^R_{dr} + j\Psi^I_{dr}\right)\\ \left(\Psi^R_{qr} + j\Psi^I_{qr}\right)\end{bmatrix} = \begin{bmatrix}1 & 1\\ j & -j\end{bmatrix}\begin{bmatrix}\left(\Psi^R_f + j\Psi^I_f\right)\\ \left(\Psi^R_b + j\Psi^I_b\right)\end{bmatrix} \tag{3.12}$$

$$\begin{bmatrix}\left(\mathrm{I}^R_f + j\mathrm{I}^I_f\right)\\ \left(\mathrm{I}^R_b + j\mathrm{I}^I_b\right)\end{bmatrix} = \left(\frac{1}{2}\right)\begin{bmatrix}1 & -jn\\ 1 & jn\end{bmatrix}\begin{bmatrix}\left(\mathrm{I}^R_{ds} + j\mathrm{I}^I_{ds}\right)\\ \left(\mathrm{I}^R_{qs} + j\mathrm{I}^I_{qs}\right)\end{bmatrix} \tag{3.13}$$

$$\begin{bmatrix}(\mathrm{I}_{ds}^{R}+j\mathrm{I}_{ds}^{I})\\(\mathrm{I}_{qs}^{R}+j\mathrm{I}_{qs}^{I})\end{bmatrix}=\begin{bmatrix}1 & 1\\ jn & -jn\end{bmatrix}\begin{bmatrix}(\mathrm{I}_{f}^{R}+j\mathrm{I}_{f}^{I})\\(\mathrm{I}_{b}^{R}+j\mathrm{I}_{b}^{I})\end{bmatrix} \tag{3.14}$$

$$T_o'\frac{d}{dt}\left(\Psi_f^R+j\Psi_f^I\right)=X_m\left(\mathrm{I}_f^R+j\mathrm{I}_f^I\right)-\left(sat\left(\Psi_f,\Psi_b\right)+j(\omega_s-\omega_r)T_o'\right)\left(\Psi_f^R+j\Psi_f^I\right) \tag{3.15}$$

$$(\Psi_b^R+j\Psi_b^I)=\frac{X_m(\mathrm{I}_b^R+j\mathrm{I}_b^I)}{\left(sat\left(\Psi_f,\Psi_b\right)+j(\omega_s+\omega_r)T_o'\right)} \tag{3.16}$$

$$\frac{2H}{\omega_b}\frac{d\omega_r}{dt}=\frac{X_m}{X_r}2\left(I_f^I\Psi_f^R-I_f^R\Psi_f^I-I_b^I\Psi_b^R+I_b^R\Psi_b^I\right)-T_{mech} \tag{3.17}$$

$$I_s=\left[(\mathrm{I}_{ds}^{R}+j\mathrm{I}_{ds}^{I})+\left(\mathrm{I}_{qs}^{R}+j\mathrm{I}_{qs}^{I}\right)\right]e^{j\phi} \tag{3.18}$$

$$sat\left(\Psi_f,\Psi_b\right)=\begin{cases}1, & \Psi\le b_{sat}\\ 1+A_{sat}(\Psi-b_{sat})^2, & \Psi>b_{sat}\end{cases} \tag{3.19}$$

$$\Psi=\sqrt{\left(\Psi_f^R\right)^2+\left(\Psi_f^I\right)^2+(\Psi_b^R)^2+(\Psi_b^I)^2} \tag{3.20}$$

$$T_o'=\frac{X_r}{\omega_b R_r} \tag{3.21}$$

Here V_s is the terminal voltage for the motor, ω_b is the base angular speed, ω_s is the angular speed of the stator voltage signal, ω_r is the rotor angular speed, ϕ is the phase angle of the dq frame, r and X represent resistance and reactance, I represents currents, Ψ represents the magnetic fields, subscript s represents stator, subscript r represents rotor, subscripts d, q represent the d and q axes, superscript R represents a real part and superscript I represents an imaginary part. Also, X_m is the magnetizing reactance, X_c is the capacitor reactance (negative), n is the ratio of the stator auxiliary winding turns to

stator main winding turns, H is the inertia constant of the motor, T_{mech} is the mechanical torque, and A_{sat} and b_{sat} are the parameters used for defining the saturation function.

Note, this dissertation does not present a T&D co-simulation case with the motor model implemented, however, it is provided here to identify the appropriate model that can be used in conjunction with the rest of the framework and models to study the interactions of the motor model with the rest of the dynamic models and network.

4 DYNAMIC SIMULATION OF A FEEDER WITH SOLAR PV MODELS

The process for creating a detailed and accurate feeder model for a real feeder in Arizona is described in the Chapter 2. For this modeled feeder, it is observed that when an unbalanced fault is applied to the feeder, one of the non-faulted phases shows a high voltage swell during the fault. Occurrences of such voltage swell from the literature are presented and analyzed in Section 4.1. The reason/mechanism behind this voltage swell for the modeled feeder is studied in Section 4.2, and Section 4.3 explores the impact various controls from the solar PV units have on this voltage swell and whether the solar PV resources on the feeder can be used to mitigate the voltage swell.

The work related to the voltage swell given in this chapter is published in [107].

4.1 Voltage Swell in Non-faulted Phases During Unbalanced Faults on the Distribution Feeder

One of the phenomena studied by utilizing the developed detailed distribution system model is the occurrence of voltage impact on the modeled distribution feeder during unbalanced faults on the distribution system. For single line to ground faults, as expected, the faulted phases experience a very low voltage. However, one of the non-faulted phases during the unbalanced faults also experiences a high voltage swell, as will be shown in this chapter.

It is known in the literature that analysis of unbalanced faults may show adverse voltage impacts on non-faulted phases in power systems [108]. Further, such adverse voltage impacts have also previously been reported from recorded data for utility circuits through a survey conducted in early 1990s [109]. Analytically, the ratio of zero and positive

sequence equivalent impedance at the fault location is shown to play a large role in determining the voltage swell on the non-faulted phases during unbalanced faults by calculating the effective impedances and voltages for all three phases using sequence component analysis [108], [110]. However, while this analysis provides an explanation for the voltage swell, the physical reason/physical network situation(s) which lead to this phenomenon are not revealed through this analysis.

The authors of [111] compare different grounding schemes for multi-grounded neutral in three-phase distribution systems and discuss the impact of these grounding schemes on the voltage swell. They also show that the voltage swell experienced by different non-faulted phases might be different. The impacts of different neutral to grounding impedances at the substation on the voltage swell are discussed in [112]. A case study for an industrial system is provided in [113], showing the impact of the substation transformer neutral grounding on the voltage swells on non-faulted phases during unbalanced faults. Another factor which is shown to impact the voltage swell is the substation transformer configuration [112], [114], where [114] shows the impact for a synthetic IEEE test feeder. In chapter 5, for the modeled feeder, the mutual coupling for the three-phase cables/cable impedance for the three-phase cables is shown to lead to the voltage swell on the non-faulted phases during unbalanced faults.

It is important to note that studying the impact of the voltage swell on the non-faulted phases is important from the perspective that the voltage swell can cause disruptions to customer service and may damage customer equipment. The IEEE Standard 1159 for power quality [115] defines voltage swell as an event where the root mean square (RMS)

voltage goes above 1.1 p.u. for more than half cycle. Many household appliances may start failing for severe voltage swells, as shown in [116]. The severity here could be in terms of voltage swell magnitude as well as the duration of the voltage swell. The reference [116] presents results from laboratory tests performed on 60 different household appliances where different overvoltages were applied – it is seen that the appliances may start to fail especially above 1.2 p.u. voltages. There are also different power acceptability curves such as the CBEMA curve provided by the Computer Business Equipment Manufacturers Association specifying the acceptable voltage levels [117]. According to such curves, usually a voltage above 1.2 p.u. is not considered acceptable except for a very short period. Hence, the customer equipment may be adversely impacted by the voltage swell above 1.2 p.u.

In addition, for distribution systems with a high penetration of solar PV generation, it is important to note how the solar PV inverters respond to the voltage swell – on one hand, the voltage swell may result in the disconnection of a large number of solar PV units, adversely impacting the system, but on the other hand, with advanced controls, the solar PV units can be seen as resources which can be utilized to potentially alleviate the voltage swell, as will be discussed in Chapter 5. The IEEE Standard 1547-2018 [91] requires DERs to trip over 1.2 p.u. voltage. In fact, this standard is relatively recent, and the inverters already installed in the field might not even be compliant with this standard and may trip for a smaller voltage swell. The voltage sensitivity of twenty-five, off-the-shelf residential solar PV inverters was tested in 2021, as presented in [118] and it is found that some of those inverters disconnected when a voltage swell was applied. Hence, a voltage swell may result in a large amount of solar PV generation tripping.

However, the solar PV units can also help alleviate the adverse conditions during the faults. In [119], the authors show that with dynamic voltage support capabilities the inverters are able to help alleviate the voltage sag and frequency drop during balanced three-phase faults. The solar PV units have also been useful in mitigating/reducing the voltage sags and swells during unbalanced faults using positive and negative sequence reactive power injections [120] or independent phase control [121]. However, the distribution networks modeled in these papers are small synthetic networks. Further, most of the literature assumes the presence of a large three-phase DER, which may not be true for a residential feeder where the majority of the DERs may be residential rooftop solar PV units.

4.2 Voltage Swell on Non-faulted Phases for Unbalanced Faults

A dynamic simulation for the modeled feeder is run by first solving the power flow and then using the OpenDSS dynamics mode. OpenDSS supports applying balanced as well as unbalanced faults in the dynamic mode. When an unbalanced SLG fault is applied to the modeled feeder, it is seen that the feeder experiences a large voltage swell. This section explores the reason/mechanism behind this voltage swell and its potential impacts on the feeder.

For the dynamic simulation, a snapshot corresponding to 15 March 2019 at 1 PM was chosen as the base operating point. At this operating point, the feeder experiences a large reverse active power flow of approx. 2.1 MW, since the total active load at this operating point is approx. 1.6 MW while the generation from the solar PV units is 3.8 MW. A SLG fault is applied to the feeder starting from this base operating point near the middle of the

feeder on the main three-phase trunk of the feeder, as shown in Figure 4.1. The fault resistance is selected to be 0.05 Ω. For this fault, it is observed that the faulted phase (chosen to be phase A) experiences a large fault current at the feeder-head and low voltage, while the other two phases experience voltage swell during the fault, with the phase C voltage swell being worse than phase B. Phase B has a small voltage swell where the voltages remain below 1.2 p.u., while a large number of buses on phase C experience voltages of more than 1.2 p.u. as shown in the feeder voltage profile in Figure 4.2. The reason for this voltage swell is the equivalent impedance at the fault location, and, in particular, is shown to be the large unbalanced fault current flowing through the impedances of the cables comprising the main three-phase trunk of the feeder.

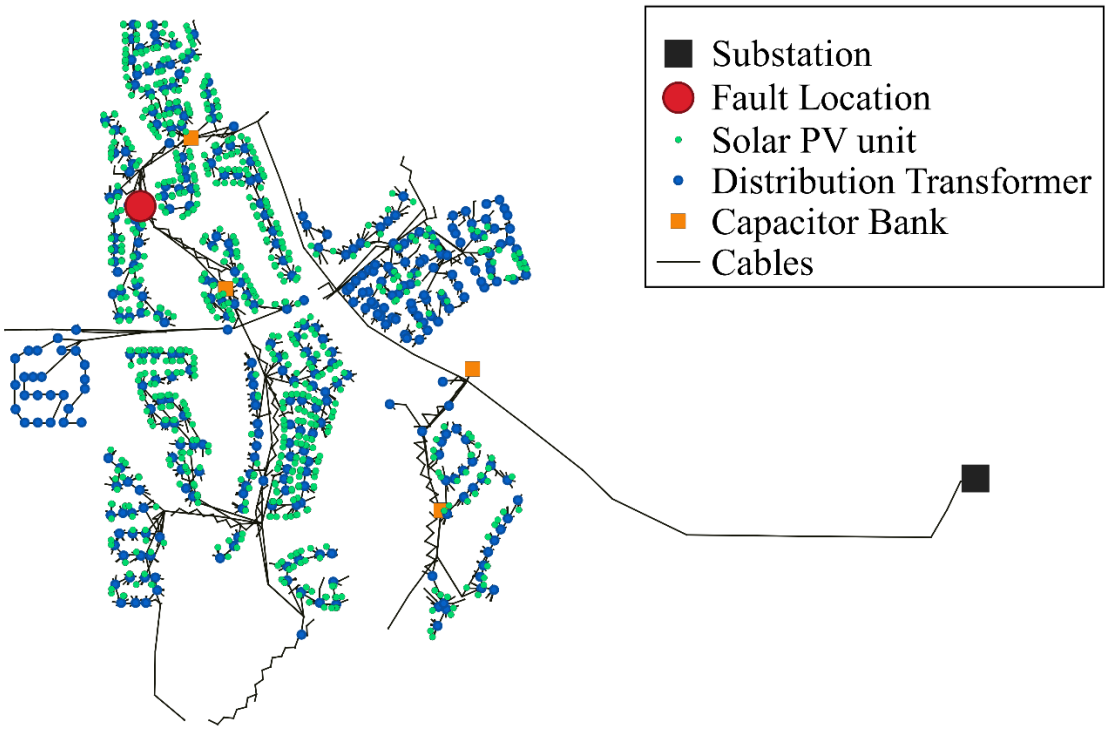

Figure 4.1 Circuit Diagram of the Modeled Feeder Showing the Fault Location

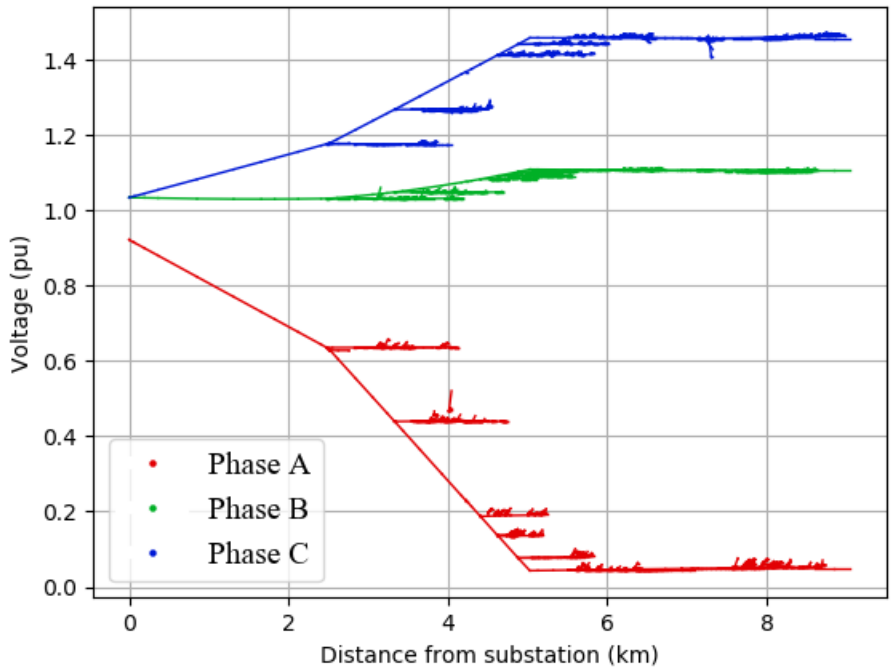

Figure 4.2 The Voltage Profile of the Feeder under a SLG Fault at the Middle of the Feeder.

For the applied fault, it is seen that a large number of phase C buses (including 507 customer loads) experience voltage of more than 1.2 p.u. For several of these buses with high voltage, the voltage is much higher than 1.2 p.u. and even higher than 1.4 p.u. This can be very detrimental to the customer equipment, resulting in potential degradation/loss of some of the equipment. Additionally, the solar PV units connected to the phase C buses experiencing such overvoltages would also trip, resulting in lost generation. Depending on the solar PV units, it may or may not be possible to connect these units back to the grid automatically even when the fault is cleared - hence it is possible that this loss of generation might sustain for a longer period. In addition, if the solar PV units

connected to the faulted phase A do not ride-through the low voltage during the fault, they may also be lost. For a feeder with a very high penetration level of solar PV resources, the loss of solar PV units connected to two of the three phases would mean a very unbalanced current even when the fault is cleared, and this may trigger a ground/neutral protection device upstream, leading to more disruption to the service – this aspect is explored further in Chapter 6.

To examine and demonstrate the impact of positive and zero sequence impedances on the voltage swell in non-faulted phases, a smaller three-bus circuit is constructed, as shown in Figure 4.3. Here the source is an ideal source operating at 1.0 p.u. on a 12.47 kV line-to-line (LL) root mean square (RMS) voltage base, denoted by V_s. The source bus is connected via a 'long' cable of length around 4000 m to another bus via a shorter cable (having a length of 100 m). The cable impedances used (per unit length) are the same as those for the cable in the actual feeder as obtained from the utility, given in Table 4.1. A load is applied at the end of the shorter cable. A SLG fault is applied at the end of the long cable. The fault response is analyzed analytically to show a similar voltage swell as is seen in the feeder, and this small circuit is also reconstructed in OpenDSS and PLECS simulation as a validation.

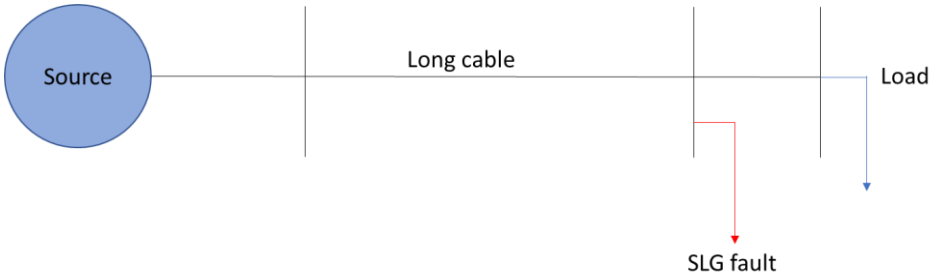

Figure 4.3 Small Three Bus Circuit Constructed to Show the Impact of the Cable Impedance and Unbalanced Fault Currents on the Voltage Swell Caused During the SLG Fault on the Feeder

Table 4.1 The Cable Impedances for the Small Circuit

Quantity	Value (Ω/m)
Zero sequence resistance $\boldsymbol{R_0}$	2.79E-04
Positive sequence resistance $\boldsymbol{R_1}$	5.49E-05
Zero sequence reactance $\boldsymbol{X_0}$	5.13E-05
Positive sequence reactance $\boldsymbol{X_1}$	5.83E-05

Considering the voltage and power bases of 12.47 kV (LL,RMS) and 100 MVA, the total impedance of the fault ("Z_f") would be 0.032 p.u. Note that the equivalent impedances at the fault location for zero and positive sequence (Z_{kk0} and Z_{kk1}) are equal to the total zero and positive sequence impedances for the long cable, since the voltage source considered is ideal. These are computed to be 0.72+j0.13 p.u. and 0.14+j0.15 p.u. respectively. The positive and negative sequence impedances are assumed to be equal. Now, for a SLG fault, we can compute the fault current using the following formula by constructing an equivalent sequence impedance network:

$$I_f = \frac{V_s}{Z_{kk0} + Z_{kk1} + Z_{kk2} + 3Z_f} \tag{4.1}$$

The value of the fault current thus computed is 0.790 -j0.311 p.u. The three sequence voltages at the fault location are given by:

$$V_{ka0} = -Z_{kk0} I_f, \tag{4.2}$$

$$V_{ka1} = V_s - Z_{kk1} I_f \tag{4.3}$$

$$V_{ka2} = -Z_{kk2} I_f \tag{4.4}$$

The sequence voltages calculated using these formulae have magnitudes of 0.62 p.u.,0.85 p.u. and 0.17 p.u. for the zero, positive and negative sequence voltages respectively. Converting the sequence voltages to the phase voltages, we get magnitudes of phase A, B and C voltages to be of magnitudes of 0.08 p.u., 1.16 p.u., and 1.42 p.u. respectively, which is close to the voltages seen for the feeder. This small circuit is also constructed in OpenDSS and PLECS and the simulations in both packages yield similar values for the voltages at the fault location, as shown in Figure 4.4.

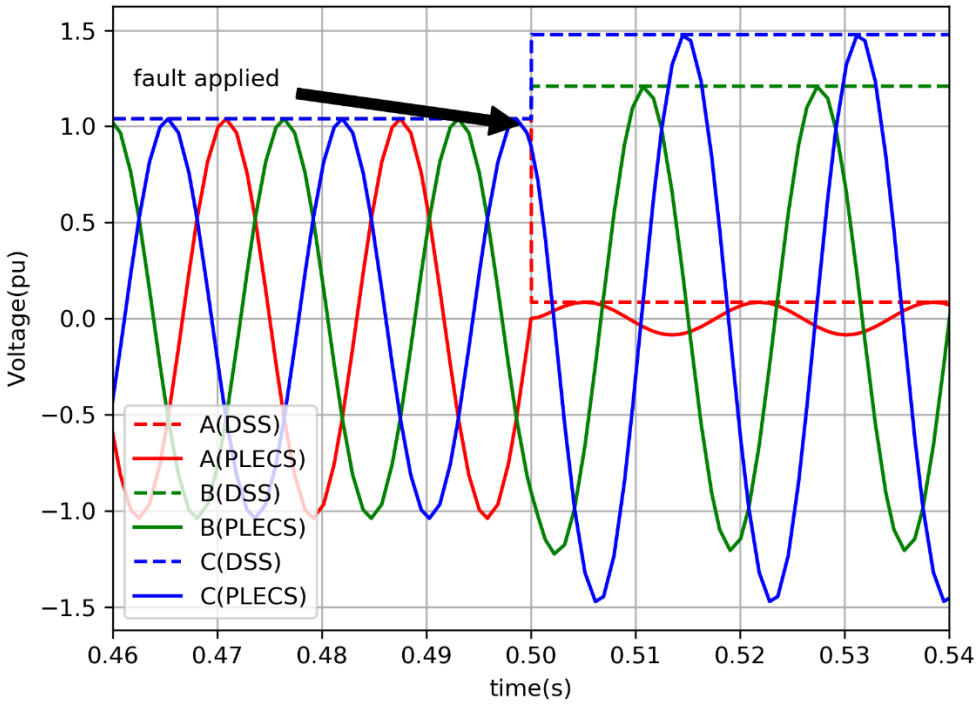

Figure 4.4 The Three Phase Voltages at the Fault Location for the Small Circuit in OpenDSS and PLECS.

The ratio of zero and positive sequence impedance has been shown in the literature as to be a potential reason for the voltage swell on the non-faulted phases. In [112], it is discussed that for a SLG fault, the voltage in the non-faulted voltage can take values of more than 1.2 p.u. for the values of X_0/X_1 of more than 2 or for the values of R_0/X_1 of more than approx. 0.8 depending on the grounding. However, the analysis presented in [112] pertains to the fault at the substation. In [108], it is shown that the non-faulted phases experience voltages above 1.2 p.u. when a SLG fault is applied to the system for X_0/X_1 between 0.5 and 5 for the values of R_0/X_1 above 1. In both these references, R_1 is

considered to be very small, which is not true for the modeled feeder/representative circuit. The zero and positive sequence impedances at the fault location for the representative circuit yield X_0/X_1=0.86 and R_0/X_1=4.5 while for the modeled feeder X_0/X_1=1.24 and R_0/X_1=1.5 at the fault location, where the differences in the values between the feeder and the representative circuit are due to different representations of the substation and the presence of different types of cables in the feeder.

4.3 Possible Alleviation of the Voltage Swell Using Solar PV Resources

For a feeder with a very high penetration level of solar PV units, the DERs installed on the feeder may be able to alleviate the voltage swell during the fault to an extent. It was assumed in this part of the study that all the installed inverters in the feeder would be capable of staying connected to the feeder and implementing advanced inverter controls. Unity power factor was selected as the base control scenario, and the results presented in the previous section model all solar PV inverters to be using unity power factor control. Unity power factor is also found in most residential solar PV units presently installed in the field. For volt-VAr and volt-watt control, the default values of the Q vs V or P vs V curves were used from the IEEE 1547-2018 Standard. In each control scenario, a fault with the same fault impedance was applied at the same location. The voltage profiles for phase C voltages for these three control scenarios are shown in Figure 4.5. It is seen that the volt-VAr and volt-watt controls with the chosen Q vs V or P vs V curves only slightly reduce the voltage swell, having a small impact.

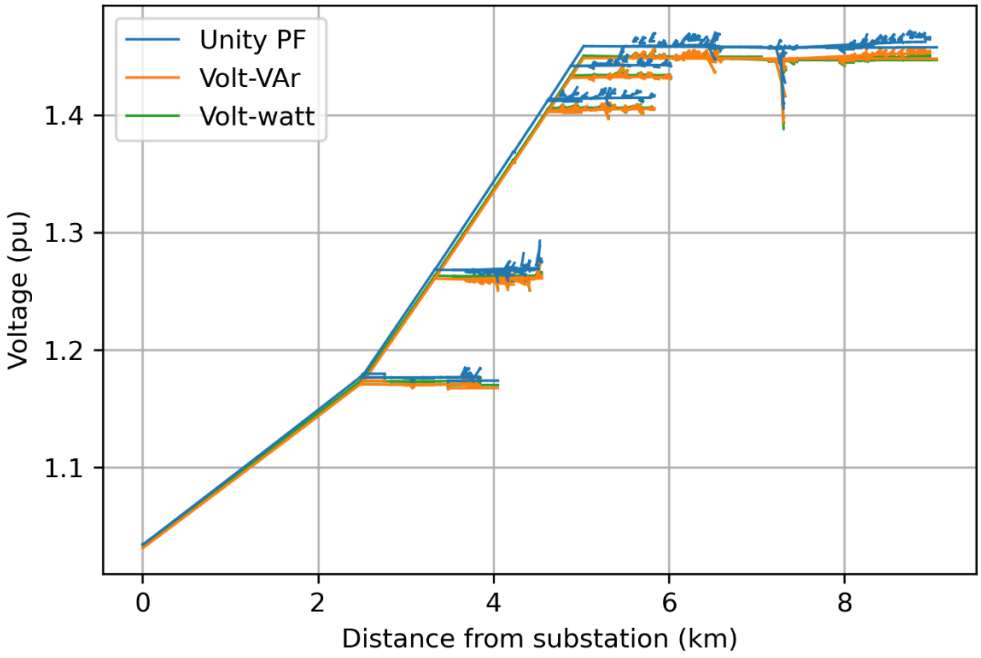

Figure 4.5 The Phase C Voltage Profile for the Feeder under SLG Fault under Different Solar PV Control Scenarios

To find a control suitable for reducing the voltage swell, various levels of reactive power absorption/injection were tried for the solar PV units connected to one of the three phases. In each case, the active power was set according to the apparent power rating of the inverter, giving preference to the reactive power. Unity power factor was used as the control strategy for the inverters in the other two phases. The inverters in phases A and B were not found to be very effective in reducing the voltage swell for phase C, regardless of the reactive power injection/absorption. Figure 4.6 presents the number of buses on phase C at various voltage levels (bins) for the different reactive power injections/absorptions by the inverters connected to phase C. The maximum reduction in

the voltage swell was when the solar PV inverters connected to phase C absorbed reactive power equal to their apparent power ratings.

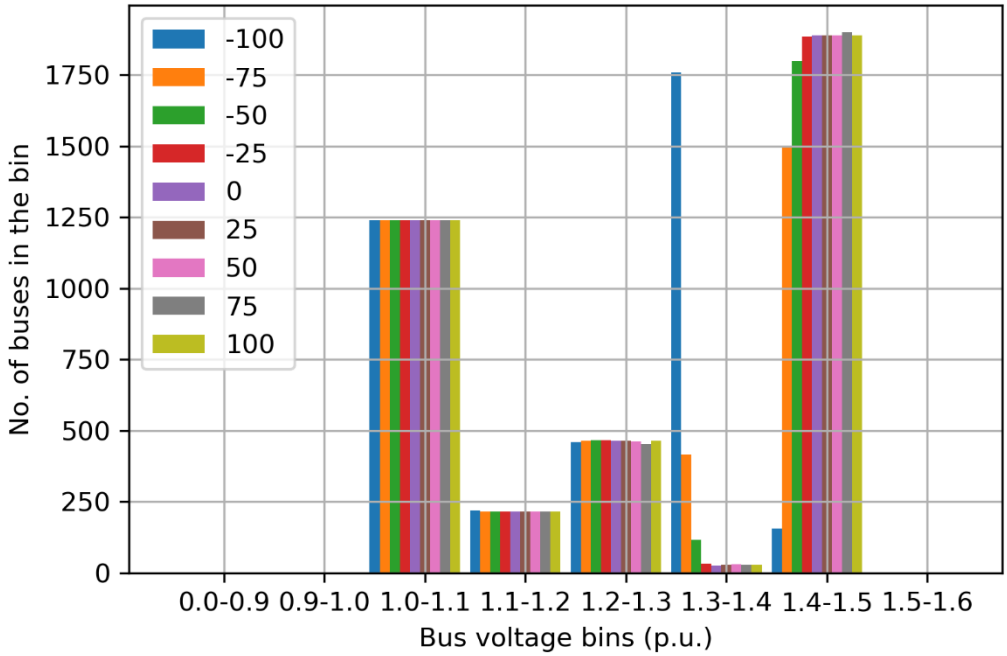

Figure 4.6 Histogram of the Phase C Voltages for Different Reactive Power Absorption/Injection Control Implemented for Phase C Inverter for Feeder under SLG Fault. The Numbers in the Legend Indicate the Reactive Power as a Percentage of the Apparent Power Rating

Hence, this control was tested for different penetration cases developed (Section 3.4) where if the voltage at the inverter terminal is very high (true for solar PV inverters connected to phase C), it would absorb reactive power equal to its apparent power rating, otherwise (for solar PV inverters connected to phases A and B) it would use unity power factor control. With this control, the voltage profile for the feeder under the fault is plotted for varying solar PV penetration levels in Figure 4.7. It is seen that the solar PV

units are able to reduce the severity of the voltage swell using this control, however, the voltage swell is not completely eliminated even at the highest penetration scenario of around 801% instantaneous solar PV penetration level. Nevertheless, the reduced severity of the voltage swell would still lessen the impact of the voltage swell on the feeder since many buses would not experience voltages above 1.2 p.u. because of this reduced severity of the voltage swell. At the present penetration of 237%, implementing the proposed control would bring down the maximum voltage from 1.47 to 1.41 p.u., and to 1.32 p.u. at 801% penetration level. At this high penetration level, 1914 buses and 341 customer loads would face voltages above 1.2 p.u. compared to 2376 buses and 532 loads at the present penetration level. Another benefit is that because of the implemented control, instead of all solar PV units (1.3 MW) connected to phase C being tripped due to the SLG fault, 1.2 MW generation would be lost for the present penetration level. Another feature seen from Figure 4.6. and Figure 4.7. is that there is a significant voltage drop which is seen across the secondary circuits, highlighting the importance of modeling the secondary circuit to accurately capture the voltage at the terminal of the solar PV units.

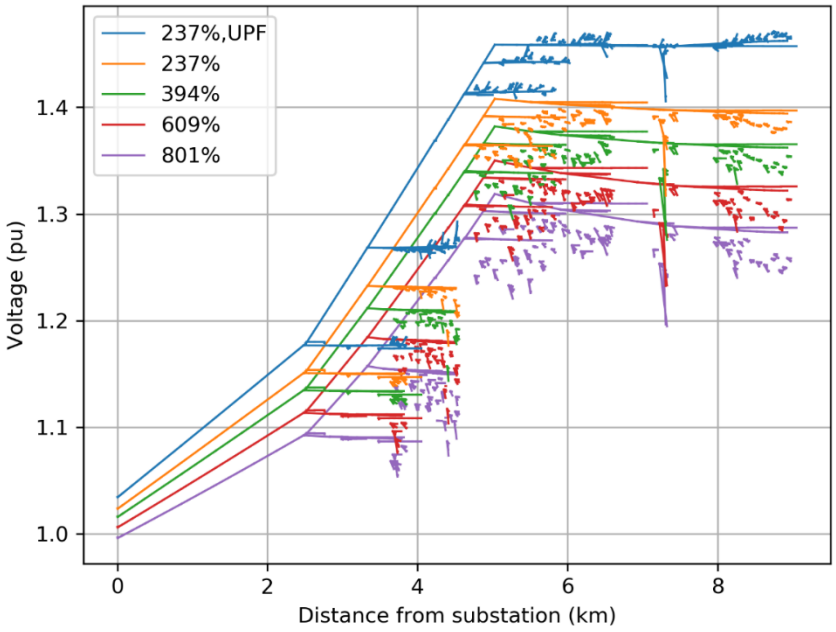

Figure 4.7 The Phase C Voltage Profile for the Faulted Feeder under Different Solar PV Penetration Levels for the Described Control, with the Base Penetration Unity Power Factor Voltage Profile (Blue) as a Comparison

5 SUB-TRANSMISSION-DISTRIBUTION CO-SIMULATION: POWER FLOW

In addition to describing the co-simulation framework, an extended network model is developed adding more feeders and sub-transmission network to the feeder model developed in Chapter 2. This chapter begins by describing the T&D network model developed and presenting the validation of the network model in Section 5.1. In Section 5.2, the process followed in creating time-series models for the T&D network is given, along with the validation of the T&D co-simulation power flow time series simulations against field measurements. Section 5.3 presents the steady-state aspects highlighting the importance of modeling the secondary network.

5.1 Validation of the T&D Power Flow: Snapshot

The feeder model described in Chapter 2 is extended to include a larger network in the distribution system, and the sub-transmission network in the vicinity of this distribution system is also modeled, thus extending the network representation to perform T&D co-simulation studies. The selected distribution network comprises of four feeders in addition to the feeder model described in Chapter 2 fed by two substation transformers located at a substation. All five feeders are modeled in OpenDSS, divided into two distribution systems according to the substation transformer they are fed by. Each feeder has around 1660 primary sections and around 300 distribution transformers. Here, "Feeder 1" is the feeder modeled in detail, described and used in this dissertation thus far. The OpenDSS models for the other four feeders are created from CYME models provided by the utility using the developed CYME to OpenDSS tool [22]. These four feeders are modeled in 'primary-only' fashion i.e., till the distribution secondary transformers. At each distribution transformer, an aggregate load (and an aggregate solar

PV unit where applicable) is added. Some key characteristics of the five feeders are given in Table 5.1. Compared to Feeder 1 modeled in detail which has a very high solar PV penetration, the other four feeders have relatively less solar PV penetration. Figure 5.1 shows the single line diagrams of all five feeders.

Table 5.1 Key Characteristics of the Modeled Feeders

Primary sections	1790	1784	1897	1160	1697
Distribution transformers	371	382	391	201	284
Capbanks (1.2 MVAr each)	4	3	2	4	4
Peak active power requirement (MW) on July 15, 2019	7.35	6.57	10.02	5.6	6.62
Peak solar PV production (MW) on March 15, 2019	3.82	1.94	1.81	1.90	0.78
Peak reverse power flow (MW) on March 15, 2019	2.13	0.5	0.17	0.54	0

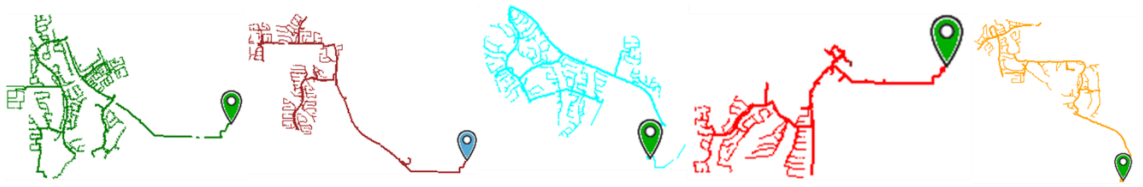

Figure 5.1 Single Line Diagrams of the Five Modeled Feeders. The Pin Indicates the Location of the Substation.

The sub-transmission system modeled includes the selected substation ("S1") and two other substations connected to it ("S2" and "S3"). These two substations connect to the bulk transmission network; hence the rest of the network is modeled using a Thévenin equivalent voltage source representation at S2 and S3 including the transfer impedance, using the equivalent impedances for the rest of the transmission network at the three

substation locations obtained from the utility. This choice of retaining the two substations directly connected to S1 was made in order to capture the redundancy which is inherently required to keep the distribution system operational even if one of the sub-transmission lines/sources fail. However, the formulation is general, and it is possible to extend the representation of the sub-transmission network to include a wider area or higher voltage levels without loss of generality. For such an extension, one needs to model the appropriate network including the sub-transmission/transmission lines and the step-up transformers. Further, in this case the generating stations are electrically distant from the chosen sub-transmission circuits, so the Thévenin equivalent voltage representation of the bulk transmission network is sufficient to examine the T&D interactions.

For modeling the sub-transmission network, the positive sequence line data was obtained from the utility, and negative and zero sequence data were generated using the negative and zero sequence to positive sequence impedance ratios of lines of similar length. The impedance of the substation transformers and the substation circuity was also obtained from the utility. The two substation transformers have delta to wye-grounded configuration, with delta configuration on the high voltage side. Substation transformer T1 is connected to Feeder 1, Feeder 4, and Feeder 5, whereas substation transformer T2 is connected to Feeder 2 and Feeder3. The high voltage (69 kV) bus at substation S1 is selected as the boundary between the distribution and sub-transmission networks. Figure 5.2 describes the circuit schematic and the division of the overall system into transmission and distribution subsystems.

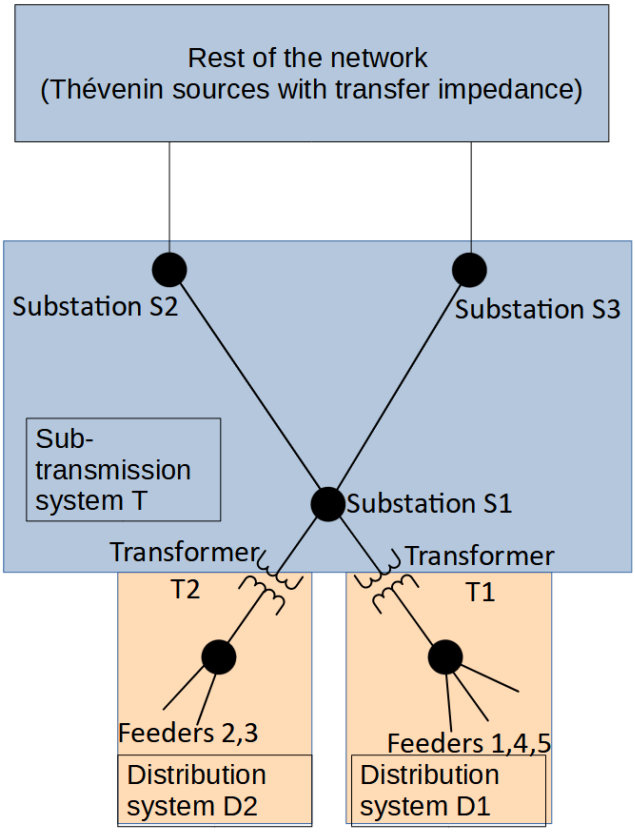

Figure 5.2 Schematic of the Sub-transmission and Distribution Networks Modeled

The validation of the co-simulation is performed by considering the values from the T&D co-simulation in two stages. In the first stage, the values at the boundary bus are compared. For a successful T&D co-simulation, the values of currents and voltages across the boundary would be consistent in the distribution and sub-transmission models. A good match here would indicate that the co-simulation power flow is run successfully. In the second stage, the values obtained from the co-simulation power flow for the sub-transmission and distribution feeder-head power flows and distribution AMI voltages. A

good match for this stage would indicate that the co-simulation power flow accurately represents the network conditions for the selected snapshot.

The operating point chosen for the validation corresponds to the utility network on July 15, 2019 at 17:00 (5 PM). At this operating point, the total load in the distribution systems is approximately 33.9 MW, while the solar PV generation in the distribution system is approximately 2.9 MW. This operating point is selected keeping in mind that the utility network experiences the highest loading conditions during summer evenings.

After running the co-simulation power flow, the boundary values at the boundary bus are shown in Table 5.2. Note that in the distribution system, the boundary bus is on the delta (high voltage) side of the delta-wye substation transformers, hence, the boundary bus is disconnected from the rest of the distribution systems in zero sequence. Consequently, the zero sequence values exchanged between the distribution and sub-transmission systems are very small.

Table 5.2 Boundary Values from Co-simulation Power Flow

Boundary Value	**T**	**D1**	**D2**	**Boundary Value**	**T**	**D1**	**D2**	**D1+D2**
V1, p.u.	1.0307	1.0307	1.0307	I1real, p.u.	0.3114	0.1670	0.1444	0.3114
V1, angle (deg)	0.0580	0.0580	0.0580	I1imag, p.u.	-0.0299	0.0029	-0.0328	-0.0299
V2real, p.u.	-1.06E-04	-1.06E-04	-1.06E-04	I2real, p.u.	0.0060	0.0022	0.0038	0.0060
V2imag, p.u.	-2.60E-04	-2.60E-04	-2.60E-04	I2imag, p.u.	-0.0013	0.0033	-0.0046	-0.0013
V0real, p.u.	-6.73E-12	-6.73E-12	-6.73E-12	I0real, p.u.	-7.50E-11	1.06E-10	-1.81E-10	-7.50E-10
V0imag, p.u.	-3.62E-11	-3.62E-11	-3.62E-11	I0imag, p.u.	1.88E-10	2.85E-10	-9.67E-11	1.88E-10

In the second stage, the results from the co-simulation power flow are validated against field measurements. The following field measurements are available for validation:

- Active and reactive power measurements at the heads of the feeder for all five feeders
- Active power flows on the two lines modeled in the sub-transmission network
- Voltage magnitude measurements from AMI meters at 1179 locations on Feeder 1

The errors between the co-simulation and field measurements for active and reactive powers at the heads of the feeders for all five feeders are less than 2%, and the errors for the active power flows on the two lines in the sub-transmission network are less than 5%. This comparison is also given in Table 5.3. A histogram of the errors between the voltage measurements at 1179 locations on Feeder 1 and the corresponding values from the co-simulation are given in Figure 5.3. The figure shows that these errors are less than 2% for most of the meters. These low errors indicate that the co-simulation model operating point closely represents the actual operating point of the system.

Table 5.3 Comparison of Co-simulation Feeder-head and Sub-transmission Values with Field Measurements, July Snapshot

Location	Quantity	Measured value (MVA)	Co-simulation value (MVA)	Error (%)
Feeder 1	P	5.9789	5.9847	0.10
Feeder 1	Q	0.5228	0.5169	1.14
Feeder 2	P	5.6638	5.6658	0.03
Feeder 2	Q	1.1451	1.1477	0.23
Feeder 3	P	9.1675	9.1674	0.001
Feeder 3	Q	1.5055	1.5088	0.22
Feeder 4	P	5.1313	5.1307	0.01
Feeder 4	Q	-1.6528	-1.6448	0.48
Feeder 5	P	6.0399	6.0391	0.01
Feeder 5	Q	-0.0579	-0.0589	1.70
Line S2-S1	P	36.9	35.48	3.85
Line S3-S1	P	-3.1	-3.18	2.58

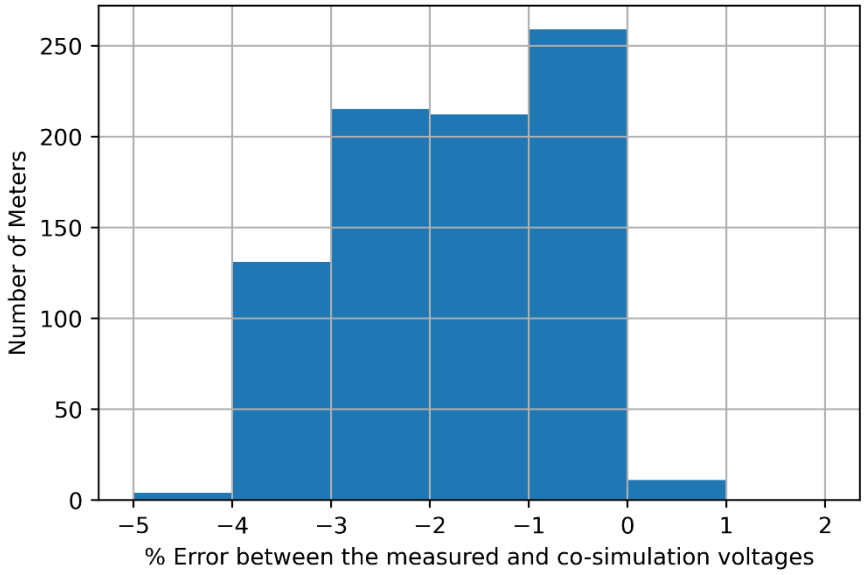

Figure 5.3 Histogram for the Errors Between the Measured and Co-simulation Voltages for the AMI Meters on Feeder 1, July Snapshot

Another operating point is chosen to correspond to 15 March 2019 at 1 PM. This operating point corresponds to a large solar PV generation and low load scenario and also corresponds to the peak reverse active power flow for this feeder for 2019. A comparison of the sub-transmission and feeder-head quantities is available in Table 5.4 and the voltages from the co-simulation are compared against the AMI voltage measurements in Figure 5.4.

Table 5.4 Comparison of Co-simulation Feeder-head and Sub-transmission Values with Field Measurements, March Snapshot

Location	**Quantity**	**Measured Value (MVA)**	**Co-simulation Value (MVA)**	**Error (%)**
Feeder1	P	-2.12846	-2.1467	0.86%
Feeder1	Q	-0.20775	-0.2017	-2.92%
Feeder2	P	-0.50923	-0.5098	0.11%
Feeder2	Q	-0.252	-0.2513	-0.29%
Feeder3	P	-0.17511	-0.1755	0.24%
Feeder3	Q	-0.08408	-0.0834	-0.77%
Feeder4	P	-0.53752	-0.5381	0.11%
Feeder4	Q	-1.26713	-1.2488	-1.45%
Feeder5	P	0.44441	0.4441	-0.06%
Feeder5	Q	-1.47952	-1.4581	-1.45%
S3-S1	P	4.7000	4.9000	4.26%
S2-S1	P	-8.0000	-7.7300	-3.37%

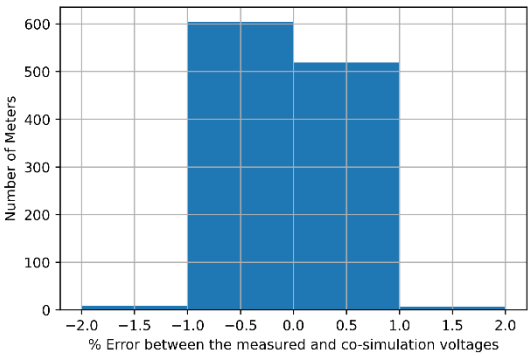

Figure 5.4 Histogram for the Errors Betwen the Measured and Co-simulation Voltages for AMI Meters on Feeder 1, March Snapshot

5.2 Time Series Power Flow T&D Co-simulation

In order to validate the T&D co-simulation over a wider range of operating points, the formulation is extended to support a time-series power flow simulation – this formulation is explained in Section 3.1. An accurate time series power flow simulation relies on: (a) accurate network model and (b) accurate time series profiles.

The process used to create an accurate T&D network model is described in Chapter 2 and Section 5.1. A time series simulation of the detailed feeder model for feeder 1 is also presented in Chapter 2 for data corresponding to two different days, and very low errors between the active and reactive powers measured at the feeder-head as well as the voltage magnitudes along the feeder available from various utility measurements and the simulation results are shown for hourly time series simulations of the feeder model. In this section, the process followed to create higher resolution time series models of the T&D co-simulation power flow is described, and the results from the T&D co-simulation time series power flow are compared against available field measurements at the feeder-heads of the feeders.

To create the time series model of the T&D network, the time series profiles for active and reactive powers from the loads and solar PV units as well as the time series profiles for the sub-transmission voltage sources are required. One of the challenges in creating these profiles is to combine the measurements available from the utility that follow different time series resolutions. The data for the feeders consisted of the head of the feeder measurements of the active and reactive power, individual phase currents and phase A voltages for all five feeders for 15 July 2019 and 15 March 2019 with a

resolution of 10 seconds. The data for the Feeder 1 loads and solar PV units measured from the AMI devices were obtained with a resolution of one hour or 15 minutes, depending on the meter. It was observed that the active power measurements for the solar PV units were available with a 15-minute resolution for the majority of the solar PV production meters, whereas the load/billing meters provided hourly measurements for a majority of the meters. For other four feeders, only the AMI meter measurements from solar PV units were available with a 15-minute resolution. The data for the sub-transmission system consisted of the active power and ampere flows on the two lines connected to the modeled substation and the voltage magnitude at one of the substations which we have modeled as a source. The sub-transmission data were available with a resolution of 5-minutes.

The data available from these sources were combined to create time series profiles with 15-minute, 5-minute and 1-minute resolutions. When creating the time series models with this data and running time series co-simulations, Feeder 1 was represented in detail, including the primary and secondary circuits, whereas the other feeders were represented using aggregated 3 phase unbalanced models. Whenever higher resolution data were not available from a particular source, interpolation was used when combining the data. This procedure is shown in Figure 5.5. It is seen that for the hourly model, the loads and solar PV units as well as the feeder-head measurements and sub-transmission measurements are available. For the model with 15-minute resolution, the load time series data were generated using interpolation while the solar PV generation measurements as well as feeder-head and sub-transmission measurements were available. For the time series model with 5-minute resolution, the load and solar PV generation time series models

were extended using interpolation whereas the sub-transmission time series model was formed using available measurements. The time-series model with 1-minute resolution used interpolation for the time series models of loads, solar PV generation as well as sub-transmission sources. In all cases, the feeder-head measurements of combined active and reactive powers from all three phases for all five feeders were available. For Feeder 1, these measurements were used to validate the time series co-simulation results. For other feeders, the feeder-head measurements were used to create the time series models for the feeders represented using aggregate unbalanced load and solar PV generation.

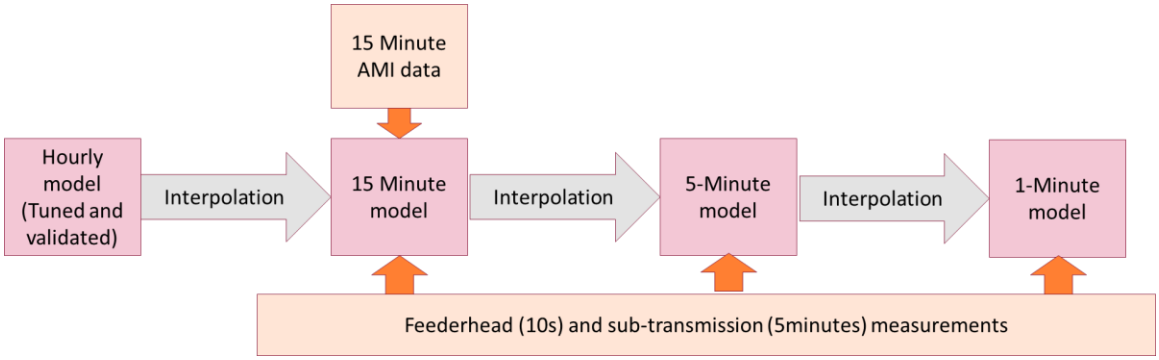

Figure 5.5 The Flow Chart Illustrating the Process Followed to Create the High Resolution Time Series Data

The procedure described above was followed to create time series models corresponding to the day with the high reverse active power case, 15 March 2019. It is seen that the time series models thus created match well with the available field measurements, as seen in Figure 5.6 and Figure 5.7.

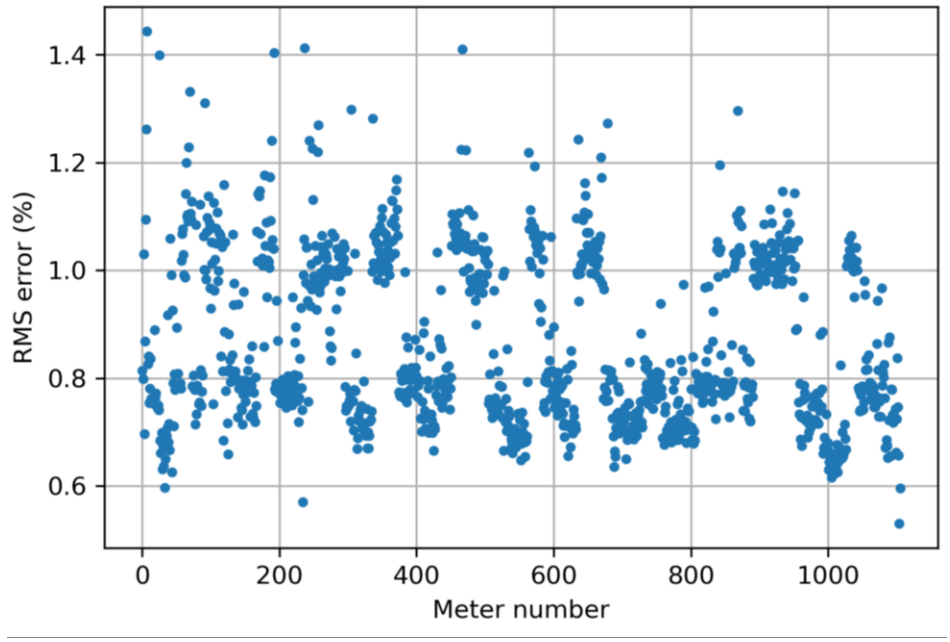

Figure 5.6 RMS Errors for the Comparison Between the Voltage Meter Hourly Measurements and Corresponding Values from the 1-minute T&D Co-simulation Time Series Power Flow

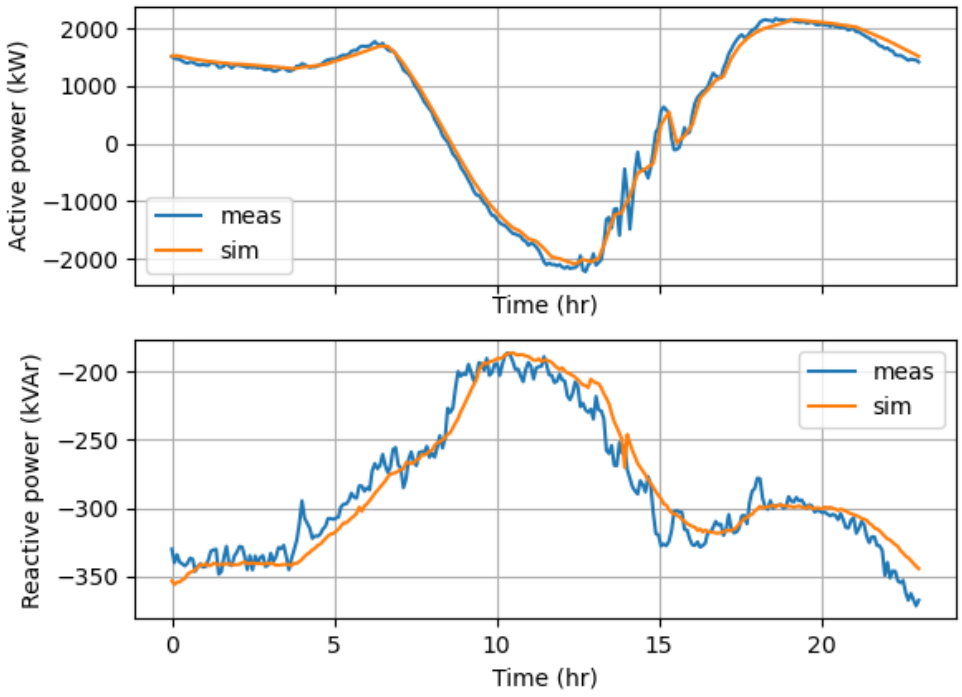

Figure 5.7 Comparison Between the Feeder-head Active and Reactive Power Flow Measured Values Versus 5-minute T&D Co-simulation Time Series for March 15, 2019

5.3 Importance of Modeling the Secondary Network

It is seen throughout the voltage profiles shown in this chapter so far that there is a significant voltage rise across the network due to the reverse active power flow, and some of this voltage rise is across the secondary network. In this section, the importance of modeling the secondary network is assessed. For this purpose, two models of Feeder 1 are considered. The "secondary" model which is described and used so far, where the secondary network is modeled in detail for Feeder 1, and the loads and the solar PV units are located at the household/user locations. Another model, called "primary" model in this dissertation, models Feeder 1 similar to the models of other four feeders, with the load and solar PV units represented in an aggregate manner at the secondary terminal of the distribution transformers, and no representation of the secondary network. These two network paradigms can be explained using Figure 5.8.

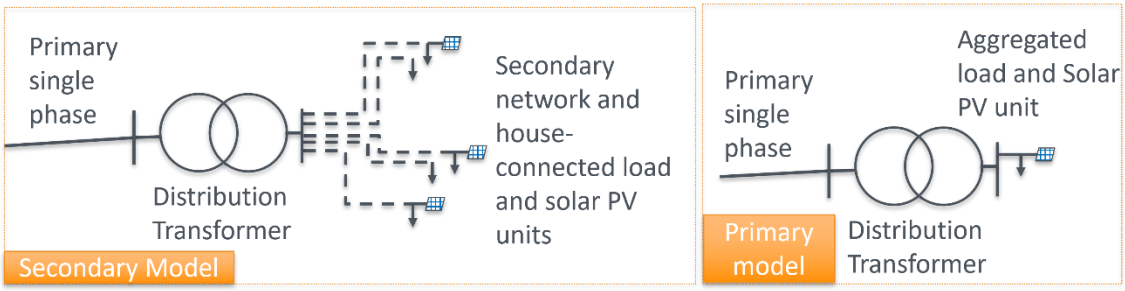

Figure 5.8 A Schematic Explaining the Primary and Secondary Models

It was found that for the steady state, for both unity power factor control and volt-VAr control, the voltages along the feeders as well as the active and reactive powers seen at the head of the feeder for the feeder modeled with the secondary networks were similar

between the primary and secondary models, however, it is noted that there are certain overvoltages observed in the secondary model not observed in the primary model because the voltage rise across the secondary network is not captured, as seen in Figure 5.9.

Due to this voltage difference, the reactive power from the inverters absorbed/injected at the transformer can have a significant difference for volt-VAr control (up to 44% difference for certain transformers) when comparing the two models. This difference between the reactive powers injected/absorbed by the inverters connected to that transformer is shown as a bar chart in Fig. Figure 5.10 for three transformers connected to Feeder 1. Considering all the solar PV units, the combined reactive power injected from all the solar PV units is different by 68 kVAr for the selected operating point (~10% of the total reactive power from all the inverters or 14% of the feeder-head reactive power for this operating point).

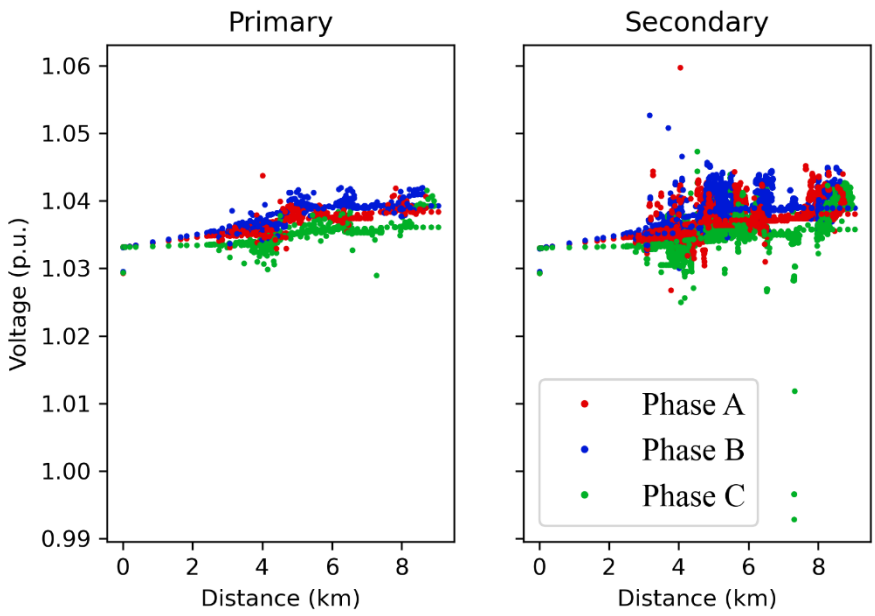

Figure 5.9 Feeder Voltages for Feeder 1 for the Primary and Secondary Models in Steady State with Inverters in Volt-VAr Mode

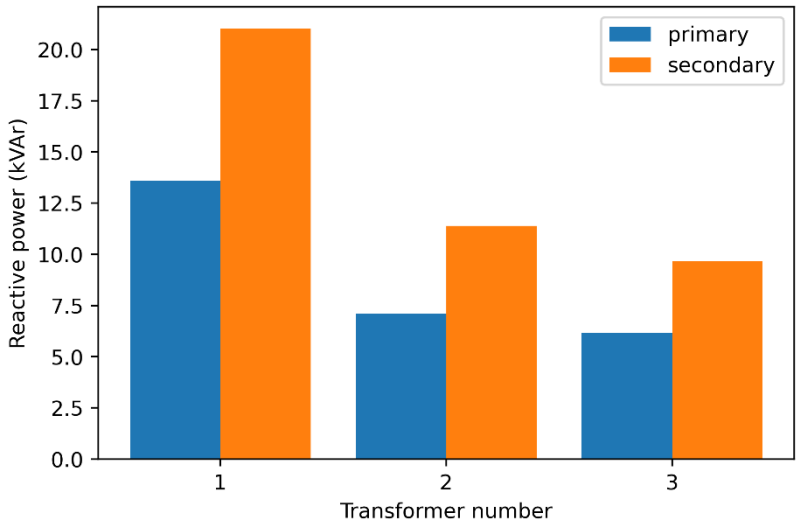

Figure 5.10 The Reactive Power Recorded at Three Transformers When Primary and Secondary Network Models Are Used, with Inverters in Volt-VAr Mode

6 SUB-TRANSMISSION-DISTRIBUTION DYNAMIC CO-SIMULATION

The formulation used in this project for the T&D power flow and dynamic co-simulation is described in the Chapter 3. The previous chapter describes the data creation process and validation of the steady state T&D power flow model. This chapter discusses several case studies using the dynamic T&D co-simulation to highlight the importance of detailed distribution system modeling in/via a dynamic T&D co-simulation.

Four case studies are presented in this chapter. Sections 6.1-6.4 study the response of the feeder modeled in detail to various faults. In Chapter 4, an unbalanced fault on the distribution system was studied. The response of the distribution system to that fault is further investigated in Section 6.1. In Section 6.2, a balanced fault on Feeder 1 is considered. Section 6.3 and Section 6.4 explore the response of the T&D combined system to the unbalanced and balanced sub-transmission faults, highlighting the importance of having a detailed model for representing the distribution systems in T&D co-simulations and the impact different inverter control strategies have on the distribution system response. Section 6.5 explores the importance of modeling the secondary network and its impact on the fault response of the distribution system for certain faults. Section 6.6 presents a preliminary study including grid forming inverter models in the T&D dynamic co-simulation and comparing the response to a fault with grid following and grid forming models.

For all the studies in this chapter, the base operating point is selected to be the snapshot corresponding to 15 March 2019 at 1 PM. This snapshot is selected since it corresponds

to the highest reverse active power flow on the feeder for that year, so the solar PV generation will likely have a large impact on the feeder behavior.

Starting from this operating point, four faults are applied in Section 6.1-6.4, considered as four cases:

- Unbalanced SLG fault on the middle of the feeder
- Balanced 3ϕG fault on the middle of the feeder
- Unbalanced SLG fault on the sub-transmission network
- Balanced 3ϕG fault on the sub-transmission network

In each case, the fault is applied for five cycles (for faults on the sub-transmission network) or fifteen cycles (for faults on the distribution network) and cleared/removed after the fault duration. The fault locations on the distribution system are shown in Figure 6.1. For distribution system faults, the fault location is the same as that discussed in Chapter 5. For the sub-transmission faults, the fault location is selected to be at the middle of one of the sub-transmission lines. For all the faults, the response of the feeder modeled in detail is studied. The solar PV inverters are assumed to have the trip/no-trip response corresponding to the category I inverters from IEEE 1547-2018, so they are assumed to trip for voltages below 0.45 p.u. and above 1.2 p.u. within one cycle. Furthermore, unless otherwise mentioned, the results correspond to solar PV inverters operating at unity power factor mode (similar to how they operate in the field). However, the impact of different inverter abnormal categories as well as advanced inverter controls is also discussed for these faults.

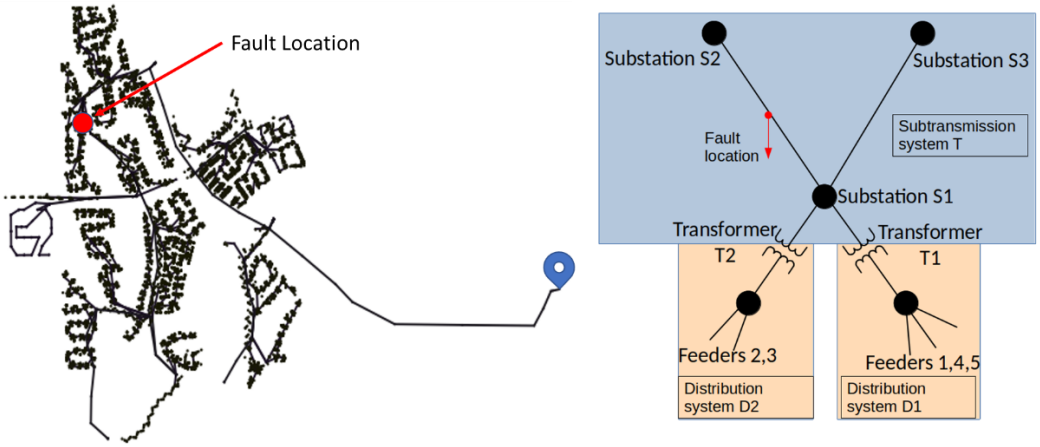

Figure 6.1 The Fault Locations for the Faults on the Distribution and Sub-transmission Network

6.1 Unbalanced Fault on the Distribution System

When a SLG fault is applied on Feeder 1, the voltage profile for the feeders connected to the substation transformer for this feeder is plotted in Figure 6.2. In the figure, for Feeder 1, as seen in Chapter 4, the faulted phase A voltages are very low while phase C experiences a high voltage swell. As a result, within one cycle after the fault is applied, a high number of solar PV units trip for phases A and C. However, for the other feeders connected to the substation transformer, only a small voltage dip at the feeder-head is observed for the faulted phase A, corresponding to the voltage drop across the substation transformer. Hence, the voltage profiles for all three phases for the other phases are relatively flat, as seen in the figure. This phenomenon of a fault on the distribution feeder not affecting the voltage profiles of the other feeders very severely is also observed later in Section 6.2 for a balanced fault applied on Feeder 1.

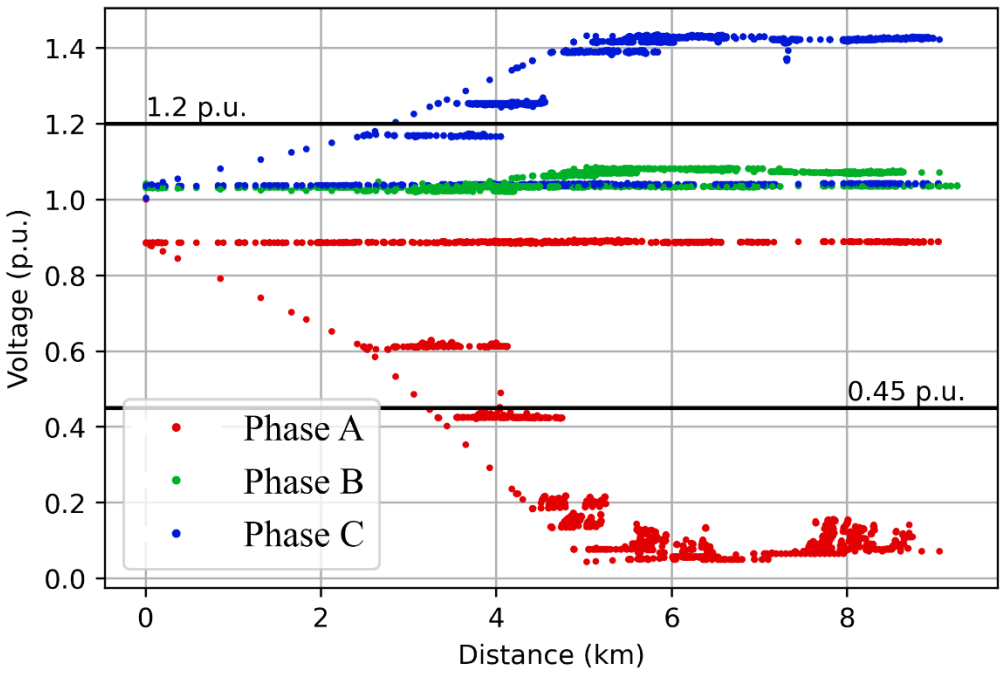

Figure 6.2 The Voltage Profile for the Distribution System with Unbalanced Single Line to Ground Fault on the Distribution Feeder 1

The feeder-head active power for Feeder 1 is plotted in Figure 6.3. When the fault is applied, there is a large increase in the faulted phase A current and power seen at the feeder-head to feed the fault. This results in a loss of approximately 1099 kW generation for phase A and 1314 kW generation for phase C. It should be noted that instead of inverter abnormal response category I from IEEE 1547-2018, a more aggressive category III implementation would see the phase A inverters kept connected though the fault. Hence, there would be a reduction in the solar PV generation lost and no generation would be lost for phase A. However, even the most aggressive Category III mandates the solar PV units disconnect for voltages of more than 1.2 p.u., and the loss of generation

from phase C would be the same even for Category III inverters. The disconnection of the solar PV is reflected in this figure as changes to the active power observed at the feeder-head for phases A and C. When the fault is cleared, this results in phases A and C with forward active power flow while the phase B still has a reverse active power flow because the solar PV units connected to phase B are not tripped – thus creating an unbalance in the post-fault clearance condition.

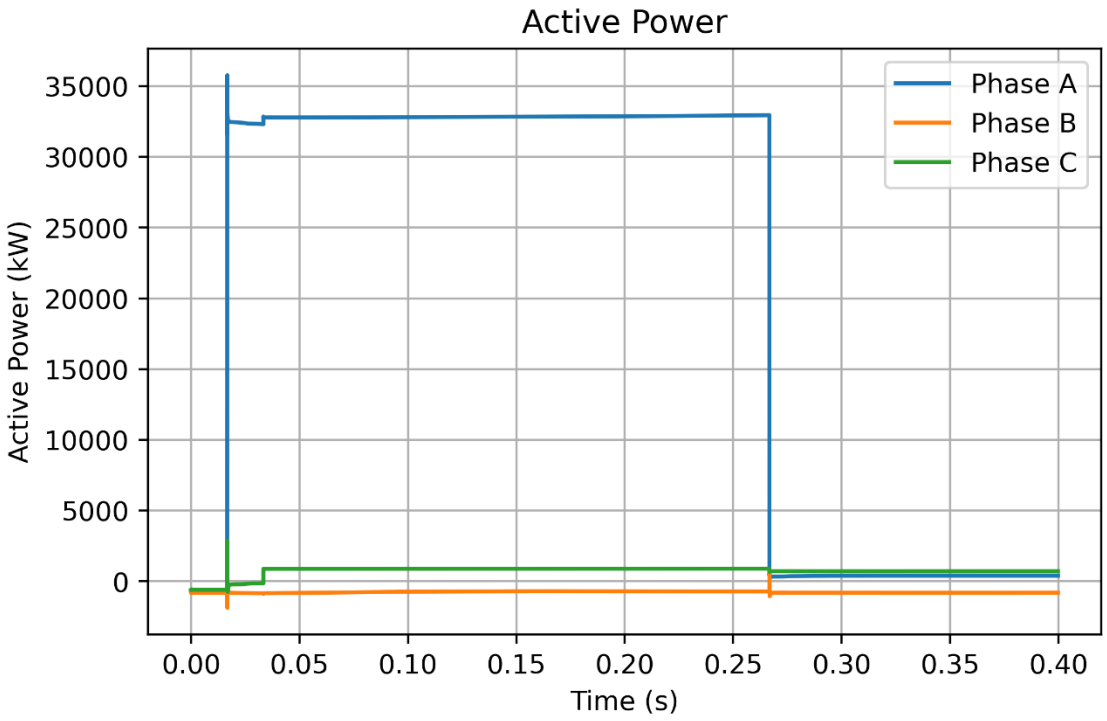

Figure 6.3 Feeder-head Active Power for Feeder 1 for Unbalanced Single Line to Ground Fault

This unbalance is noteworthy since this is a steady-state unbalance. When calculated, the ground current measured at the feeder-head is approximately 190.45 A. For this feeder, there are phase and ground protection relays installed at the feeder-head. While the fault

duration is not high enough where the delayed response phase or ground relays would trip the feeder for these five cycle faults, the ground current in the post-fault clearance condition being comparable to the ground relay pickup current of 300 A is a larger concern, since it will persist much longer as long as no solar PV units connect back automatically. A similar SLG fault was also applied to the modeled T&D network by increasing the penetration of solar PV resources on Feeder 1, and at higher penetrations. It is seen from Figure 6.4 that at 418% penetration level the post-fault clearance ground current goes above the pickup current and would result in the relay tripping the feeder in steady-state even when the fault is already successfully cleared, resulting in a loss of connection for all the customers on this feeder.

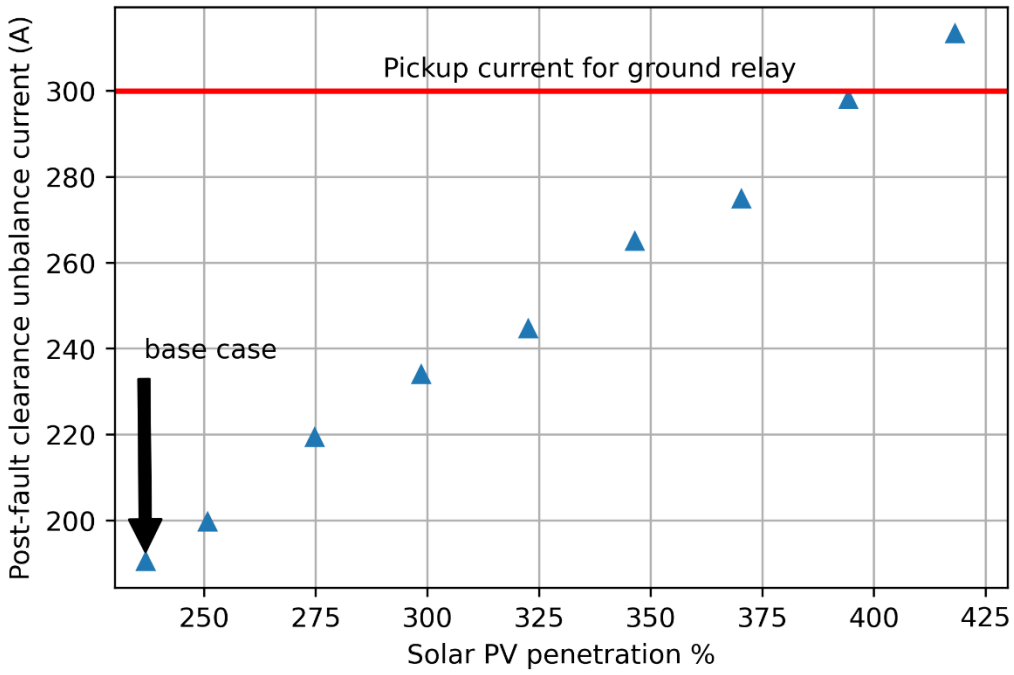

Figure 6.4 The Post-fault Clearance Ground Current for Feeder 1 after Applying a SLG Fault for Different Solar PV Penetration Cases

6.2 Balanced Fault on the Distribution System

For the balanced fault on the distribution system, the voltage profile is shown in Figure 6.5. The figure shows the voltage profiles for all feeders connected to the substation feeding the faulted feeder (Feeder 1 which is faulted, and Feeder 4 and Feeder 5). It is seen that all three phases for the faulted feeder experience very low voltages, with the voltage near the fault location being nearly zero while the other feeders do not experience such low voltages (resulting in a relatively flat voltage profile for those feeders, similar to the observation for unbalanced fault in Section 6.1). This results in most of the solar PV units on the faulted feeder experiencing very low voltages at the terminal, and hence a large amount of solar PV generation trips within one cycle for this fault. This can be also seen in Figure 6.6, which shows the feeder-head active power for the faulted feeder. In this figure, it is noted that before the fault was applied, since the selected base operating point corresponds to a reverse active power flow case, that there is substantial reverse active power flow at the feeder-head for all three phases. When the fault is applied, there is a high current/power in the forward direction from the substation feeding the fault in all three phases. One cycle after the fault is applied, the solar PV units on the feeder trip, which is reflected as a small increase in the active power at the feeder-head. In this case, it is seen that the solar PV units tripping does not have a large impact on the fault current seen at the feeder-head. However, assuming that the tripped solar PV units do not automatically reconnect after the fault is cleared, there is a forward active power demand seen from the feeder due to the loss of generation from the solar PV units. Overall, there is a loss of approximately 1171 kW generation on phase A, 1341 kW on phase B and

1314 kW on phase C. While for the selected operating point, this may not be an issue from the perspective of the overall demand increase from the feeder since the operating point corresponds to a low load scenario, a similar increase in demand when the feeder is operating near the peak demand would be more significant. Note, however, that using category III inverters instead of category I inverters would result in the inverters not disconnecting due to the low voltages caused during the short-duration fault considered and no generation would be lost in such a case.

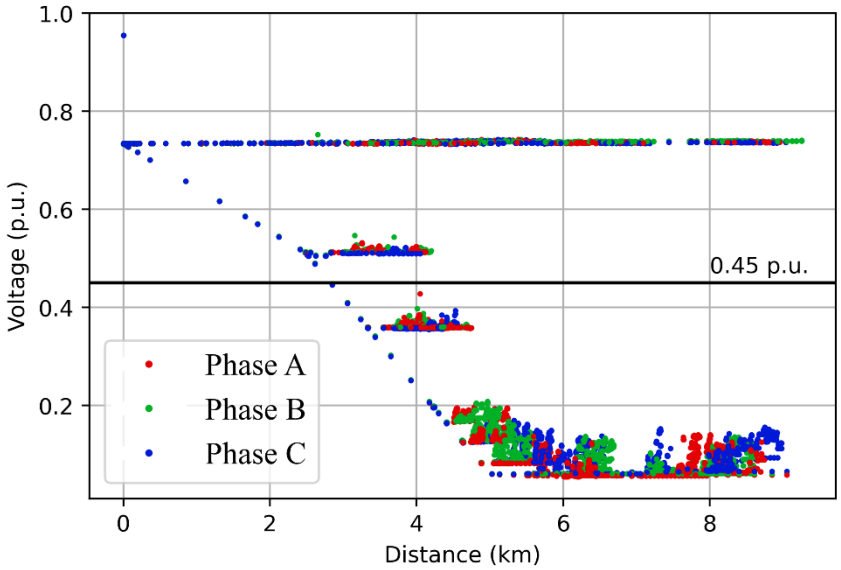

Figure 6.5 The Voltage Profile for the Distribution System with a Balanced Three-phase to Ground Fault on the Distribution Feeder

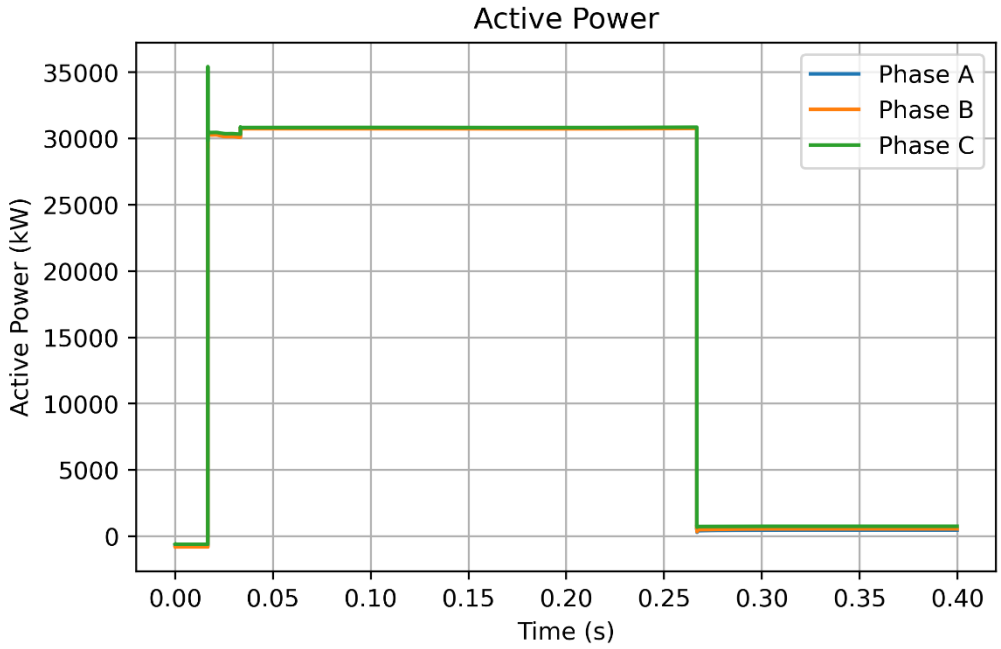

Figure 6.6 Feeder-head Active Power for the Faulted Feeder, Feeder 1, for Balanced Three-phase to Ground Fault

6.3 Unbalanced Fault on the Sub-transmission System

When a SLG fault is applied on the sub-transmission system, assuming the fault is applied on phase A, it is seen that at the boundary bus, the voltage for the faulted phase A has approximately 0.37 p.u. voltage, whereas the other two phases have voltages between 1.13 and 1.15 p.u. However, these voltages are on the high voltage/delta side of the substation transformer. Due to the delta-wye transformer at the substation, two of the phases (A and B) on the feeder experience low voltages between 0.7 and 0.9 p.u. while the phase C voltage is between 1 and 1.1 p.u., as shown in Figure 6.7. These voltages are not so low as to cause any generation to trip. However, due to the low voltages on phases A and B of the feeder, there is an increased reverse active power flow at the feeder-head

for these phases, and a corresponding increased current. It is notable that advanced control modes such as volt-VAr show a greater increase in the current magnitude at the feeder-head, as shown in Figure 6.8.

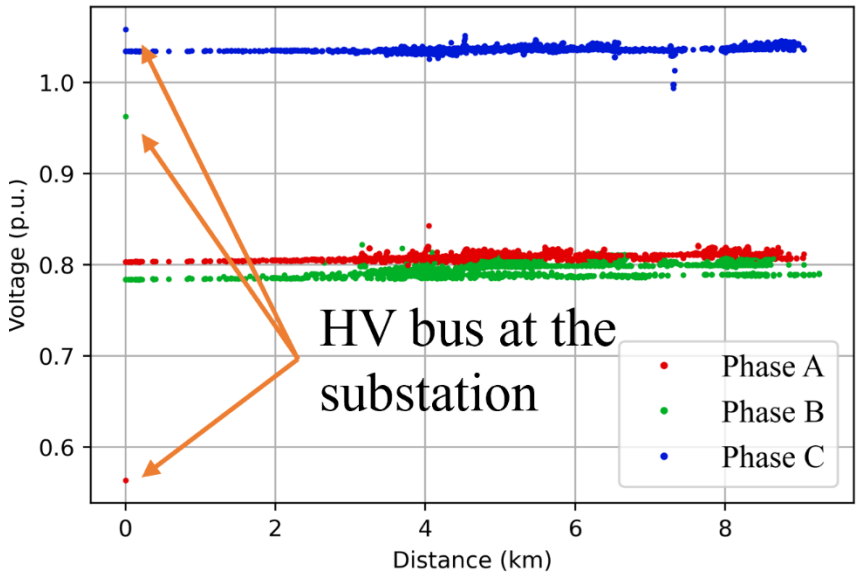

Figure 6.7 The Voltages Profiles for Feeders 1,4,5 Under a Single Line to Ground Fault on the Sub-transmission System

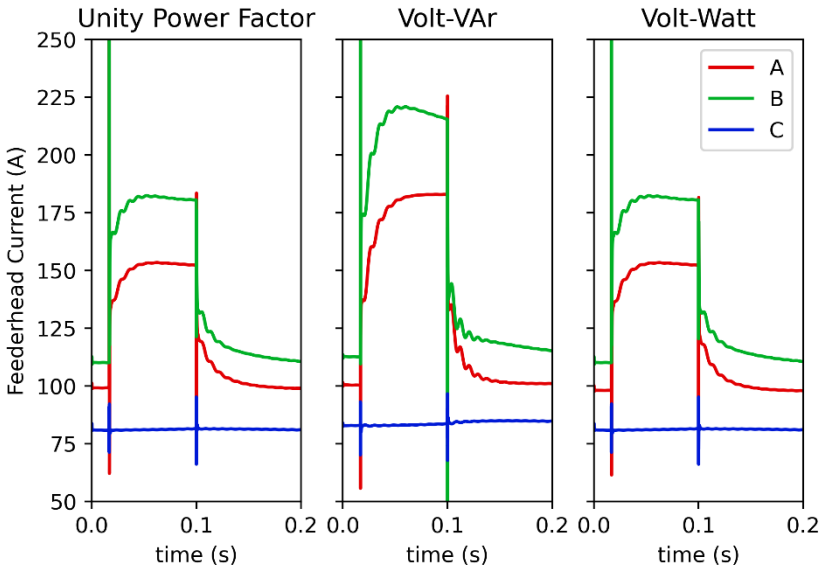

Figure 6.8 Feeder-head Current for Feeder 1 When a Single Line to Ground Fault Is Applied on the Sub-transmission System under Different Inverter Controls

6.4 Balanced Fault on the Sub-transmission System

When a balanced fault is applied at the middle of the sub-transmission network, the boundary bus experiences a low voltage of approximately 0.41 p.u. This results in all three phases on all the feeders experiencing a low voltage. The voltage profile for the feeders Feeder 1, Feeder 4 and Feeder 5 (fed by substation transformer T1) during this fault is shown in Figure 6.9. As seen from the figure, while not all solar PV units experience a voltage below 0.45 p.u. and trip, there is still a loss of 1065 kW, 751 kW and 742 kW on phases A, B and C respectively for Feeder 1.

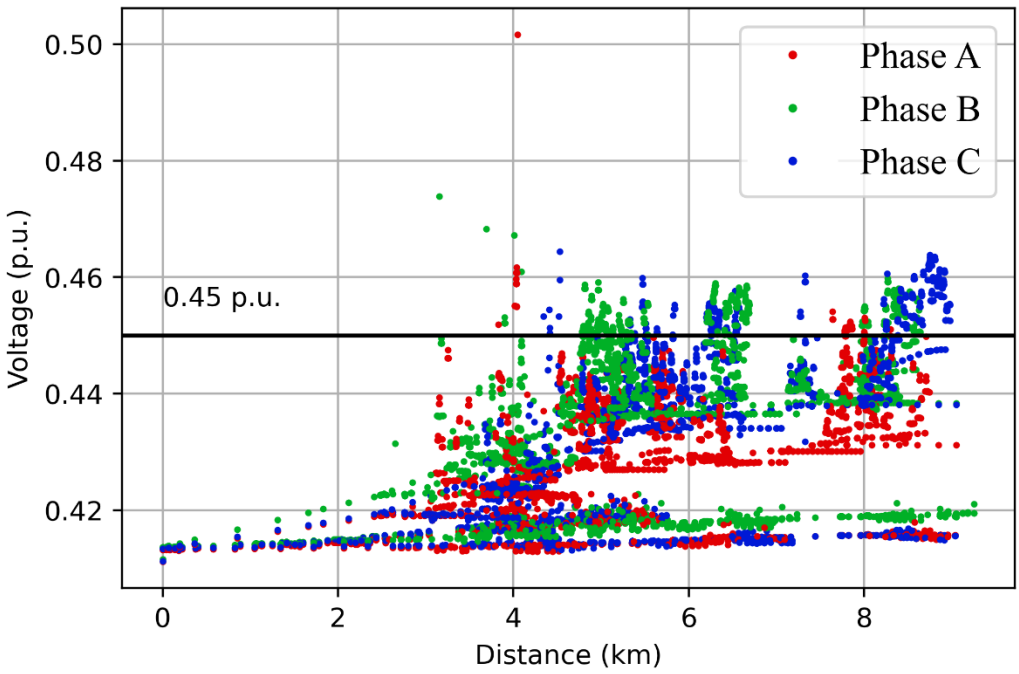

Figure 6.9 The Voltage Profile for the Distribution Feeders 1,4,5 with Balanced Three-phase to Ground Fault on the Sub-transmission System

In terms of the active power seen at the feeder-head of Feeder 1 (shown in Figure 6.10), it is seen that when the fault is applied, the solar PV units on the feeder continue to feed the fault for one cycle. One cycle after the fault is applied, the solar PV units with voltage below 0.45 p.u. trip and there is some loss of generation. After clearing the fault, the active power flow is still in the reverse direction, the magnitude is somewhat less due to the loss of some solar PV generation. However, it is seen from Figure 6.9 that while a lot of the solar PV units experience a voltage above 0.45 p.u., at the feeder-head the voltage is approximately 0.413 p.u. and there is a significant voltage rise along the feeder which allows some of the solar PV units connected to have voltages higher than 0.45 p.u.

However, the other feeders do not have such a high reverse active power flow and corresponding voltage rise, hence, the solar PV units connected to the other feeders would all trip for this case. Hence, for this case it is seen that different feeders may behave differently – this behavior would not be captured by aggregating all the feeders together as a single load while studying this sub-transmission fault.

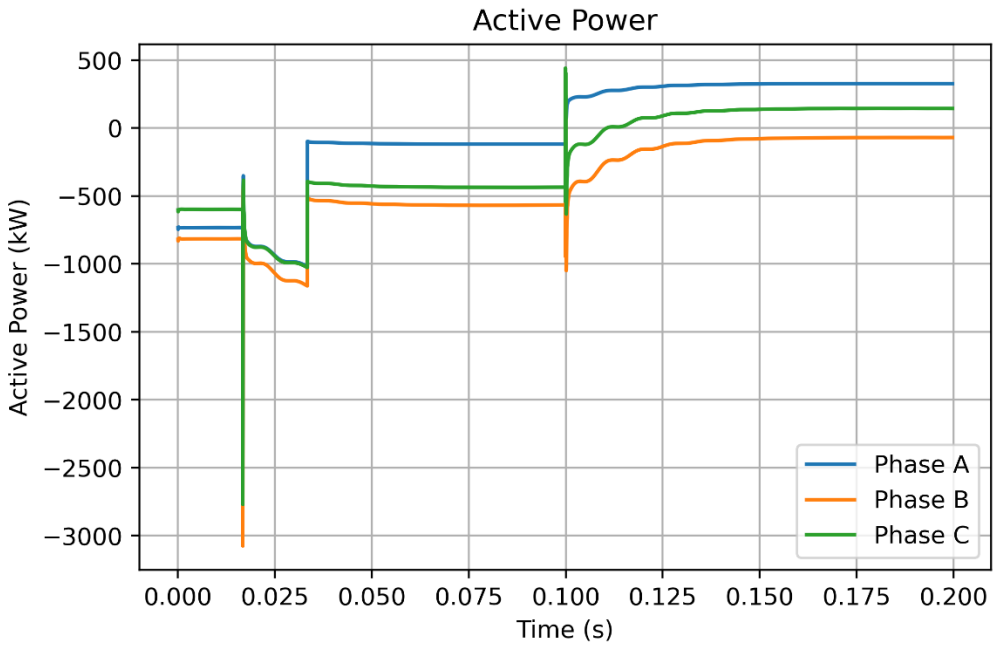

Figure 6.10 The Active Power Observed at the Feeder-head of Feeder 1 When a Balanced Three-phase to Ground Fault Is Applied on the Sub-transmission System

For this fault, it is observed that the voltages for Feeder 1 are close to 0.45 p.u. threshold below which the category I inverters would trip. Hence, instead of using unity power factor mode, if all the solar PV units on Feeder 1 operate in volt-VAr mode, there is a slightly extra voltage rise owing to the extra reverse reactive power, as seen in Figure 6.11. Hence, the solar PV generation lost in this case is reduced to 137 kW for phase A,

81 kW for phase B and 40 kW for phase C. This example shows that the advanced control modes from inverters such as volt-VAr mode could have an impact in terms of generation tripped due to certain sub-transmission events.

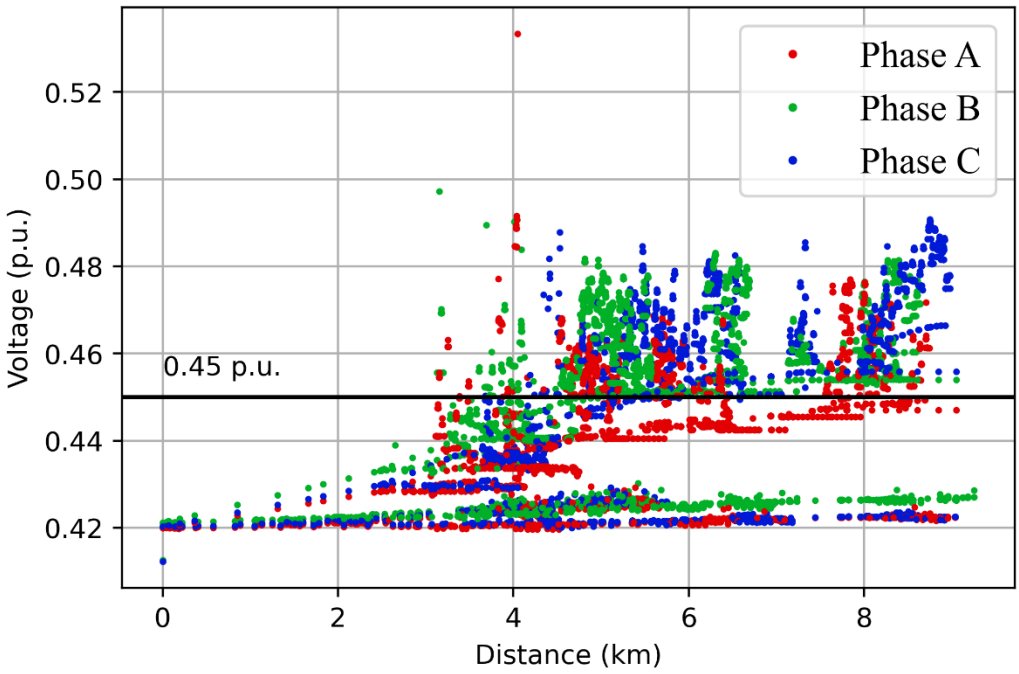

Figure 6.11 The Voltage Profile for the Distribution Feeders 1,4,5 with Balanced Three-phase to Ground Fault in the Sub-transmission System, with Feeder 1 Solar PV Units Operating in Volt-VAr Control

6.5 Importance of Modeling the Secondary Network

In Section 5.3, the steady-state differences between the primary and secondary model are discussed. In addition to the differences in the steady-state such as overvoltages and reactive power from DERs with volt-VAr controls, the similarities and differences between the primary and the secondary model are discussed in this section.

For several balanced/unbalanced faults applied on the distribution and sub-transmission systems, the response for both the systems is similar. For example, Figure 6.12 and Figure 6.13 show the voltage profiles during fault and active powers at the feeder-head of feeder 1 for primary and secondary models when an unbalanced SLG fault is applied on the distribution system as described in Section 6.1.

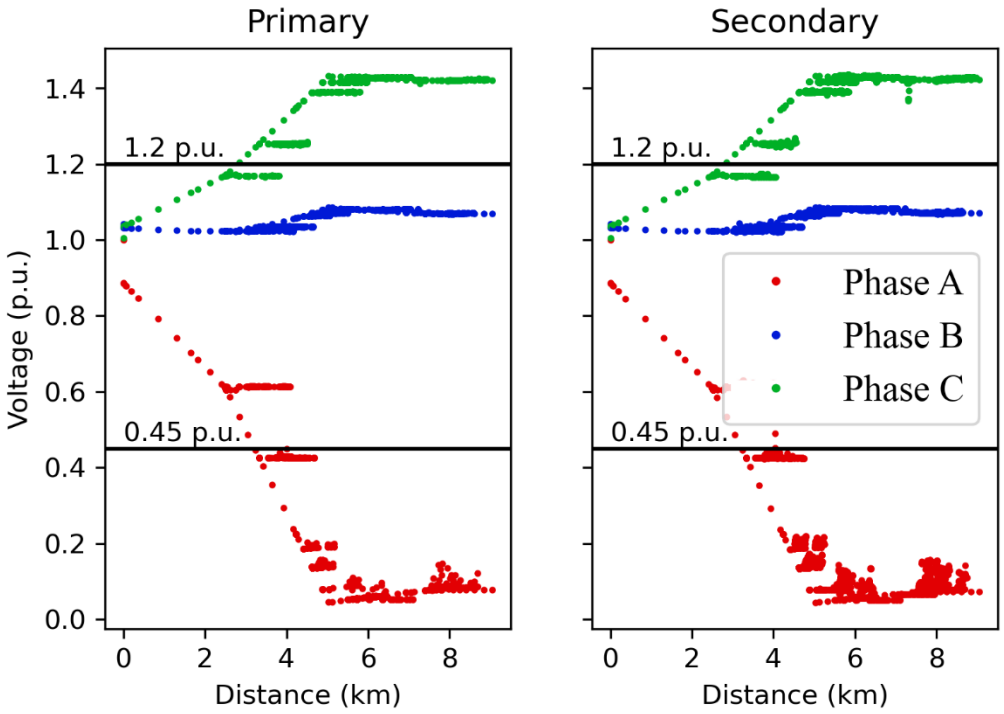

Figure 6.12 Feeder 1 Voltages for Primary and Secondary Model for SLG Fault on the Distribution System

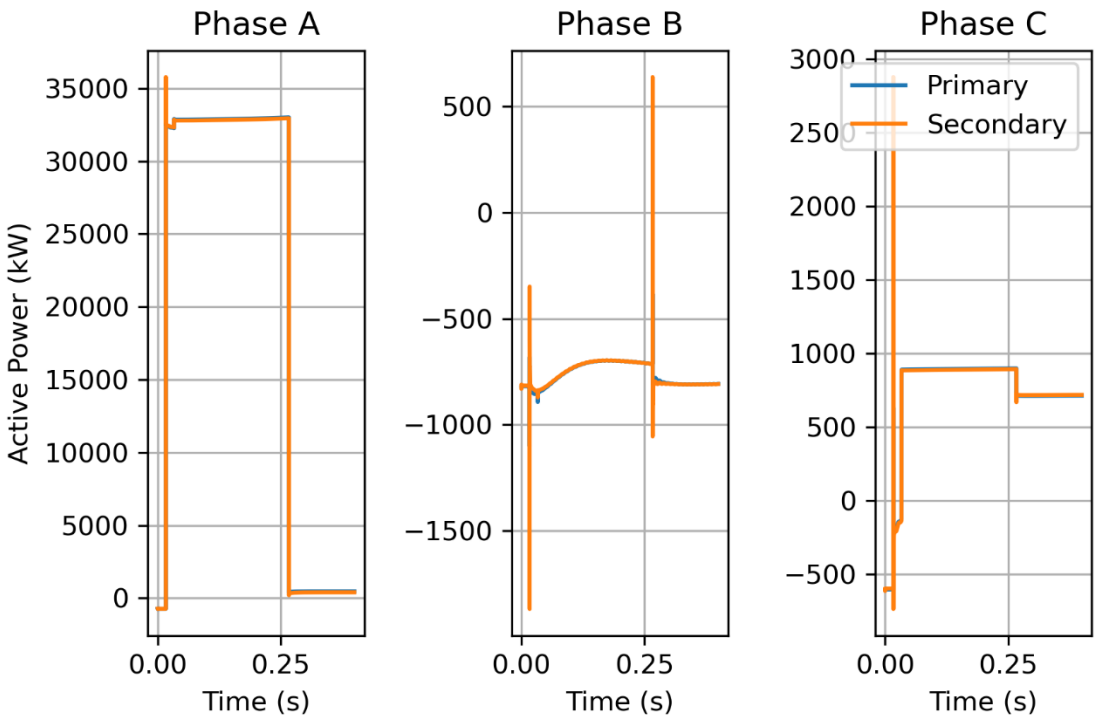

Figure 6.13 Feeder-head Active Power for Feeder 1 During SLG Fault on the Distribution System

However, for certain faults, the voltage at the inverter terminal is above 0.45 p.u. after capturing the voltage rise across the secondary network whereas it is below 0.45 p.u. for the primary model – resulting in a difference in the number of solar PV units which are registered as tripped in both models. For one such case, where a balanced 3ϕG fault on the sub-transmission system applied at the middle of one of the sub-transmission lines, the Feeder 1 voltage profile and the feeder-head active power are shown in Figure 6.14 and Figure 6.15. For this fault, in the primary model, the solar PV generation tripped in phases A, B and C is 1219 kW, 1335 kW and 1175 kW respectively, while in the secondary model, the tripped generation is much less, 1065 kW, 751 kW and 742 kW

respectively. Note that for this study the inverters are kept at unity power factor mode. Hence, it is important to model the secondary network in detail and not modeling the secondary network can lead to an inaccurate response from the distribution model.

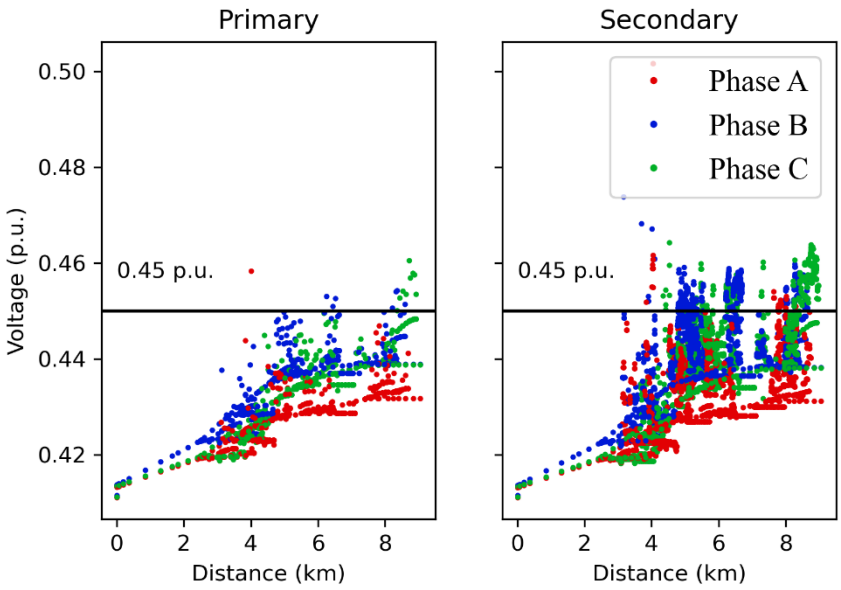

Figure 6.14 Feeder 1 Voltages for Primary and Secondary Model During a Balanced Fault on the Sub-transmission Model

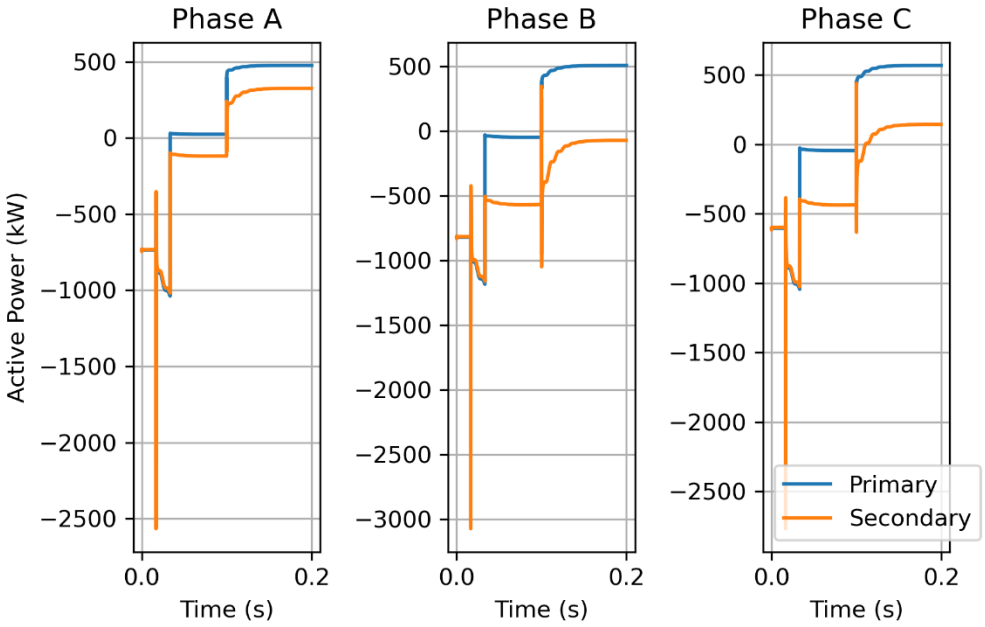

Figure 6.15 Feeder-head Active Power for Feeder 1 Primary and Secondary Model During a Balanced Fault on the Sub-transmission Network

6.6 Grid Forming Inverter Models Simulation with the T&D Network

In this section, an application of T&D dynamic co-simulation using the grid forming inverter model described in Section 4.5 is presented. For this purpose, two network models are considered, denoted by 'detailed' and 'reduced' feeder models. The detailed feeder model represents the network in detail, with both the primary and secondary networks and the loads and solar PV units installed at their actual secondary network locations – the 'detailed' network model is same as the model described and used for various simulations throughout Sections 6.1-6.4. The reduced model is designed to mimic the response of the detailed model by representing the feeder as a three-phase three-segment model. After selecting the initial operating point (March 15, 2019 at 13:00), the

constructed three-segment model can be constructed, as shown in Figure 6.16. For the reduced OpenDSS model, the loads are considered to be constant active and reactive power loads, and the grid following/forming inverter models from Section 4.4 and Section 4.5 are considered. The procedure to create the reduced model from [122] is used.

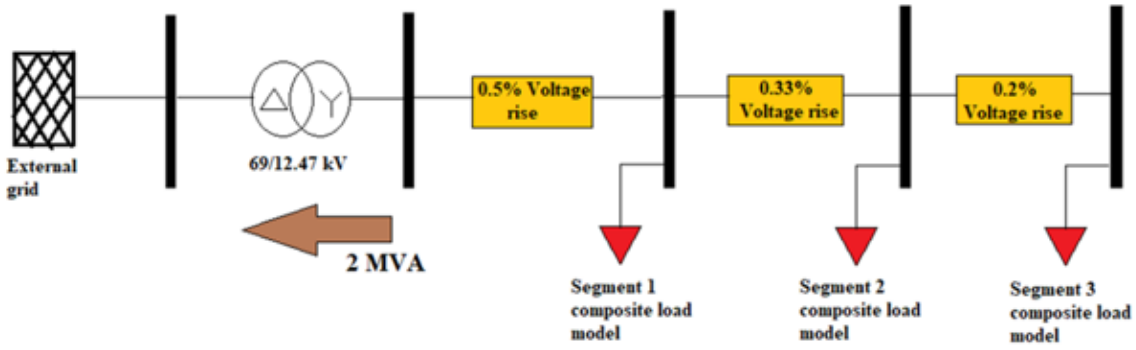

Figure 6.16 Three-phase Three-segment Model of Feeder 1 for March Case

In order to test the efficacy of the developed GFM models with the detailed and the reduced feeder, two co-simulation cases are considered, with (a) the detailed and with (b) the reduced feeder model. In both cases, a five-cycle balanced fault is applied on the sub-transmission system at the middle of one of the sub-transmission lines, as in Section 6.4. This dynamic co-simulation is conducted for (a) 100% GFL, (b) 100% GFM, with m_p =20, and (c)100% GFM, with m_p =100. The current magnitude for phase A for the detailed simulation with all PV units represented in Feeder 1 is shown in Figure 6.17, and the voltages at the end of the feeder for the detailed model are plotted in Figure 6.18. It is seen that the GFL and GFM models lead to differences at the feeder-head current during

the fault (as well as in the steady state) and that the voltages seen for the GFM and GFL inverters are similar but with the reactive power and active power control strategies being different for the GFM, the voltage recovery portion of the GFM plots are slightly different from that of GFL. The difference in the feeder-head currents during the fault can be explained by the differences between the current limit in the GFM and GFL models – for the GFM model, a limit based on the rated apparent power and nominal voltage (1 p.u.) is used, whereas the rated current for the GFL model is calculated based on the rated apparent power and the lowest continuous operating voltage (0.88 p.u.). Further, another difference visible in Figure 6.17 is that the GFL model results in a quicker increase in the current at the feeder-head. This difference can be attributed to the detailed representation of current control for the GFL model versus the representation of current control using delay blocks for the GFM model.

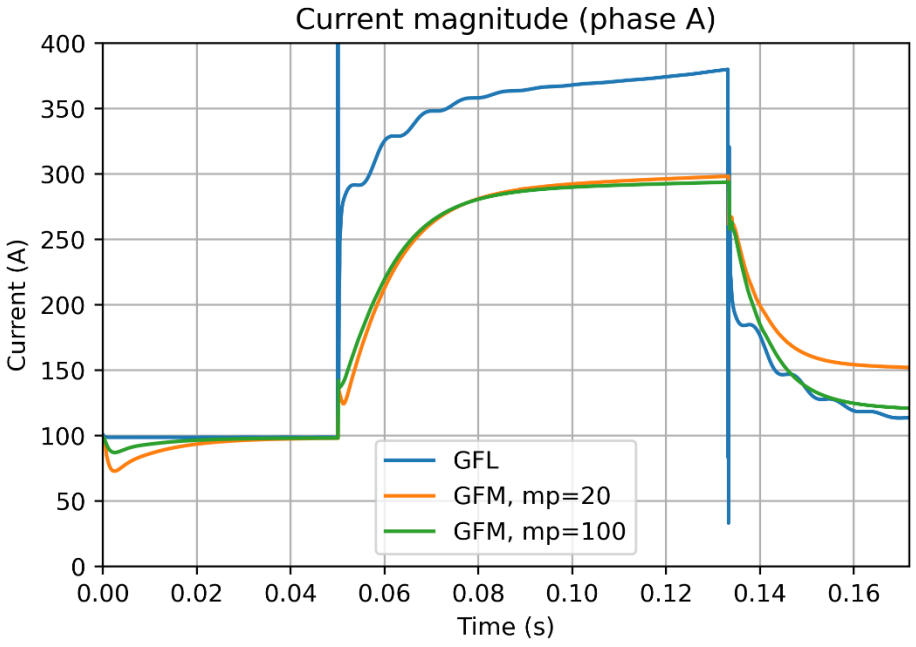

Figure 6.17 The Current at the Feeder-head for Phase a for Different Combinations of GFM and GFL Devices for the Detailed Feeder Model

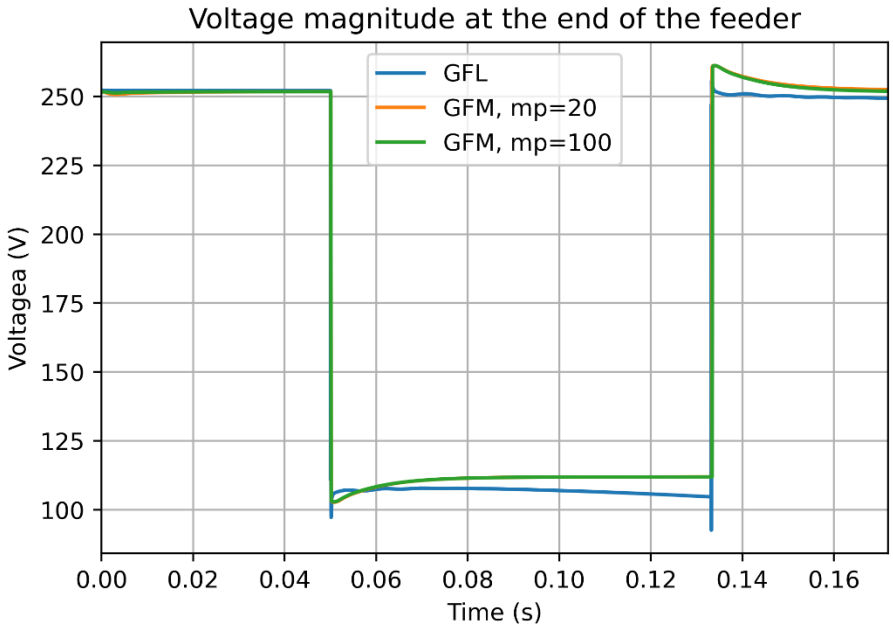

Figure 6.18 The Voltage Magnitude at the End of the Feeder for Phase a for Different Combinations of GFM and GFL Devices for the Detailed Feeder Model

The same three scenarios of (a) 100% GFL, (b) 100% GFM, with m_p=20, and (c)100% GFM, with m_p=100 are considered for the reduced feeder model. Figure 6.19 shows the current at the feeder-head for phase A. Figure 6.20 displays the voltage magnitude at the end of the feeder for the reduced order model. It is seen that the reduced model plots for both feeder-head current and end of the feeder voltage compare well with the detailed model plots of the corresponding quantities. The differences in the feeder-head current plots for the simulation cases with GFL and GFM models from Figure 6.19 can be explained similar to the differences found for the reduced model in Figure 6.17.

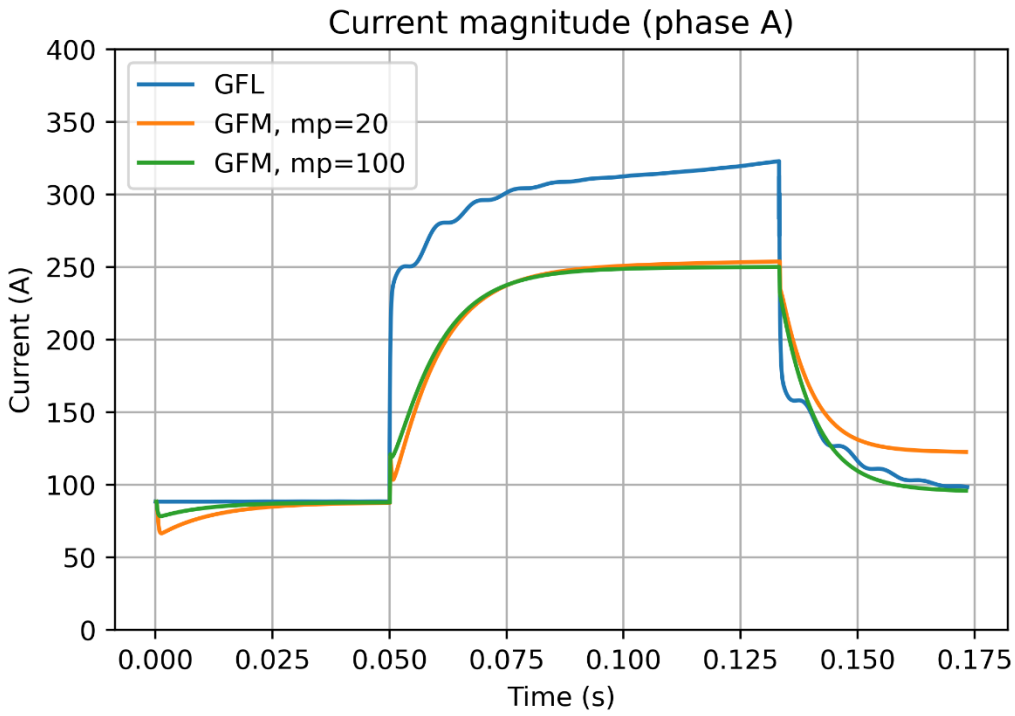

Figure 6.19 The Current at the Feeder-head for Phase a for Different Combinations of GFM and GFL Devices for the Reduced Feeder Model

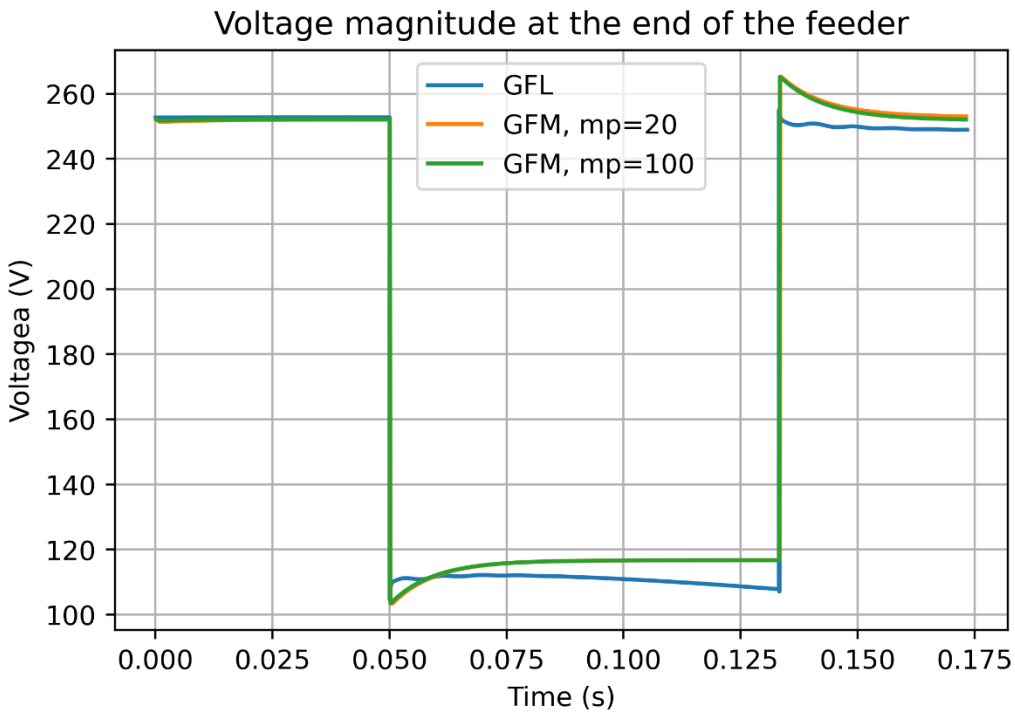

Figure 6.20 The Voltage Magnitude at the End of the Feeder for Phase a for Different Combinations of GFM and GFL Devices for the Reduced Feeder

Note that the study presented here is just a preliminary study. It is seen that the detailed and reduced feeder model lead to qualitatively similar responses in terms of the current at the feeder-head and the voltage at the end of the feeder. However, there is a difference in the current magnitude that must be investigated further to create a better reduced model. Such reduced model may be relevant for representing the feeder in a large study where the representation of a large number of feeders across the bulk power system is necessary. Further, a simple control was used to represent the grid forming devices in this dissertation, the impacts of various parameters considered and the impact of different grid

forming control architectures under different disturbances would need to be undertaken to study the impact of grid forming inverters on T&D networks more thoroughly.

7 CONCLUSIONS AND FUTURE WORK

7.1 Conclusions

In this dissertation, the importance of modeling the distribution network in detail is highlighted. A detailed model for a real distribution-sub-transmission network has been created by combining various field data and validated against field measurements. A procedure has been developed to combine various data sources to form an accurate and field-validated feeder model. One of the feeders has been modeled in detail including the primary and secondary network models.

A dynamic model for solar PV units including advanced inverter control is developed and implemented as an OpenDSS user defined model. User defined models allow for representations of components such as inverters in detail and capturing the response of these components in power flow and dynamic simulations. For the feeder modeled in detail, it is seen that during unbalanced faults on the feeder, the mutual cable impedances for the main three-phase trunk of the feeder result in such equivalent network impedances at the fault location that there is a voltage swell observed during the fault on non-faulted phases. This voltage swell can cause voltages above 1.2 p.u. and can have detrimental impacts on the solar PV generation installed on the feeder as well as on customer devices. It is shown that with appropriate control, the solar PV units on the feeder can alleviate this voltage swell to some extent, but to completely eliminate the voltage swell other interventions might be needed in addition to the advanced inverter controls.

A framework for distribution-transmission co-simulation has been developed for both power flow as well as dynamic simulations. The integrated modeling of the two systems

allows the accurate capture of the impact of one system on the other. The co-simulation framework and the model at the base operating point have been validated against field measurements and the model is found to match well with the field measurements. The distribution system is represented using OpenDSS in a three-phase unbalanced detail whereas the sub-transmission network is represented in three-sequence domain in InterPSS. HELICS software is used for coordinating the co-simulation. The co-simulation power flow is further developed as a module that can be implemented on a cloud based platform and that can be used as an input for running various analytics modules.

Using the dynamic co-simulation, the impacts of distribution and sub-transmission faults on the combined T&D system are studied. It is found that the distribution and sub-transmission faults can cause a large amount of solar PV to trip resulting in a loss of generation which may persist even after the fault is cleared. In case of faults tripping the generation on two of the three phases, such as due to an unbalanced SLG fault on the distribution feeder, the post-fault clearance currents at the feeder-head have a very high unbalance for high penetration feeders, and may cause ground protection at the feeder-head to trip the feeder even after clearing the fault due to this unbalance.

Further, it is found that advanced inverter controls such as volt-VAr are able to improve the response to some of the faults and that more aggressive abnormal voltage controls with larger ride-through requirements can reduce the amount of solar PV generation tripping due to faults. Grid forming inverter controls are also considered in terms of a simple grid forming inverter model using a custom OpenDSS user defined model, and a preliminary study with this user defined model is conducted.

Modeling the different feeders in a sub-transmission-distribution network are found to be important, since different feeders may have very different fault responses due to the differences in the feeder loads and solar PV generation. An aggregate model may not be able to capture this different behavior of different feeders. Further, it is found that both in steady-state and dynamic simulations, the voltage rise or drop across the secondary network is important to accurately capture the voltages seen at the solar PV units and at the customer locations and not modeling the secondary network can result in an inaccurate assessment of the voltage violations in the feeder as well as the fault response of the feeder in terms on the amount of generation tripping due to certain faults.

7.2 Future Work

A detailed model of the distribution-sub-transmission network has been created and studied in this dissertation. However, a static model is used for the loads. For distribution feeders, one of the important dynamic characteristics is the fault induced delayed voltage recovery (FIDVR) which occurs because of the single-phase motor loads (installed in houses commonly for applications such as air conditioning) stalling during low voltage. FIDVR is an important phenomenon considered when the modeling of distribution systems in transmission/sub-transmission networks is considered, and one avenue to further enhance the systems modeled and studies performed would be to model single-phase motor loads in the network and study the interactions between the solar PV units installed on the system and the motor loads especially during faults for feeders with high solar PV penetration. To this end, a suitable motor model is presented in Section 3.7, the next steps for this research can be to create a custom user defined model for OpenDSS for

this motor model and study the impact of motor stalling on the feeder response to faults and if the DERs on the distribution network can be utilized to mitigate this impact.

A simple representation for the grid forming inverters is created in Section 3 and a preliminary study of the T&D network with grid forming inverters is reported in Section 6.6. Grid forming inverters are increasingly looked at as the inverter architecture of the future for the systems with a very high penetration of inverter-based resources. There are different control architectures to enable a grid forming mode possible. The impact of such architectures and different control parameters on the response of the T&D network needs to be studied. Further, future works may include studies of special cases involving grid forming inverters such as intentional islanding of certain parts of the distribution network enabled by these inverters.

There are several new technologies such as battery storage and electric vehicles which are being increasingly considered when the distribution and sub-transmission operation is concerned. On one hand, grid-connected battery storage enables grid operators an extra resource which can be utilized to combat the adverse impacts of the variability of distributed solar PV generation as well as during dynamic events. The operation of battery storage considering the distribution-sub-transmission network would add value to the grid operator. On the other hand, as more and more people shift to using electric vehicles instead of internal combustion engine vehicles, a new type of load is added to the network both on the residential level (people charging their cars in their houses) as well as larger grid level (charging stations). This would impact the load profiles of the

distribution and sub-transmission network and might warrant changes to the network operation which can be studied using a T&D co-simulation.

REFERENCES

[1] G. Carpinelli, G. Celli, S. Mocci, F. Mottola, F. Pilo, and D. Proto, "Optimal Integration of Distributed Energy Storage Devices in Smart Grids," *IEEE Trans. Smart Grid*, vol. 4, no. 2, pp. 985–995, Jun. 2013, doi: 10.1109/TSG.2012.2231100.

[2] "Technical Reference Document: Dynamic Load Modeling," North American Electric Reliability Corporation, Altanta, GA, Dec. 2016. [Online]. Available: https://www.nerc.com/comm/PC/LoadModelingTaskForceDL/Dynamic%20Load%20Modeling%20Tech%20Ref%202016-11-14%20-%20FINAL.PDF

[3] R. Quint *et al.*, "Transformation of the Grid: The Impact of Distributed Energy Resources on Bulk Power Systems," *IEEE Power Energy Mag.*, vol. 17, no. 6, pp. 35–45, Nov. 2019, doi: 10.1109/MPE.2019.2933071.

[4] "IEEE Standard for Interconnection and Interoperability of Distributed Energy Resources with Associated Electric Power Systems Interfaces--Amendment 1: To Provide More Flexibility for Adoption of Abnormal Operating Performance Category III," IEEE. doi: 10.1109/IEEESTD.2020.9069495.

[5] J. Matevosyan *et al.*, "A Future With Inverter-Based Resources: Finding Strength From Traditional Weakness," *IEEE Power Energy Mag.*, vol. 19, no. 6, pp. 18–28, Nov. 2021, doi: 10.1109/MPE.2021.3104075.

[6] "DIgSILENT PowerFactory." DIgSILENT GmbH. [Online]. Available: https://www.digsilent.de/en/powerfactory.html

[7] R. C. Dugan, D. Montenegro, and A. Ballanti, *Reference Guide The Open Distribution System Simulator (OpenDSS)*. EPRI, 2018.

[8] K. Montano-Martinez, S. Thakar, V. Vittal, R. Ayyanar, and C. Rojas, "Detailed Primary and Secondary Distribution System Feeder Modeling Based on AMI Data," in *2020 52nd North American Power Symposium (NAPS)*, Tempe, AZ, USA: IEEE, Apr. 2021, pp. 1–6. doi: 10.1109/NAPS50074.2021.9449779.

[9] W. H. Kersting, *Distribution system modeling and analysis*, Fourth edition. Boca Raton: CRC Press, Taylor & Francis Group, CRC Press is an imprint of the Taylor & Francis Group, an informa business, 2018.

[10] T. Gönen, *Electric power distribution system engineering*, 3rd ed. Boca Raton: CRC Press, 2014.

[11] J. Guerrero *et al.*, "Distributed Generation: Toward a New Energy Paradigm," *IEEE Ind. Electron. Mag.*, vol. 4, no. 1, pp. 52–64, Mar. 2010, doi: 10.1109/MIE.2010.935862.

[12] F. Bu, Y. Yuan, Z. Wang, K. Dehghanpour, and A. Kimber, "A Time-Series Distribution Test System Based on Real Utility Data," in *2019 North American Power Symposium (NAPS)*, Wichita, KS, USA: IEEE, Oct. 2019, pp. 1–6. doi: 10.1109/NAPS46351.2019.8999982.

[13] Y. Tang and R. Ayyanar, "Modeling and validation of a distribution system with high PV penetration using zone division method," in *2014 IEEE PES T&D Conference and Exposition*, Chicago, IL: IEEE, Apr. 2014, pp. 1–5. doi: 10.1109/TDC.2014.6863357.

[14] T. J. Morrell, V. Venkataramanan, A. Srivastava, A. Bose, and C.-C. Liu, "Modeling of Electric Distribution Feeder Using Smart Meter Data," in *2018 IEEE/PES Transmission and Distribution Conference and Exposition (T&D)*, Denver, CO: IEEE, Apr. 2018, pp. 1–9. doi: 10.1109/TDC.2018.8440540.

[15] G. J. Shirek, B. A. Lassiter, W. C. Carr, and W. H. Kersting, "Modeling Secondary Services in Engineering and Mapping," *IEEE Trans. Ind. Appl.*, vol. 48, no. 1, pp. 254–262, Jan. 2012, doi: 10.1109/TIA.2011.2175874.

[16] P. Balakrishna, K. Rajagopal, and K. S. Swarup, "AMI/GIS based distribution system load flow for extended situational awareness," in *2014 Eighteenth National Power Systems Conference (NPSC)*, Guwahati, India: IEEE, Dec. 2014, pp. 1–6. doi: 10.1109/NPSC.2014.7103790.

[17] J. Giraldez, P. Gotseff, A. Nagarajan, R. Ueda, J. Shindo, and S. Suryanarayanan, "Distribution Feeder Modeling for Time-Series Simulation of Voltage Management Strategies," in *2018 IEEE/PES Transmission and Distribution Conference and Exposition (T&D)*, Denver, CO: IEEE, Apr. 2018, pp. 1–5. doi: 10.1109/TDC.2018.8440379.

[18] J. A. Taylor, T. A. Short, and B. Bushey, "Efficiency impacts of distribution secondaries," in *PES T&D 2012*, Orlando, FL, USA: IEEE, May 2012, pp. 1–6. doi: 10.1109/TDC.2012.6281661.

[19] J. Peppanen, M. J. Reno, M. Thakkar, S. Grijalva, and R. G. Harley, "Leveraging AMI Data for Distribution System Model Calibration and Situational Awareness," *IEEE Trans. Smart Grid*, vol. 6, no. 4, pp. 2050–2059, Jul. 2015, doi: 10.1109/TSG.2014.2385636.

[20] B. Wang and W. Luan, "Generate distribution circuit model using AMI data," in *2014 China International Conference on Electricity Distribution (CICED)*, Shenzhen, China: IEEE, Sep. 2014, pp. 1251–1255. doi: 10.1109/CICED.2014.6991907.

[21] "CYME." CYME International. [Online]. Available: https://www.cyme.com/software/

[22] S. Thakar and K. Montano-Martinez, "Distribution System Model Transformation Tool (DISMOTT)." Arizona State University, 2020. [Online]. Available: https://github.com/thakars/dismott

[23] QGIS Development Team, "QGIS Geographic Information System." Open Source Geospacial Foundation, 2020.

[24] K. Montano-Martinez *et al.*, "Detailed Primary and Secondary Distribution System Model Enhancement Using AMI Data," *IEEE Open Access J. Power Energy*, vol. 9, pp. 2–15, 2022, doi: 10.1109/OAJPE.2021.3125900.

[25] B. Palmintier *et al.*, "Chapter 7: Distribution System Analysis," National Renewable Energy Laboratory, Golden, CO, Chapter NREL/TP-6A20-79444-7, 2021. [Online]. Available: https://www.nrel.gov/docs/fy21osti/79444-7.pdf

[26] S. Thakar, V. Vittal, and R. Ayyanar, "An Integrated Transmission-Distribution Co-Simulation for a Distribution System with High Renewable Penetration," in *2021 IEEE 48th Photovoltaic Specialists Conference (PVSC)*, Fort Lauderdale, FL, USA: IEEE, Jun. 2021, pp. 0672–0679. doi: 10.1109/PVSC43889.2021.9518452.

[27] N. Panossian, T. Elgindy, B. Palmintier, and D. Wallison, "Synthetic, Realistic Transmission and Distribution Co-Simulation for Voltage Control Benchmarking," in *2021 IEEE Texas Power and Energy Conference (TPEC)*, College Station, TX, USA: IEEE, Feb. 2021, pp. 1–5. doi: 10.1109/TPEC51183.2021.9384935.

[28] M. Gupta and A. R. Abhyankar, "Coordinated Load Flow Solution for Coupled Transmission-Distribution System Incorporating Load Modeling," in *2018 20th National Power Systems Conference (NPSC)*, Tiruchirappalli, India: IEEE, Dec. 2018, pp. 1–6. doi: 10.1109/NPSC.2018.8771708.

[29] H. Jain, B. Palmintier, I. Krad, and D. Krishnamurthy, "Studying the Impact of Distributed Solar PV on Power Systems Using Integrated Transmission and Distribution Models," in *2018 IEEE/PES Transmission and Distribution Conference and Exposition (T&D)*, Denver, CO: IEEE, Apr. 2018, pp. 1–5. doi: 10.1109/TDC.2018.8440457.

[30] H. Jain, B. Palmintier, D. Krishnamurthy, I. Krad, and E. Hale, "Evaluating the Impact of Price-Responsive Load on Power Systems Using Integrated T&D Simulation," in *2019 IEEE Power & Energy Society Innovative Smart Grid Technologies Conference (ISGT)*, Washington, DC, USA: IEEE, Feb. 2019, pp. 1–5. doi: 10.1109/ISGT.2019.8791634.

[31] M. Sarstedt, S. Garske, C. Blaufus, and L. Hofmann, "Modelling of Integrated Transmission and Distribution Grids based on Synthetic Distribution Grid Models,"

in *2019 IEEE Milan PowerTech*, Milan, Italy: IEEE, Jun. 2019, pp. 1–6. doi: 10.1109/PTC.2019.8810823.

[32] H. Jain, K. Rahimi, A. Tbaileh, R. P. Broadwater, Akshay Kumar Jain, and M. Dilek, "Integrated transmission & distribution system modeling and analysis: Need & advantages," in *2016 IEEE Power and Energy Society General Meeting (PESGM)*, Boston, MA, USA: IEEE, Jul. 2016, pp. 1–5. doi: 10.1109/PESGM.2016.7741235.

[33] B. Mather and F. Ding, "Distribution-connected PV's response to voltage sags at transmission-scale," in *2016 IEEE 43rd Photovoltaic Specialists Conference (PVSC)*, Portland, OR, USA: IEEE, Jun. 2016, pp. 2030–2035. doi: 10.1109/PVSC.2016.7749985.

[34] R. W. Kenyon, B. Mather, and B.-M. Hodge, "Coupled transmission and distribution simulations to assess distributed generation response to power system faults," *Electr. Power Syst. Res.*, vol. 189, p. 106746, Dec. 2020, doi: 10.1016/j.epsr.2020.106746.

[35] G. Chaspierre, G. Denis, P. Panciatici, and T. Van Cutsem, "A Dynamic Equivalent of Active Distribution Network: Derivation, Update, Validation and Use Cases," *IEEE Open Access J. Power Energy*, vol. 8, pp. 497–509, 2021, doi: 10.1109/OAJPE.2021.3102499.

[36] F. Escobar, J. M. Viquez, J. Garcia, P. Aristidou, and G. Valverde, "Coordination of DERs and Flexible Loads to Support Transmission Voltages in Emergency Conditions," *IEEE Trans. Sustain. Energy*, vol. 13, no. 3, pp. 1344–1355, Jul. 2022, doi: 10.1109/TSTE.2022.3154716.

[37] A. Pandey and L. Pileggi, "Steady-State Simulation for Combined Transmission and Distribution Systems," *IEEE Trans. Smart Grid*, vol. 11, no. 2, pp. 1124–1135, Mar. 2020, doi: 10.1109/TSG.2019.2932403.

[38] A. Suresh, S. Kamalasadan, and S. Paudyal, "A Novel Three-Phase Transmission and Unbalance Distribution Co-Simulation Power Flow Model For Long Term Voltage Stability Margin Assessment," in *2021 IEEE Power & Energy Society General Meeting (PESGM)*, Washington, DC, USA: IEEE, Jul. 2021, pp. 1–5. doi: 10.1109/PESGM46819.2021.9638047.

[39] H. Jain, A. Parchure, R. P. Broadwater, M. Dilek, and J. Woyak, "Three-Phase Dynamic Simulation of Power Systems Using Combined Transmission and Distribution System Models," *IEEE Trans. Power Syst.*, vol. 31, no. 6, pp. 4517–4524, Nov. 2016, doi: 10.1109/TPWRS.2016.2535297.

[40] P. Aristidou and T. Van Cutsem, “Dynamic simulations of combined transmission and distribution systems using decomposition and localization,” in *2013 IEEE Grenoble Conference*, Grenoble, France: IEEE, Jun. 2013, pp. 1–6. doi: 10.1109/PTC.2013.6652146.

[41] P. Aristidou and T. Van Cutsem, “Dynamic simulations of combined transmission and distribution systems using parallel processing techniques,” in *2014 Power Systems Computation Conference*, Wrocław, Poland: IEEE, Aug. 2014, pp. 1–7. doi: 10.1109/PSCC.2014.7038478.

[42] P. Aristidou, S. Lebeau, and T. Van Cutsem, “Power System Dynamic Simulations Using a Parallel Two-Level Schur-Complement Decomposition,” *IEEE Trans. Power Syst.*, vol. 31, no. 5, pp. 3984–3995, Sep. 2016, doi: 10.1109/TPWRS.2015.2509023.

[43] T. Fu, D. Wang, X. Fan, H. Ren, J. Ogle, and Y. Chen, “Efficient Topology Assessment for Integrated Transmission and Distribution Network with 10,000+ Inverter-based Resources,” in *2022 IEEE Power & Energy Society General Meeting (PESGM)*, Denver, CO, USA: IEEE, Jul. 2022, pp. 1–5. doi: 10.1109/PESGM48719.2022.9916770.

[44] M. A. I. Khan, A. Suresh, S. Paudyal, and S. Kamalasadan, “Decoupled and Unified Approaches for Solving Transmission and Distribution Co-Simulations,” in *2019 North American Power Symposium (NAPS)*, Wichita, KS, USA: IEEE, Oct. 2019, pp. 1–6. doi: 10.1109/NAPS46351.2019.9000279.

[45] B. A. Bhatti, R. Broadwater, and M. Delik, “Integrated T&D Modeling vs. Co-Simulation – Comparing Two Approaches to Study Smart Grid,” in *2019 IEEE Power & Energy Society General Meeting (PESGM)*, Atlanta, GA, USA: IEEE, Aug. 2019, pp. 1–5. doi: 10.1109/PESGM40551.2019.8973761.

[46] Q. Nguyen, S. N. Ananthan, and S. Santoso, “Power Flow Solution Methods for Combined Transmission and Distribution Systems,” in *2019 IEEE Power & Energy Society General Meeting (PESGM)*, Atlanta, GA, USA: IEEE, Aug. 2019, pp. 1–5. doi: 10.1109/PESGM40551.2019.8973391.

[47] Y. N. Velaga, A. Chen, P. K. Sen, G. Krishnamoorthy, and A. Dubey, “Transmission-Distribution Co-Simulation: Model Validation with Standalone Simulation,” in *2018 North American Power Symposium (NAPS)*, Fargo, ND: IEEE, Sep. 2018, pp. 1–6. doi: 10.1109/NAPS.2018.8600591.

[48] G. R. Bharati, S. Chakraborty, C. Duan, and T. Nishikawa, “An Integrated Transmission-Distribution Modeling for Phasor-Domain Dynamic Analysis in Real-time,” in *2020 IEEE Power & Energy Society Innovative Smart Grid Technologies Conference (ISGT)*, Washington, DC, USA: IEEE, Feb. 2020, pp. 1–5. doi: 10.1109/ISGT45199.2020.9087705.

[49] V. Jalili-Marandi and J. Belanger, “Real-Time Transient Stability Simulation of Confederated Transmission-Distribution Power Grids With More Than 100,000 Nodes,” in *2018 IEEE Power & Energy Society General Meeting (PESGM)*, Portland, OR: IEEE, Aug. 2018, pp. 1–5. doi: 10.1109/PESGM.2018.8585930.

[50] S. M. Mohseni-Bonab, I. Kamwa, and A. Moeini, “IC-GAMA: A Novel Framework for Integrated T&D Co-Simulation,” in *2019 IEEE PES Innovative Smart Grid Technologies Europe (ISGT-Europe)*, Bucharest, Romania: IEEE, Sep. 2019, pp. 1–5. doi: 10.1109/ISGTEurope.2019.8905571.

[51] S. M. H. Rizvi, S. K. Sadanandan, and T. Ghaoud, “TDS-CoSim: A Static Co-simulation Tool for Integrated T & D Snapshot Analysis Considering Large Penetration of DERs,” in *2022 IEEE Industrial Electronics and Applications Conference (IEACon)*, Kuala Lumpur, Malaysia: IEEE, Oct. 2022, pp. 67–72. doi: 10.1109/IEACon55029.2022.9951837.

[52] G. Krishnamoorthy and A. Dubey, “A Framework to Analyze Interactions between Transmission and Distribution Systems,” in *2018 IEEE Power & Energy Society General Meeting (PESGM)*, Portland, OR: IEEE, Aug. 2018, pp. 1–5. doi: 10.1109/PESGM.2018.8585926.

[53] R. Venkatraman, S. K. Khaitan, and V. Ajjarapu, “A combined transmission-distribution system dynamic model with grid-connected DG inverter,” in *2017 IEEE Power & Energy Society General Meeting*, Chicago, IL: IEEE, Jul. 2017, pp. 1–5. doi: 10.1109/PESGM.2017.8274593.

[54] K. Balasubramaniam and S. Abhyankar, “A combined transmission and distribution system co-simulation framework for assessing the impact of Volt/VAR control on transmission system,” in *2017 IEEE Power & Energy Society General Meeting*, Chicago, IL: IEEE, Jul. 2017, pp. 1–5. doi: 10.1109/PESGM.2017.8274633.

[55] X. Fang, M. Cai, and A. Florita, “Cyber-Physical Event Emulation-Based Transmission-and-Distribution Co-simulation for Situational Awareness of Grid Anomalies (SAGA),” in *2021 IEEE Power & Energy Society General Meeting (PESGM)*, Washington, DC, USA: IEEE, Jul. 2021, pp. 1–5. doi: 10.1109/PESGM46819.2021.9637866.

[56] K. Balasubramaniam *et al.*, “Co-Simulation of Transmission and Distribution Systems—From Modeling to Software Development,” *IEEE Access*, vol. 10, pp. 127061–127072, 2022, doi: 10.1109/ACCESS.2022.3224939.

[57] A. K. Bharati, V. Ajjarapu, W. Du, and Y. Liu, “Role of Distributed Inverter-Based-Resources in Bulk Grid Primary Frequency Response Through HELICS Based SMTD Co-Simulation,” *IEEE Syst. J.*, vol. 17, no. 1, pp. 1071–1082, Mar. 2023, doi: 10.1109/JSYST.2022.3218117.

[58] A. Mohammed and H. Abu-Rub, “A Co-Simulation Platform for Microgrid Integration into Transmission System - Power Quality Study,” in *2022 10th International Conference on Smart Grid (icSmartGrid)*, Istanbul, Turkey: IEEE, Jun. 2022, pp. 319–324. doi: 10.1109/icSmartGrid55722.2022.9848679.

[59] T. M. Hansen *et al.*, “Enabling Smart Grid Cosimulation Studies: Rapid Design and Development of the Technologies and Controls,” *IEEE Electrification Mag.*, vol. 4, no. 1, pp. 25–32, Mar. 2016, doi: 10.1109/MELE.2015.2509899.

[60] B. Palmintier *et al.*, “IGMS: An Integrated ISO-to-Appliance Scale Grid Modeling System,” *IEEE Trans. Smart Grid*, vol. 8, no. 3, pp. 1525–1534, May 2017, doi: 10.1109/TSG.2016.2604239.

[61] T. S. Nouidui, J. Coignard, C. Gehbauer, M. Wetter, J.-Y. Joo, and E. Vrettos, “CyDER – an FMI-based co-simulation platform for distributed energy resources,” *J. Build. Perform. Simul.*, vol. 12, no. 5, pp. 566–579, Sep. 2019, doi: 10.1080/19401493.2018.1535623.

[62] R. Huang, R. Fan, J. Daily, A. Fisher, and J. Fuller, “Open-source framework for power system transmission and distribution dynamics co-simulation,” *IET Gener. Transm. Distrib.*, vol. 11, no. 12, pp. 3152–3162, Aug. 2017, doi: 10.1049/iet-gtd.2016.1556.

[63] Q. Huang *et al.*, “Simulation-Based Valuation of Transactive Energy Systems,” *IEEE Trans. Power Syst.*, vol. 34, no. 5, pp. 4138–4147, Sep. 2019, doi: 10.1109/TPWRS.2018.2838111.

[64] B. Palmintier, D. Krishnamurthy, P. Top, S. Smith, J. Daily, and J. Fuller, “Design of the HELICS high-performance transmission-distribution-communication-market co-simulation framework,” in *2017 Workshop on Modeling and Simulation of Cyber-Physical Energy Systems (MSCPES)*, Pittsburgh, PA: IEEE, Apr. 2017, pp. 1–6. doi: 10.1109/MSCPES.2017.8064542.

[65] N. Duan *et al.*, “Parallel Transmission Distribution Co-simulation Leveraging A Commercial Distribution Simulator,” in *2020 IEEE PES Innovative Smart Grid Technologies Europe (ISGT-Europe)*, The Hague, Netherlands: IEEE, Oct. 2020, pp. 894–898. doi: 10.1109/ISGT-Europe47291.2020.9248879.

[66] A. K. Bharati and V. Ajjarapu, “SMTD Co-Simulation Framework With HELICS for Future-Grid Analysis and Synthetic Measurement-Data Generation,” *IEEE Trans. Ind. Appl.*, vol. 58, no. 1, pp. 131–141, Jan. 2022, doi: 10.1109/TIA.2021.3123925.

[67] “An Overview of Co-Simulation Platforms for Transmission Planning,” Electric Power Research Institute, Technical Update 000000003002017494, Dec. 2019. [Online]. Available: https://www.epri.com/research/products/000000003002017494

[68] R. Sadnan, G. Krishnamoorthy, and A. Dubey, “Transmission and Distribution (T&D) Quasi-Static Co-Simulation: Analysis and Comparison of T&D Coupling Strength,” *IEEE Access*, vol. 8, pp. 124007–124019, 2020, doi: 10.1109/ACCESS.2020.3006058.

[69] G. Krishnamoorthy, A. Dubey, and P. K. Sen, “Iteratively-Coupled Co-simulation Framework for Unbalanced Transmission-Distribution System,” in *2019 IEEE Milan PowerTech*, Milan, Italy: IEEE, Jun. 2019, pp. 1–6. doi: 10.1109/PTC.2019.8810625.

[70] E. Schweitzer, J. Hansen, and J. Fuller, “Transmission and Distribution Co-Simulation with Possible Distribution Loops,” in *2018 IEEE Power & Energy Society General Meeting (PESGM)*, Portland, OR: IEEE, Aug. 2018, pp. 1–5. doi: 10.1109/PESGM.2018.8586619.

[71] Q. Huang *et al.*, “A Comparative Study of Interface Techniques for Transmission and Distribution Dynamic Co-Simulation,” in *2018 IEEE Power & Energy Society General Meeting (PESGM)*, Portland, OR: IEEE, Aug. 2018, pp. 1–5. doi: 10.1109/PESGM.2018.8586046.

[72] Q. Li and S. Abhyankar, “Evaluation of High Solar Penetration Impact on Bulk System Stability through a Transmission-Distribution Dynamics Co-simulation,” in *2019 IEEE Power & Energy Society General Meeting (PESGM)*, Atlanta, GA, USA: IEEE, Aug. 2019, pp. 1–5. doi: 10.1109/PESGM40551.2019.9119339.

[73] R. Venkatraman, S. K. Khaitan, and V. Ajjarapu, “Dynamic Co-Simulation Methods for Combined Transmission-Distribution System With Integration Time Step Impact on Convergence,” *IEEE Trans. Power Syst.*, vol. 34, no. 2, pp. 1171–1181, Mar. 2019, doi: 10.1109/TPWRS.2018.2874807.

[74] S. M. Mohseni-Bonab, A. Hajebrahimi, I. Kamwa, and A. Moeini, “Transmission and distribution co-simulation: a review and propositions,” *IET Gener. Transm. Distrib.*, vol. 14, no. 21, pp. 4631–4642, Nov. 2020, doi: 10.1049/iet-gtd.2020.0244.

[75] H. Jain, B. A. Bhatti, T. Wu, B. Mather, and R. Broadwater, “Integrated Transmission-and-Distribution System Modeling of Power Systems: State-of-the-Art and Future Research Directions,” *Energies*, vol. 14, no. 1, p. 12, Dec. 2020, doi: 10.3390/en14010012.

[76] G. Krishnamoorthy, R. Sadnan, A. Dubey, Y. N. Velaga, and P. K. Sen, “Distributed PV Penetration Impact Analysis on Transmission System Voltages using Co-Simulation,” in *2019 North American Power Symposium (NAPS)*, Wichita, KS, USA: IEEE, Oct. 2019, pp. 1–6. doi: 10.1109/NAPS46351.2019.9000281.

[77] S. M. H. Rizvi and A. K. Srivastava, “Integrated T&D Voltage Stability Assessment Considering Impact of DERs and Distribution Network Topology,” *IEEE Access*, vol. 11, pp. 14702–14714, 2023, doi: 10.1109/ACCESS.2023.3243100.

[78] A. R. R. Matavalam, R. Venkatraman, and V. Ajjarapu, “Mitigating Delayed Voltage Recovery Using DER & Load Control in Distribution Systems,” in *2022 IEEE Power & Energy Society General Meeting (PESGM)*, Denver, CO, USA: IEEE, Jul. 2022, pp. 1–5. doi: 10.1109/PESGM48719.2022.9916669.

[79] M. M. Rezvani, S. Mehraeen, J. R. Ramamurthy, and T. Field, “Dynamic Interaction of Distribution-Connected DER_A With Transmission System Via Co-Simulation Analysis,” *IEEE Trans. Ind. Appl.*, vol. 58, no. 2, pp. 1502–1511, Mar. 2022, doi: 10.1109/TIA.2021.3137087.

[80] S. Abhyankar, K. Balasubramaniam, and B. Cui, “Load Model Parameter Estimation by Transmission-Distribution Co-Simulation,” in *2018 Power Systems Computation Conference (PSCC)*, Dublin, Ireland: IEEE, Jun. 2018, pp. 1–7. doi: 10.23919/PSCC.2018.8442939.

[81] R. Venkatraman, S. K. Khaitan, and V. Ajjarapu, “Application of Combined Transmission-Distribution System Modeling to WECC Composite Load Model,” in *2018 IEEE Power & Energy Society General Meeting (PESGM)*, Portland, OR: IEEE, Aug. 2018, pp. 1–5. doi: 10.1109/PESGM.2018.8585910.

[82] P. Dattaray, D. Ramasubramanian, P. Mitra, J. C. Boemer, M. Bello, and A. Gaikwad, “Bulk System Impact of DER and Loads using T &D Cosimulation and Aggregate models,” in *2021 IEEE PES Innovative Smart Grid Technologies Europe (ISGT Europe)*, Espoo, Finland: IEEE, Oct. 2021, pp. 01–05. doi: 10.1109/ISGTEurope52324.2021.9640042.

[83] W. Wang, X. Fang, H. Cui, F. Li, Y. Liu, and T. J. Overbye, “Transmission-and-Distribution Dynamic Co-Simulation Framework for Distributed Energy Resource Frequency Response,” *IEEE Trans. Smart Grid*, vol. 13, no. 1, pp. 482–495, Jan. 2022, doi: 10.1109/TSG.2021.3118292.

[84] Y. Liu, R. Huang, W. Du, A. Singhal, and Z. Huang, “High-Performance Transmission and Distribution Co-simulation with 10,000+ Inverter-Based Resources,” in *2022 IEEE Industry Applications Society Annual Meeting (IAS)*, Detroit, MI, USA: IEEE, Oct. 2022, pp. 1–5. doi: 10.1109/IAS54023.2022.9940149.

[85] J. Yusuf, A. S. M. Jahid Hasan, and S. Ula, “EV Penetration Impact Analysis on Transmission System using Co-Simulation,” in *2022 IEEE Transportation Electrification Conference & Expo (ITEC)*, Anaheim, CA, USA: IEEE, Jun. 2022, pp. 1154–1158. doi: 10.1109/ITEC53557.2022.9814058.

[86] Y. Liu *et al.*, “Transmission-Distribution Dynamic Co-simulation of Electric Vehicles Providing Grid Frequency Response,” in *2022 IEEE Power & Energy Society General Meeting (PESGM)*, Denver, CO, USA: IEEE, Jul. 2022, pp. 1–5. doi: 10.1109/PESGM48719.2022.9917027.

[87] M. Zhou and S. Zhou, “Internet, Open-source and Power System Simulation,” in *2007 IEEE Power Engineering Society General Meeting*, Tampa, FL, USA: IEEE, Jun. 2007, pp. 1–5. doi: 10.1109/PES.2007.385492.

[88] J. J. Grainger and W. D. Stevenson, *Power system analysis*. in McGraw-Hill series in electrical and computer engineering. New York: McGraw-Hill, 1994.

[89] P. Meira, “dss-python.” [Online]. Available: https://github.com/dss-extensions/dss_python/releases

[90] Z. Yu, Y. Tang, T. Yao, and R. Ayyanar, “Dynamic simulation of CIG in large unbalanced distribution systems using an open source tool,” *IET Gener. Transm. Distrib.*, vol. 13, no. 9, pp. 1638–1645, May 2019, doi: 10.1049/iet-gtd.2018.6089.

[91] “IEEE Standard for Interconnection and Interoperability of Distributed Energy Resources with Associated Electric Power Systems Interfaces,” IEEE. doi: 10.1109/IEEESTD.2018.8332112.

[92] “PLECS.” Plexim. [Online]. Available: https://www.plexim.com/products/plecs

[93] J. M. Guerrero, J. C. Vasquez, J. Matas, L. G. de Vicuna, and M. Castilla, “Hierarchical Control of Droop-Controlled AC and DC Microgrids—A General Approach Toward Standardization,” *IEEE Trans. Ind. Electron.*, vol. 58, no. 1, pp. 158–172, Jan. 2011, doi: 10.1109/TIE.2010.2066534.

[94] J. Alipoor, Y. Miura, and T. Ise, “Power System Stabilization Using Virtual Synchronous Generator With Alternating Moment of Inertia,” *IEEE J. Emerg. Sel. Top. Power Electron.*, vol. 3, no. 2, pp. 451–458, Jun. 2015, doi: 10.1109/JESTPE.2014.2362530.

[95] M. Lu, “Virtual Oscillator Grid-Forming Inverters: State of the Art, Modeling, and Stability,” *IEEE Trans. Power Electron.*, vol. 37, no. 10, pp. 11579–11591, Oct. 2022, doi: 10.1109/TPEL.2022.3163377.

[96] D. Ramasubramanian, P. Pourbeik, E. Farantatos, and A. Gaikwad, “Simulation of 100% Inverter-Based Resource Grids With Positive Sequence Modeling,” *IEEE Electrification Mag.*, vol. 9, no. 2, pp. 62–71, Jun. 2021, doi: 10.1109/MELE.2021.3070938.

[97] W. Du *et al.*, “Modeling of Grid-Forming and Grid-Following Inverters for Dynamic Simulation of Large-Scale Distribution Systems,” *IEEE Trans. Power Deliv.*, vol. 36, no. 4, pp. 2035–2045, Aug. 2021, doi: 10.1109/TPWRD.2020.3018647.

[98] A. Quedan, W. Wang, D. Ramasubramanian, E. Farantatos, and S. Asgarpoor, "Behavior of a High Inverter-Based Resources Distribution Network with Different Participation Ratios of Grid-Forming and Grid-Following Inverters," in *2021 North American Power Symposium (NAPS)*, College Station, TX, USA: IEEE, Nov. 2021, pp. 1–6. doi: 10.1109/NAPS52732.2021.9654448.

[99] A. Quedan, D. Ramasubramanian, and E. Farantatos, "Virtual Oscillator Controlled Grid Forming Inverters Modelling and Testing in Phasor Domain," in *2021 IEEE 12th Energy Conversion Congress & Exposition - Asia (ECCE-Asia)*, Singapore, Singapore: IEEE, May 2021, pp. 2375–2380. doi: 10.1109/ECCE-Asia49820.2021.9479398.

[100] Y. Liu, V. Vittal, J. Undrill, and J. H. Eto, "Transient Model of Air-Conditioner Compressor Single Phase Induction Motor," *IEEE Trans. Power Syst.*, vol. 28, no. 4, pp. 4528–4536, Nov. 2013, doi: 10.1109/TPWRS.2013.2275256.

[101] B. Lesieutre, D. Kosterev, and J. Undrill, "Phasor modeling approach for single phase A/C motors," in *2008 IEEE Power and Energy Society General Meeting - Conversion and Delivery of Electrical Energy in the 21st Century*, Pittsburgh, PA, USA: IEEE, Jul. 2008, pp. 1–7. doi: 10.1109/PES.2008.4596554.

[102] "Load Characteristic INDMOT1P: Dynamic Phasor Model of a single-phase induction motor load model," PowerWorld Corporation, Apr. 2021. [Online]. Available: https://www.powerworld.com/WebHelp/Content/TransientModels_HTML/Load%20Characteristic%20INDMOT1P.htm

[103] F. K. Tuffner, K. P. Schneider, J. Hansen, and M. A. Elizondo, "Modeling Load Dynamics to Support Resiliency-Based Operations in Low-Inertia Microgrids," *IEEE Trans. Smart Grid*, vol. 10, no. 3, pp. 2726–2737, May 2019, doi: 10.1109/TSG.2018.2809452.

[104] D. Mohammadi, "Dynamic Modeling of Single-Phase Induction Motor Loads," Boise State University, Boise, Idaho, 2012. [Online]. Available: https://scholarworks.boisestate.edu/td/294

[105] A. M. Stankovic, B. C. Lesieutre, and T. Aydin, "Modeling and analysis of single-phase induction machines with dynamic phasors," *IEEE Trans. Power Syst.*, vol. 14, no. 1, pp. 9–14, Feb. 1999, doi: 10.1109/59.744460.

[106] J. Zhang, "Dynamic Simulation and Load Modeling for Voltage Recovery Studies with Three-Phase and Single-Phase Induction Motors," M.S., Illinois Institute of Technology, United States -- Illinois, 2017. [Online]. Available: http://login.ezproxy1.lib.asu.edu/login?url=https://www.proquest.com/dissertations-theses/dynamic-simulation-load-modeling-voltage-recovery/docview/1916573899/se-2?accountid=4485

[107] S. Thakar, V. Vittal, and R. Ayyanar, “Mitigation of fault related voltage swell on distribution feeders using DER-based advanced inverter controls,” presented at the IEEE Power and Energy Society General Meeting, Denver, CO, Denver, CO: IEEE, Aug. 2022.

[108] C. F. (Charles F. Wagner, *Symmetrical components as applied to the analysis of unbalanced electrical circuits*, 1st ed. New York: McGraw-Hill, 1933.

[109] E. W. Gunther and H. Mebta, “A survey of distribution system power quality-preliminary results,” *IEEE Trans. Power Deliv.*, vol. 10, no. 1, pp. 322–329, Jan. 1995, doi: 10.1109/61.368382.

[110] G. Ramos, A. Espin-Delgado, and J. Camarillo-Penaranda, “Behavior of phase voltages due to faults in radial power systems: An educational tool,” in *2017 IEEE Workshop on Power Electronics and Power Quality Applications (PEPQA)*, Bogota, Colombia: IEEE, May 2017, pp. 1–6. doi: 10.1109/PEPQA.2017.7981686.

[111] J. Acharya and W. Xu, “Characteristics of Voltage Swell in Multigrounded Systems,” *IEEE Trans. Power Deliv.*, vol. 22, no. 2, pp. 1259–1260, Apr. 2007, doi: 10.1109/TPWRD.2007.893384.

[112] M. Vaziri and D. R. Smith, “Grounding of Primary System for LV Networks,” *IEEE Trans. Power Deliv.*, vol. 31, no. 2, pp. 419–427, Apr. 2016, doi: 10.1109/TPWRD.2014.2363175.

[113] L. A. da Costa, Y. Mohammadi, R. C. Leborgne, and D. da S. Gazzana, “Impact Evaluation of the Neutral-Grounding Resistance on Short-Duration RMS Voltage Variations,” in *2020 19th International Conference on Harmonics and Quality of Power (ICHQP)*, Dubai, United Arab Emirates: IEEE, Jul. 2020, pp. 1–6. doi: 10.1109/ICHQP46026.2020.9177891.

[114] L. A. da Costa, D. da S. Gazzana, and R. C. Leborgne, “Investigation of Main and Secondary Transformers on Mitigation of Voltage Sags, Swells and Interruptions in Unbalanced Medium Voltage Distribution Systems,” *Electr. Power Compon. Syst.*, vol. 48, no. 8, pp. 858–869, May 2020, doi: 10.1080/15325008.2020.1821835.

[115] “IEEE Recommended Practice for Monitoring Electric Power Quality,” IEEE. doi: 10.1109/IEEESTD.2019.8796486.

[116] S. Helge, T. Rump, and K. L. Haugen, “Overvoltage Immunity of Electrical Appliances – Laboratory Test Results from 60 Appliances,” presented at the CIRED, 21st International Conference on Electricity Distribution, Frankfurt, Germany, Frankfurt, Germany, Jun. 2011, pp. 1–4. [Online]. Available: http://www.cired.net/publications/cired2011/part1/papers/CIRED2011_0946_final.pdf

[117] G. T. Heydt, G. G. Karady, Barry Cummi, “Improved Application of Power Acceptability Curves and Their Application to Certain Three-Phase Loads,” *Electr. Mach. Power Syst.*, vol. 27, no. 7, pp. 737–751, Jun. 1999, doi: 10.1080/073135699268984.

[118] H. D. Tafti, A. Ahmad, L. Callegaro, G. Konstantinou, and J. E. Fletcher, “Sensitivity of Commercial Rooftop Photovoltaic Inverters to Grid Voltage Swell,” in *2021 IEEE 12th Energy Conversion Congress & Exposition - Asia (ECCE-Asia)*, Singapore, Singapore: IEEE, May 2021, pp. 308–313. doi: 10.1109/ECCE-Asia49820.2021.9479029.

[119] K. Kawabe, Y. Ota, A. Yokoyama, and K. Tanaka, “Novel Dynamic Voltage Support Capability of Photovoltaic Systems for Improvement of Short-Term Voltage Stability in Power Systems,” *IEEE Trans. Power Syst.*, vol. 32, no. 3, pp. 1796–1804, May 2017, doi: 10.1109/TPWRS.2016.2592970.

[120] M. Islam, M. Nadarajah, and M. J. Hossain, “A Grid-Support Strategy With PV Units to Boost Short-Term Voltage Stability Under Asymmetrical Faults,” *IEEE Trans. Power Syst.*, vol. 35, no. 2, pp. 1120–1131, Mar. 2020, doi: 10.1109/TPWRS.2019.2942094.

[121] M. Ghorbani, A. Mosallanejad, and S. Mohamadian, “A new method to point of common coupling voltage control in distribution grid-connected photovoltaic systems,” *Int. Trans. Electr. Energy Syst.*, vol. 28, no. 2, p. e2491, Feb. 2018, doi: 10.1002/etep.2491.

[122] S. Nekkalapu, V. Vittal, J. Undrill, B. Keel, B. Gong, and K. Brown, “Synthesis of Load and Feeder Models Using Point on Wave Measurement Data,” *IEEE Open Access J. Power Energy*, vol. 8, pp. 198–210, 2021, doi: 10.1109/OAJPE.2021.3079724.